



2,  
59662032

This is to certify that the  
dissertation entitled

RETINOPATHY, GLOBE ENLARGED

presented by

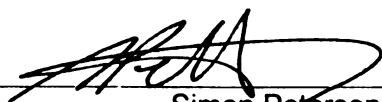
Fabiano Montiani-Ferreira

has been accepted towards fulfillment  
of the requirements for the

PhD

degree in

Comparative Medicine &  
Integrative Biology



Simon Petersen-Jones

3/3/04

Date





**PLACE IN RETURN BOX** to remove this checkout from your record.  
**TO AVOID FINES** return on or before date due.  
**MAY BE RECALLED** with earlier due date if requested.

| DATE DUE | DATE DUE | DATE DUE |
|----------|----------|----------|
|          |          |          |
|          |          |          |
|          |          |          |
|          |          |          |
|          |          |          |
|          |          |          |
|          |          |          |
|          |          |          |
|          |          |          |
|          |          |          |

**RETINOPATHY, GLOBE ENLARGED**

**By**

**Fabiano Montiani-Ferreira**

**A DISSERTATION**

**Submitted to  
Michigan State University  
in partial fulfillment of the requirements  
for the degree of**

**DOCTOR OF PHILOSOPHY**

**Comparative Medicine Integrative Biology  
College of Veterinary Medicine**

**2004**

## ABSTRACT

### RETINOPATHY, GLOBE ENLARGED

By

Fabiano Montiani-Ferreira

The purpose of this study was to perform a detailed characterization of the clinical, electroretinographic and morphological aspects and a preliminary molecular characterization of the autosomal recessive retinopathy, globe enlarged (*rge*) phenotype in chickens. *Rge* affected, carrier and normal birds were examined in detail ophthalmoscopically. A morphometric assessment of the eye globe and vision testing with an optokinetic device were performed. Scotopic and photopic electroretinography (ERG) and visually evoked potentials (VEPs) were recorded. Pharmacological investigation of abnormal ERG responses of *rge* birds was carried out. Morphological features were examined by light and electron microscopy. Retinal cell counting and measurement of the thickness of retinal layers were performed. Immunohistochemical staining with a panel of several antibodies was also investigated. *Rge* chicks lose vision over the first few weeks of life and are functionally blind by 30 days of age. They develop thicker corneas with a larger radius of curvature, hyperopia, and enlarged globes both radially and axially. At 1 day of age they have an elevated photopic and scotopic ERG response threshold, lower amplitude for a-wave and a substantial decrease of both oscillatory responses (OPs) and c-waves. With bright flash intensities, a supernormal b-wave response is present during the first weeks of life. All ERG responses decrease with increasing age. Naka-Rushton analysis of the ERG shows it is clearly abnormal from 1

day of age. After the *rge* chicks are functionally blind, optokinetic and cortical responses suggest some degree of vision (judged by the optokinetic performance) remains, although very reduced. Failure to block the b-wave responses with intravitreal injections of glutamate analogues (PDA and APB) provides strong evidence that the cells that normally generate this response in normal chicks do not originate the b-wave of *rge* chicks. Intravitreal injections of  $\text{BaCl}_2$  enhanced the supernormal b-wave response and ornithine nearly abolished it. Early morphological changes observed in *rge* retinas were disorganization of the outer plexiform layer and abnormal location of the smooth endoplasmic reticulum of the photoreceptors. In *rge* retinas, photoreceptor pedicles were abnormally shaped, usually containing multivesicular bodies. Furthermore, synaptic ribbons were less numerous and large glycogen deposits progressively accumulated in the perinuclear cytoplasm. Retinal thickness and numbers of rod outer segments (OSs) and inner nuclear layer nuclei decreased with age. A decrease in tyrosine hydroxylase-positive neurites, mislocalization, disorganization and a decrease in number of opsin-positive rod OSs, with activation of glial cells were all present in *rge* birds. The *rge* defect results in a severe visual deficit with a major effect on photoreceptors. Morphological changes consistent with retinal stretch due to excessive ocular growth and with progressive photoreceptor degeneration were present. A microsatellite marker (MCW0318) co-segregated with the *rge* locus, indicating that human chromosome region 12 p11-13 is the most likely region to contain the human homolog of the *rge* gene. Future identification of the causal gene mutation should help explain the morphological and ERG abnormalities of the *rge* phenotype and account for the rapid development of vision deficits.

## ACKNOWLEDGMENTS

I am deeply grateful for the guidance and friendship that Dr. Simon Petersen-Jones has given me during this past period of my life. His participation was indispensable for the progress and completion of this project. I truly value his never-ending patience, British humor and willingness to help during the countless times I have knocked at his door, whether it was his office or his home. I also must thank him for his power of persuasion, making sure that I kept my focus on this project by keeping me from going astray and thus basically saving me from “myself”. However, I also would like to express gratitude for the few times that he pretended he did not see me going astray so I could work in other related endeavors during these four years. That was perhaps an attempt to save me from “himself”. An old academic saying (possibly a Brazilian one) goes like this: From the advisor standpoint, the worst types of graduate students that can exist are: 1) the ones that do not do anything you say and 2) the ones that do everything you say. I am pretty sure I was not the latter type.

Furthermore, I really would like to apologize to my wife, Larissa Reifur, and my close friends for my chronic grumpiness, which started since I left my teaching position. Thank you, Larissa, for all the encouragement and the bravery that was to move to another country with me. Special thanks and acknowledgement go to my family as well.

Several collaborators, students, technicians and friends were crucial for the completion of this project. To appropriately thank them all it would take up a lot of space. Some of these exceptional people include: Rafael Cernuda, Andy Fischer, Kathleen Gustafson, Paul Sieving, Matti Kiupel, Vilma Yuzbasiyan-Gurkan, Andrew Geller, Hans

Cheng, David Sherry, Howard Howland, Tong Li, Wim DeGrip, Michelle Curcio, Mark Evans (and the great people at Pfizer), Michael Lavagnino and Fernando Cardoso.

Furthermore, I also would like to acknowledge the fantastic people from the Comparative Ophthalmology lab (past and present) and the staff of both graduate programs, Comparative Medicine and Integrative Biology (CMIB) and Pathobiology and Diagnostic Investigation (DPDI). I particularly would like to thank Denise Harrison, Victoria Hoelzer-Maddox and Sherrie Lenneman.

I cannot forget to express my gratitude to Paul Hocking for “saving” the *rge* birds in the UK, to Lisa Allen for being so competent in her job at MSU’s Vivarium, and to Theodore C. Sieving for helping with the “automation” of the optokinetic device.

At last, I would like to acknowledge all the help, suggestions and encouragement that I received from my committee members: Mark Evans, John C. Fyfe, Jon Patterson, Ben Yamini, and Mary Rheuben. A special recognition goes to Jon Patterson for conducting all the committee meetings.

Obrigado!



## TABLE OF CONTENTS

|   |      |
|---|------|
| LIST OF TABLES .....  | xii  |
| LIST OF FIGURES .....   | xiii |
| CHAPTER 1 - INTRODUCTION.....   | 1    |
| 1.1. Development of the vertebrate retina .....                         | 1    |
| 1. 2. Structure of the adult chicken ( <i>Gallus gallus</i> ) eye ..... | 6    |
| 1.2.1. Pecten .....   | 7    |
| 1.2.2. Retina.....  | 8    |
| 1.2.2.i. Retinal pigment epithelium (RPE) .....                         | 11   |
| 1.2.2.ii. Photoreceptors.....   | 12   |
| 1.2.2.iii. Outer plexiform layer (OPL) .....                            | 14   |
| 1.2.2.iv. Inner nuclear layer (INL).....                                | 17   |
| 1.2.2.iv.a. Horizontal and amacrine cells .....                         | 17   |
| 1.2.2.iv.b. Bipolar cells .....   | 18   |
| 1.2.2.iv.c. Müller cells .....  | 18   |
| 1.2.2.v. Inner plexiform layer (IPL).....                               | 19   |
| 1.2.2.vi. Ganglion cell and nerve fiber layer (GCL+NFL).....            | 19   |
| 1.3. Central visual pathways .....                                      | 20   |
| 1.4. The visual transduction pathway.....                               | 21   |
| 1.5. Electroretinogram (ERG) .....                                      | 25   |
| 1.6. Inherited retinal dystrophies.....                                 | 31   |
| 1.6.1. Globe enlargement in chicks with retinal disease .....           | 35   |

|   |    |
|---|----|
| 1.7. Position of the field when the work started.....   | 35 |
| <b>CHAPTER 2 - CLINICAL FEATURES OF THE RETINOPATHY, GLOBE</b>  |    |
| ENLARGED ( <i>rge</i> ) PHENOTYPE.....  | 37 |
| 2.1. Introduction .....   | 37 |
| 2.2. Material & Methods .....   | 37 |
| 2.2.1. General examination, observation of behavior, ophthalmic examination and<br>necropsy and preliminary histological examination..... | 38 |
| 2.2.2. Vision testing with an optokinetic device .....  | 39 |
| 2.2.3. Tonometry, central corneal pachymetry and eye dimension measurements ...   | 39 |
| 2.2.4. Refraction and measurement of corneal curvature .....  | 40 |
| 2.2.5. Statistical Analyses.....  | 41 |
| 2.3. Results .....  | 41 |
| 2.3.1. Physical examination, post mortem and preliminary histopathologic<br>examinations.....   | 43 |
| 2.3.2. Vision testing.....  | 44 |
| 2.3.3. Ophthalmic examination and globe biometry findings .....   | 46 |
| 2.4. Discussion .....   | 53 |
| <b>CHAPTER 3 - ELECTRORETINOGRAPHIC FEATURES OF THE <i>rge</i> CHICK</b>  |    |
| PHENOTYPE .....   | 57 |
| 3.1. Introduction .....   | 57 |
| 3.2. Material & Methods .....   | 58 |
| 3.2.1. Animals.....   | 58 |
| 3.2.2. ERG recording.....   | 58 |

|  |    |
|--|----|
| 3.2.3. Electrophysiological test protocols.....  | 59 |
| 3.2.4. Data analysis.....  | 61 |
| 3.3. Results .....   | 64 |
| 3.3.1. A-wave responses .....  | 68 |
| 3.3.1.i. <i>A-wave threshold</i> .....   | 69 |
| 3.3.1.ii. <i>A-wave amplitudes</i> .....   | 69 |
| 3.3.1.iii. <i>Slope of the a-wave leading edge</i> .....   | 70 |
| 3.3.1.iv. <i>A-wave implicit times</i> .....   | 71 |
| 3.3.1.v. <i>Subtraction of intensity matched photopic a-wave from scotopic a-wave to reveal rod-mediated a-wave response</i> ..... | 74 |
| 3.3.2. B-wave responses .....  | 75 |
| 3.3.2.i. <i>B-wave threshold (Figure 3.4)</i> .....  | 76 |
| 3.3.2.ii. Naka-Rushton fitting of the first limb of the I:R curves (Figure 3.8) .....  | 76 |
| 3.3.2.iii. Maximal amplitude of the b-wave - second limb of the intensity:response plot ( $B_{\max}$ ) (Figure 3.9).....           | 79 |
| 3.3.2.iv. <i>B-wave implicit times</i> .....   | 80 |
| 3.3.2.v. Ratio of b-wave to a-wave amplitudes .....  | 81 |
| 3.3.3. ERG response using color filters.....   | 81 |
| 3.3.4. 30Hz flicker ERG comparison (Figure 3.11) .....   | 84 |
| 3.3.5. VEPs (Figure 3.12).....   | 84 |
| 3.4. Discussion .....  | 86 |
| CHAPTER 4 - PHARMACOLOGICAL DISSECTION OF THE <i>rge</i>   |    |

|   |     |
|---|-----|
| ELECTRORETINOGRAM.....  | 92  |
| 4.1. Introduction .....   | 92  |
| 4.2. Materials & Methods.....   | 95  |
| 4.2.1. Animals.....   | 95  |
| 4.2.2. Pharmacological agents .....   | 95  |
| 4.2.3. Intravitreal injection .....   | 95  |
| 4.2.4. ERG recording.....   | 96  |
| 4.2.5. Statistical Analysis .....   | 97  |
| 4.3. Results .....  | 98  |
| 4.3.1. Results after the intravitreal injection of PDA (Figure 4.1) .....           | 98  |
| 4.3.2. Results after the intravitreal injection of APB (Figure 4.2.) .....          | 101 |
| 4.3.3. Results after the intravitreal injection of APB+PDA (Figure 4.3) .....       | 103 |
| 4.3.4. Results after the intravitreal injection of barium (Figure 4.4).....         | 105 |
| 4.3.5. Results after the intravitreal injection of ornithine (Figure 4.5).....      | 108 |
| 4.4 Discussion .....  | 111 |
| CHAPTER 5 - DETAILED HISTOPATHOLOGIC CHARACTERIZATION OF THE                        |     |
| <i>rge</i> CHICK PHENOTYPE .....  | 116 |
| 5.1. Introduction .....   | 116 |
| 5.2. Material & Methods .....   | 117 |
| 5.2.1. Morphometric analysis .....  | 117 |
| 5.2.2. Conventional morphologic analysis of semi-thin and ultra-thin sections ..... | 120 |
| 5.2.3. Immunocytochemistry studies on paraffin-embedded material .....              | 121 |
| 5.2.4. Immunocytochemistry studies on frozen sections.....                          | 122 |

|  |     |
|--|-----|
| 5.2.5. Terminal Deoxynucleotidyl Transferase-mediated dUTP Nick End Labeling<br>(TUNEL) Staining .....                         | 125 |
| 5.2.6. Detailed examination of the linear fundus lesions in semi-thin and ultra-thin<br>sections .....                         | 125 |
| 5.3. Results .....   | 126 |
| 5.3.1. Morphological measurements of the retina .....  | 126 |
| 5.3.2. Observations on semi-thin and ultra-thin sections, light and electron<br>microscopy .....                               | 130 |
| 5.3.2.i. Retinal sections at 1 day of age .....  | 130 |
| 5.3.2.ii. Retinal sections at 7 days of age.....   | 132 |
| 5.3.2.iii. Retinal sections at 60 to 90 days of age .....  | 136 |
| 5.3.2.iv. Retinal sections at 270 days of age .....  | 136 |
| 5.3.3. Immunohistochemistry results (paraffin-embedded and frozen sections).....   | 140 |
| 5.3.4. TUNEL Staining.....   | 149 |
| 5.3.5. Detailed examination of the linear fundus lesions in semi-thin and ultra-thin<br>sections .....                         | 150 |
| 5.4. Discussion .....  | 154 |
| CHAPTER 6 - CONTRIBUTIONS TO THE MOLECULAR CHARACTERIZATION  |     |
| OF THE <i>rge</i> DEFECT .....   | 161 |
| 6.1. Introduction .....  | 161 |
| 6.2. Material & Methods .....  | 162 |
| 6.2.1. Testing the <i>rge</i> chicken for the deletion of the guanylate cyclase gene present<br>in the <i>rd</i> chicken ..... | 162 |

|  |     |
|--|-----|
| 6.2.2. Mapping of the <i>rge</i> region .....  | 165 |
| 6.2.3. Mapping and sequencing of candidate genes .....   | 168 |
| 6.3. Results .....   | 173 |
| 6.3.1. Testing the <i>rge</i> chicken for the deletion of the guanylate cyclase gene present<br>in the <i>rd</i> chicken ..... | 173 |
| 6.3.2. Mapping of the <i>rge</i> region .....  | 174 |
| 6.3.2.i. <i>Selection of candidate genes</i> .....   | 176 |
| 6.3.2. i.a. Cyclin-dependent kinase inhibitor (Kip1) .....   | 176 |
| 6.3.2.i.b. Synaptobrevin (Vamp1) .....   | 177 |
| 6.3.3. Mapping and sequencing of candidate genes .....   | 177 |
| 6.3.3.i. <i>Radiation-hybrid (RH) mapping</i> .....  | 177 |
| 6.3.3.ii. <i>Sequencing of candidate genes</i> .....   | 178 |
| 6.4. Discussion .....  | 181 |
| <b>CHAPTER 7 - CONCLUSIONS &amp; FUTURE STUDIES</b> .....  | 183 |
| <b>BIBLIOGRAPHY</b> .....  | 188 |



## LIST OF TABLES

|  |    |
|--|----|
| <b>Table 2.1</b> – Summary of the main clinical features observed in chicks presenting the <i>rge</i> phenotype. ** $P < 0.05$ ; *** $P < 0.001$ ; **** $P < 0.0001$ ..... | 42 |
|--|----|

## LIST OF FIGURES

Images in this dissertation are presented in color

|  |    |
|--|----|
| <b>Figure 1.1-</b> Scanning electron micrographs of embryos at different stages of development.....  | 3  |
| <b>Figure 1.2</b> - Histological and structural characteristics of the chicken eye. ....   | 7  |
| <b>Figure 1.3</b> - Plastic-embedded retinal section of a normal chicken at 270 days of age.....   | 10 |
| <b>Figure 1.4</b> - Ultrastructural aspect of the chick OPL.....   | 16 |
| <b>Figure 1.5</b> - Diagram of rod phototransduction cascade.....  | 25 |
| <b>Figure 1.6</b> - Diagrammatic representation of the Granit waveforms (I, II and II) which make up the electroretinogram (ERG).....              | 28 |
| <b>Figure 2.1</b> – Results from vision testing with an optokinetic device.....  | 45 |
| <b>Figure 2.2</b> - Series of age-matched gross ophthalmic photographs from representative <i>rge</i> and control birds. ....                      | 47 |
| <b>Figure 2.3</b> - Series of micrographs of the anterior segment of the eye of representative <i>rge</i> and control birds at different ages..... | 48 |
| <b>Figure 2.4</b> - Gross photograph showing the detail of a hypermature cataract in an <i>rge</i> chick at 270 days of age. ....                  | 49 |
| <b>Figure 2.5</b> - Radial globe diameter of <i>rge</i> and control eyes at each time-point evaluated.....   | 50 |
| <b>Figure 2.6</b> - Mean axial globe length of <i>rge</i> and control eyes at each time-point evaluated.....                                       | 50 |

|   |           |
|---|-----------|
| <b>Figure 2.7 - Mean central corneal thicknesses (CCT) of <i>rge</i> and control eyes at each time-point evaluated .....</b>  | <b>52</b> |
| <b>Figure 3.1 - Representative scotopic and photopic ERG recordings from a control bird at 7 days of age.....</b>   | <b>66</b> |
| <b>Figure 3.2 - Representative scotopic and photopic ERG recordings from a control bird at 270 days of age.....</b>   | <b>67</b> |
| <b>Figure 3.3 - Representative scotopic isolated oscillatory potentials (OPs) of an ERG recording from a control bird at 1 day of age.....</b>                                  | <b>68</b> |
| <b>Figure 3.4 – Scotopic and photopic threshold using 5 <math>\mu</math>V-criterion. Mean scotopic threshold for a-wave and for b-wave for all the age groups studied .....</b> | <b>72</b> |
| <b>Figure 3.5 – Scotopic and photopic intensity: response (I:R) plot at 7 days of age in dark-adapted <i>rge</i> and control birds.....</b>                                     | <b>73</b> |
| <b>Figure 3.6 - Mean scotopic <math>A_{max}</math> at all the age groups studied.....</b>   | <b>74</b> |
| <b>Figure 3.7 - Intensity matched (<math>2.8 \log \text{cdS/m}^2</math>) a-wave tracings from a control and an <i>rge</i> chick at 160 days of age .....</b>                    | <b>75</b> |
| <b>Figure 3.8 – Naka-Rushton fit parameters. Scotopic b-wave intensity:response function from <i>rge</i> and control chicks at 56 days of age. ....</b>                         | <b>78</b> |
| <b>Figure 3.9- Mean scotopic <math>B_{max}</math> of all the age groups studied.....</b>  | <b>80</b> |
| <b>Figure 3.10 - Mean a-wave amplitudes, photopically matched, using stimuli of 3 different peak spectral transmittances .....</b>  | <b>83</b> |
| <b>Figure 3.11 - A comparison of 30 Hz flicker tracings using flash-light intensity of <math>0.4 \log \text{cdS/m}^2</math> at 1 day of age.....</b>                            | <b>85</b> |

|  |     |
|--|-----|
| <b>Figure 3.12-</b> Comparison of the VEP response at 1 day of age in a <i>rge</i> and a control chick.....  | 86  |
| <b>Figure 4.1</b> - Representative ERGs performed before and after the intravitreal application of PDA .....   | 100 |
| <b>Figure 4.2</b> - Representative ERGs performed before and after the intravitreal application of APB .....   | 102 |
| <b>Figure 4.3</b> - Representative ERGs performed before and after the intravitreal application of PDA + APB .....   | 104 |
| <b>Figure 4.4</b> - Representative ERGs performed before and after the intravitreal application of barium chloride.....  | 107 |
| <b>Figure 4.5</b> - Representative ERGs performed before and after the intravitreal application of ornithine.....  | 110 |
| <b>Figure 5.1</b> - Graphic representation of the method used for determining the retinal regions used for retinal thickness measurement.....  | 118 |
| <b>Figure 5.2</b> - Total retinal thickness of <i>rge</i> and control birds at 2, 14, 28, 56, 180, 270 and 420 days of age .....   | 127 |
| <b>Figure 5.3</b> - Mean retinal thickness of each of the different retinal layers from <i>rge</i> and control birds at two representative age groups. ....                                  | 128 |
| <b>Figure 5.4</b> - Number of rod OSs and ganglion cells per unit length and number of rows in the INL in cross sections in cross sections at 14, 21, 90, 180, 270 and 720 days of age. .... | 129 |
| <b>Figure 5.5</b> - Semi-thin and ultra-thin retinal sections of a control and of an <i>rge</i> chick at 1 and at 60 days of age .....   | 131 |

R

d

Fi

us

and

Fig

con

Figure

Figure

.....

Figure

.....

Figure

showing

|  |     |
|--|-----|
| <b>Figure 5.6</b> - Ultrastructural features of the ONL/IS interface of an <i>rge</i> chick, at 1 day of age .....   | 132 |
| <b>Figure 5.7</b> - Semi-thin and ultra-thin sections of <i>rge</i> and control retina at 7 days of age.....   | 134 |
| <b>Figure 5.8</b> - Synaptic terminal of a cone pedicle of a control chick at 7 days of age and a typical example of a synaptic terminal of a cone pedicle of an <i>rge</i> chick at 7 days of age. .... | 135 |
| <b>Figure 5.9</b> - Ultra-thin sections of retinal samples from <i>rge</i> birds at 60 days of age .....   | 138 |
| <b>Figure 5.10</b> - Semi-thin sections of retinal samples from <i>rge</i> and control birds at 270 days of age .....  | 139 |
| <b>Figure 5.12</b> - Fluorescence photomicrographs and conventional photomicrograph using brown chromogen from immunocytochemistry sections using anti-opsin antibodies.....                             | 142 |
| <b>Figure 5.13</b> - Immunocytochemical stained retinal sections using RCA-1 antibody of control and <i>rge</i> chicks at 13, 33, and 92 days of age.....  | 145 |
| <b>Figure 5.14</b> - Immunocytochemistry of retinal sections using LEP-100 antibody.   | 146 |
| <b>Figure 5.15</b> - Immunocytochemistry of retinal sections using anti-glycine antibody .....   | 147 |
| <b>Figure 5.16</b> - Immunocytochemistry of retinal sections using anti-GFAP antibody. ....  | 148 |
| <b>Figure 5.17</b> - Photograph of the posterior eyecup from a 49-day-old <i>rge</i> bird showing lacquer cracks.....  | 152 |



|  |     |
|--|-----|
| <b>Figure 5.18</b> – Plastic and resin-embedded retinal sections from <i>rge</i> birds demonstrating morphologic details of the lacquer crack lesions typical of early stage changes observed in the <i>rge</i> phenotype..... | 153 |
| <b>Figure 5.19</b> – Ultra-thin section from the eye of an <i>rge</i> bird at 336 days of age....  | 154 |
| <b>Figure 6.1</b> - Result of RT-PCR from retinal tissue from a normal, a carrier and an <i>rge</i> bird on 1.5% agarose electrophoresis gel.....  | 174 |
| <b>Figure 6.2</b> - Genetic map for the <i>rge</i> region. ....  | 175 |
| <b>Figure 6.3</b> - Interspecies comparative genetic map (chicken, human and mouse) for the <i>rge</i> region.....   | 176 |
| <b>Figure 6.4</b> - RH correlation for several microsatellite markers linked to the <i>rge</i> region.....   | 178 |
| <b>Figure 6.5</b> - Chicken Vamp1 nucleotide sequence .....  | 180 |

u

b

n

c

m

n

en

the

co.

# **CHAPTER 1**

## **INTRODUCTION**

### **1.1. Development of the vertebrate retina**

The vertebrate eye (*bulbus oculi*) develops from several embryonic tissues including neural crest cells (ocular mesenchyme), neuroectoderm (retina and neuroepithelium of the iris and ciliary body), surface ectoderm (epithelial structures and the lens), and mesoderm (extraocular muscles and vascular endothelium).

In the embryo, with the formation of the primitive streak, the classic ectoderm, mesoderm and endoderm subdivisions appear. In response to the formation of the notochord, ectoderm thickens (neural plate), and forms elevations called the neural folds (Barishak, 2001, Cook, 1995, Cook, 1999).

A specialized population of mesenchymal cells, the neural crest, emigrates from the neural ectoderm at its junction with surface ectoderm. Neural crest cells spread beneath the surface ectoderm and populate several regions of the embryo including the region around the optic vesicle, ultimately giving rise to nearly all of the ocular connective tissue structures including internal structures of the palpebra. In the eye, mesenchyme originating from the regular mesoderm (middle embryonic layer) only gives rise to the striated myocytes (muscle cells) of the extraocular muscles and the vascular endothelium (Barishak, 2001, Cook, 1995, Cook, 1999).

To generate the neural tube, the neural folds elevate and approach each other until they actually touch and fuse. Once the tube is closed, the exterior of the embryo is completely covered by surface ectoderm. The tube is lined by neural ectoderm. Neural

segmentation then occurs to form the prosencephalon (forebrain), mesencephalon (midbrain) and rhombencephalon (hindbrain) (Barishak, 2001, Cook, 1999).

Paired evaginations of neurectoderm from the developing diencephalic portion of the prosencephalon (Figure 1.1A) develop to form the optic vesicles, which are connected to the forebrain by optic stalks (Barishak, 2001). The formation of the optic vesicles occurs between chick embryonic days 1.5 and 3 (E1.5/E3) (Pittack, Grunwald & Reh, 1997). Anteriorly, the optic vesicle induces the overlying surface ectoderm to thicken, forming the lens placode (Figure 1.1 B). The optic vesicle then induces the lens placode to invaginate (Figure 1.1 C). Once the lens placode invagination is induced by the optic vesicle, the lens placode in turn induces the optic vesicle to invaginate, concurrently, to form the optic cup (this process is called reciprocal induction). As the optic cup is being formed the invaginating lens placode then detaches from the surface to form the lens vesicle (E3) . The lens vesicles are lined by a monolayer of epithelium and are completely surrounded by a basal lamina, which will become the lens capsule in the adult bird. The ocular mesenchyme invades the anterior portion of the globe (anterior segment) between the lens and the corneal epithelium. Portions of the cornea (stroma and endothelium), iridal stroma and structures of the iridocorneal angle are all formed from these invading cells of the ocular mesenchyma (formerly neural crest cells). A portion of this ocular mesenchyme forms a vascular bridge across the future pupil (pupillary membrane) . The formation of all the neural crest-derived structures, in the anterior segment of the chick eye, is regulated by signals from the lens .



**Figure 1.1-** Scanning electron micrographs of embryos at different stages of development. A) Paired evaginations of neuroectoderm (selected area) from the developing diencephalic portion of the prosencephalon, forming the optic vesicles - mouse embryo at 8.5 days of gestation. B) Optic vesicle induces the overlying surface ectoderm to thicken, forming the lens placode (arrow) - mouse embryo at 29 days of gestation. The invaginating lens placode also induces the invagination of the optic vesicle (reciprocal induction) to form the optic cup. C) Note that the formation of the lens vesicle (arrow) and optic cup (arrowhead) are nearly completed - mouse embryo at 36 days of gestation. Source: University of North Carolina - Chapel Hill Medical School, available at [http://www.med.unc.edu/embryo\\_images](http://www.med.unc.edu/embryo_images)

The optic cup then collapses to close a potential space (subretinal space) between the two layers of neural epithelium that are destined to form the neural retina and the retinal pigment epithelium (RPE). The neuroepithelial cells at the rostral margin of the optic cup form two layers of iridal epithelium (inner and outer), which are continuous with two layers of ciliary epithelium. The outer iridal epithelium gives rise to musculature of the iris. The outer ciliary epithelium is continuous with the RPE, and the inner ciliary epithelium is continuous with the neurosensory retina at the *ora serrata*. At E 6.5, pigment granules can be seen in the inner epithelium at the root of the iris. As development proceeds, the pigmentation of both epithelial layers progresses from the root of the iris to the pupillary margin. Early features of the development of the sphincter muscle can first be recognized by E7. Both smooth muscle and striated muscle are

present in the iris of the chick embryo. The smooth musculature originates by E10 from a laminar invagination (iridial lamella) of the outer iridal epithelium. The striated musculature appears slightly later than the smooth musculature and originates from undifferentiated cells, which are regarded as mesenchymal .

As the retina develops, the outer-pigmented layer becomes relatively thinner while the neural portion thickens . As with the ciliary epithelium, invagination of the optic vesicle causes the apices of the inner nonpigmented layer to be directed outward, to face the apices of the outer pigmented layer. The retina basically is a peripherally developed portion of the central nervous system . The outer-pigmented layer develops into the RPE and Bruch's membrane. In the inner nonpigmented layer, the neuroblastic cellular differentiation proceeds in an inner-to-outer, central-to-peripheral fashion . The innermost neuroblastic layer develops into ganglion cells, Müller cells, horizontal cells and amacrine cells; while the outermost layer forms the bipolar cells and photoreceptors . As in mammals, avian retinal ganglion cells are the first cells to differentiate. In chicks, during E4 ganglion cell genesis is near its peak . The ganglion cell fibers leave the eyeball and, grow along the optic stalk, reaching the chiasm around E4 arriving at the optic tectum at E6 . In E7 embryos, the eyes are approximately 0.5 cm in diameter . At this time a developing pecten structure becomes evident . Branching patterns of the ganglion cell dendrites become relatively uniform on E8 . The inner and outer plexiform layers appear during E8 to E15 . Non-specific phagocytic activity is observable in the RPE as early as E9 and continues through the rest of the developmental period and throughout adult life . Müller cells finish developing at about E11 . The bipolar cells and photoreceptors are the last retinal cells to mature. The rods and cones start to differentiate



during E12 . The long-wavelength cone opsins, red and green, are first detected in chicks at embryonic day E14. The first rhodopsin transcripts are seen at E15 in the inferior retina. In contrast, the short-wavelength cone opsins, blue and violet, were not detected until E16 . By E16 pecten development is completed . The embryonic electroretinogram (ERG) starts to be recordable by E18 , reflecting retinal function. By hatch (E21) the chick eyes have increased to 1 cm in diameter .

## **1. 2. Structure of the adult chicken (*Gallus gallus*) eye**

The avian eye follows the basic structure of the mammalian eye, consisting of three concentric tunics and the lens. The outermost tunic is divided into cornea and sclera, the middle one is the uveal tract and the innermost is the retina. The avian cornea has a microscopically evident Bowman's layer, which is also present in primates. Another anatomic feature of the avian eye globe is the presence of two specialized structures within the sclera: a bony ring and a cartilage cup. The bony ring is comprised of a variable number of thin scleral ossicles that can vary from 10 to 18 in number. The majority of birds have 15 scleral ossicles. The ossicle ring determines the shape of the anterior segment of the globe and the scleral cartilage cup maintains the structure of the posterior segment of the globe . The avian eye is large relative to the size of the head and brain. For example, human eyes make up about 1% of the total mass of the head; in birds the eyes make up about 15% of the mass of the head .

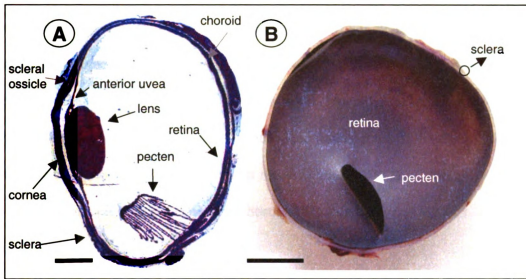


**Figure 1.2** - Histological and structural characteristics of the chicken eye. A) Paraffin-embedded cross retinal section of a chicken eye at 7 days of age, the names of the main structures are indicated in the figure. Note the comb-like appearance of the pecten, located anteriorly, on top of the optic nerve head. Stain = hematoxylin/eosin. Bar - 2.5 mm. B) Gross photograph of the posterior eyecup of a 60-day-old chicken eye after removal of the anterior segment, lens and vitreous. The retina is the transparent layer covering the eyecup. Note that the pecten projects into the inferior portion of the posterior chamber. The dorsal part of the pecten is always tilted to the temporal aspect of the eye. Thus, B shows a retinal cup from a right eye. Bar - 5 mm.

### 1.2.1. Pecten

The pecten (*pecten oculi*) is a unique structure present within the posterior segment of the avian eye. It is a highly vascular and pigmented comb-like structure that overlies the optic disc and projects into the vitreous humor (Figure 1.2 A & B). Light and electron microscope studies have shown that the pecten is a manifoldly pleated structure that consists almost exclusively of blood vessels, extravascular pigmented cells and a superficial covering membrane; it lacks both muscular and nervous tissues. Its physiological function(s) have been debated for a long time. Possible functions cited by

different authors include increasing the sensory detection of small moving objects , intraocular pressure regulation , reduction of intraocular reflection , intraocular pH regulation , magnetic sensor , blood-retinal barrier and as a source of supplemental nutrition to the retina that probably equates to the inner retinal vasculature present in many mammalian species . The latter hypothesized function has been widely accepted by contemporary researchers, since the avian retina is avascular. Thus, the avian retina has two nutrient sources: the pecten and the choroidal vasculatures.

### 1.2.2. Retina

The retina consists of two primary layers, an inner neurosensory retina and an outer simple epithelium, the RPE. The neurosensory retina is firmly attached only at its anterior termination, the *ora serrata*, and at the margins of optic nerve head.

Eight histological layers are recognized in the neurosensory retina: photoreceptor outer segments (OSs), photoreceptor inner segments (ISs), outer nuclear cells (ONL), outer plexiform (OPL), inner nuclear cells (INL), inner plexiform (IPL), ganglion cell and nerve fiber layer (GCL+NFL) (see Figure 1.3). Some alternative histological descriptions include two additional layers: the outer and inner limiting membrane. However, the idea of an outer and inner limiting membranes as actual membranes *per se* is incorrect; the dense “membrane” seen at this level with the light microscope simply consists of a line of closely opposed terminal bars joining distal processes of the Müller cells to adjacent photoreceptors. Müller cells’ endfeet also are responsible for the inner limiting membrane (Won, Kang et al. 2000).

The synaptic contact areas in the retina are named outer plexiform layer (OPL) and inner plexiform layer (IPL) (Figure 1.3 and Figure 1.4). These two areas have conventional vesicular and ribbon vesicular synapses. Transmitter release at vesicular synapses is an exocytotic process mediated by a cascade of interactions involving proteins in the synaptic vesicle membrane, presynaptic plasma membrane and presynaptic cytoplasm. Neuronal exocytosis is triggered by calcium and requires 3 SNARE proteins: synaptobrevin on the synaptic vesicle, syntaxin and SNAP25 on the plasma membrane .

By means of many complex nerve synaptic contacts within the neurosensory retina, electrical impulses generated by light reaching the photoreceptors are processed and transmitted to the nerve fiber layer and, subsequently, to the optic nerve and brain.

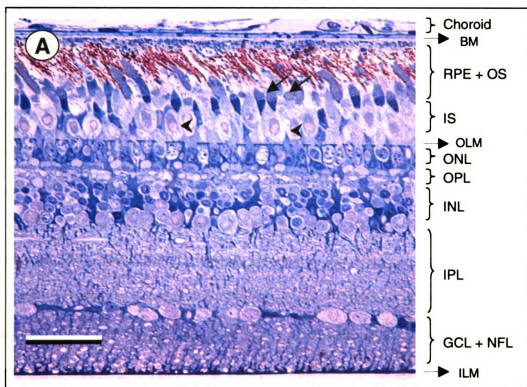


**Figure 1.3** - Plastic-embedded retinal section of a normal chicken at 270 days of age. All cell and fiber layers found in the mammalian retina are present. The oil droplets, present in some of the cone photoreceptor inner segments can be seen adjacent to the RPE (arrows). The hyperboloid and the paraboloid (arrowheads) with their characteristic metachromatic appearance in toluidine blue can also be seen. Stain – toluidine blue; Bar - 20  $\mu$ m. Key: BM - Bruch's Membrane; RPE+OS – Retinal Pigment Epithelium + Outer Segment; IS- Inner Segment; OLM – Outer Limiting Membrane; ONL- Outer Nuclear Layer; OPL- Outer Plexiform Layer; INL- Inner Nuclear Layer; IPL - Inner Plexiform Layer; GCL+NFL - Ganglion Cell Layer + Nerve Fiber Layer; ILM- Inner Limiting Membrane.

at  
is  
ve  
e  
C  
r  
f  
a  
r  
h  
c  
e

#### 1.2.2.i. Retinal pigment epithelium (RPE)

The RPE is a single layer of cuboidal cells resting on a basal lamina (Bruch's membrane), which is adjacent to the choroid. Because of its high melanin pigment content, the RPE is opaque to light (Figure 1.3). It lies adjacent to the photoreceptor cells and performs a number of functions that are critical for the viability and activity of the retina . Microvilli from the apical portion of the RPE cells usually project during the day, or in well-illuminated environments, and envelope the distal ends of the photoreceptor OSs. The microvilli are especially well developed in the avian eye and can envelope more of the photoreceptors than in the mammalian eye. At night, or after a long period of dark adaptation, they retract, and if the eye is harvested at this stage the RPE histologically looks very compact. The principal pathway by which the retina takes up nutrients and other small molecules from serum is from the choroidal circulation, via transepithelial transport, across the RPE. The RPE also engulfs, digests, and recycles approximately 10% of the mass of each OS per day , mediates the isomerization of retinal from all-trans to 11-*cis* retinal , and stores retinoid precursors for visual pigment regeneration . Phagocytosis of the OSs occurs on a diurnal schedule, with the peak of rod OS shedding occurring at dawn and the peak of cone OS disc shedding occurring at dusk . In conjunction with the retina, the RPE contributes to the generation of a standing electrical potential across the eye and to the c-wave of the electroretinogram (ERG), a voltage response to illumination that occurs on a time scale of several seconds . The isolated RPE shows an electrical response to illumination only at intensities that are well above the physiological range; this response appears to be mediated by melanin .



### 1.2.2.ii. Photoreceptors

As in mammals, the avian photoreceptor complex is arranged in a highly regular pattern, called a “retinal mosaic” . Although the avian retina has a duplex nature (i.e., containing both rods and cones) similar to that of primates, it also possesses (along with reptiles, many fish, and amphibians) photoreceptors known as double cones. Rods and cones both have four distinct functional zones: the OSs, the ISs, the cell bodies and the synaptic termini. Within the chicken retina, cone photoreceptors outnumber rod cells by six to one in the central retina and by three to one in the peripheral retina . The cone-dominant character of the avian retina contrasts with the typical mammalian retina in which rods outnumber cones. Rod OSs are packed with parallel bilaminar discs, which are separated from the cell membrane and are positioned 90° to the long axis of the cell. Rods mediate vision at low light levels and cones in bright light . Cone OSs are packed with lamellae, which, unlike the rod discs, remain continuous with the cell membrane. In both cells OS material is shed in packages from the distal end of the OS. The double cone consists of a principle cone (similar in structure to a normal single cone) and an accessory cone, which curves around the IS of the principle cone. The rod IS displays an ellipsoid of mitochondria, much rough endoplasmic reticulum (RER), numerous polysomes and a prominent hyperboloid of glycogen (Figure 1.3). The rods have no oil droplets. Single cones show a tapered OS, a large ellipsoid and a paraboloid of glycogen and an oil droplet at the apical end of the ISs. The principal cone of double cones displays a single large oil droplet and no paraboloid. The accessory cone has no oil droplet and a large paraboloid. All cones have a large ellipsoid, plentiful polysomes, RER, Golgi zones and autophagic vacuoles . Oil droplets are a common feature of the cones in many vertebrate

retinas (e.g. birds, reptiles and amphibians), but are rarely found in rods. The oil droplets consist of lipids in which carotenoid pigments are dissolved; they can appear transparent or clear, pale yellow, green, orange, or red. They are positioned at the distal end of the inner cone segments, spanning the entire width of the receptor (Figure 1.3). Light passes through the droplet before entering the photosensitive OS . Several functions have been attributed to the oil droplets. These include an ability to reduce blur, fine-tune the sensitivity spectrum of the different types of cone photoreceptors and act as an ultra-violet radiation shield . It is now believed that colored oil droplets increase the number of colors that can be discriminated, and thus are beneficial for color vision . Hence, whereas initial color processing occurs at the ganglion cell level in primates, the avian visual system may perform color-processing steps within the photoreceptors themselves. Despite the differences inherent in these retinal systems, they appear to achieve comparable color abilities. Birds appear to have excellent color vision, which may be based on as many as four or five different cone cell photopigments. Iodopsin, for instance, is a cone cell photopigment that is found exclusively in the chick retina . Not all of the other photopigments have been completely characterized. Chickens have four types of single-cone photoreceptors sensitive to ultraviolet, short-, medium- or long-wavelength light, with peak sensitivity at around 400, 475, 540 and 615 nm, respectively. The principal and accessory OSs of the double cone contain different visual pigments. The double cone has its spectral peak of sensitivity at around 575 nm. It is believed that the double cones serve luminance-based tasks, such as motion detection, and are not so important for vision . Evidence for tetra- or pentachromatic vision in birds comes from analysis of the absorption spectra of visual pigments and from behavioral discriminations .

This contrasts with the three cone pigments identified in primates and with the two cone pigments identified in ungulates and in dogs .

High densities of cones are typically correlated with high densities of their associated ganglion cells. These densities, in turn, are assumed to equate with areas of high visual acuity. There are retinal regions in which the cones are more densely packed at the expense of rods. These regions can either be circular, described as an area centralis, or elongated, called a visual streak. Some species of birds have a pit within the area of greater cone density, called a fovea, which is formed by the lateral displacement of the proximal neurons and fibers. Foveal pits tend to be more pronounced and deeper in diurnal birds in comparison to primates (including humans). Most birds have a single fovea near the center, slightly above and nasal to the optic disc. The chicken does not have a fovea and the lack of a fovea is generally regarded as a consequence of domestication. The area of densely packed cones in the chicken retina is called an afoveate area centralis .

#### 1.2.2.iii. Outer plexiform layer (OPL)

The most external area of synaptic contact in the retina is the OPL, where connections between rod and cones, vertically running bipolar cells and the horizontally oriented horizontal cells occur. In brief, photoreceptors catch light in the visual pigment-containing membranes of the OS and pass a message, concerning numbers of quanta of light and sensitivities to the different wavelengths, to the OPL where a certain degree of integration and processing of the stimulus occurs before the visual message is transmitted to the inner retina. In the bird retina, rods and double cones terminate in the outer

sublayer of the OPL, and the single cones terminate in the inner sublayer (Figure 1.4), forming a well-organized bilayered arrangement of photoreceptor terminals. The information-transmitting end of the cone cell is known as the pedicle and of the rod cell as the spherule. The cone pedicles and rod spherules make synaptic contacts with various bipolar cell and horizontal cell types. Also, cone pedicles pass electrical messages between each other and between rod spherules, so that a small amount of rod and cone signal mixing occurs at this layer. Cone pedicles are large and flat end-feet shaped. The rod spherules, in contrast, are small round enlargements of the axon or even extensions of the cell body. The synaptic endings of both photoreceptor types are filled with synaptic vesicles. At their synapses to second-order neurons (bipolar and horizontal cells), both rod spherules and cone pedicles exhibit dense structures known as synaptic ribbons pointing to the postsynaptic invaginated processes. The ribbon synapses are the principal vesicular synapses of the OPL, which tonically release the transmitter glutamate. Rod spherules have only two synaptic ribbons associated with two lateral elements that are horizontal cell axon terminals and two central invaginating dendrites of rod bipolar cells. Cones contain multiple ribbons at each area of synaptic contact. These areas are named triads. The cone triad of invaginated second-order processes consists typically of a central element, which is a dendritic terminal of an invaginating bipolar cell, and two lateral elements, which are dendritic terminals of horizontal cells.

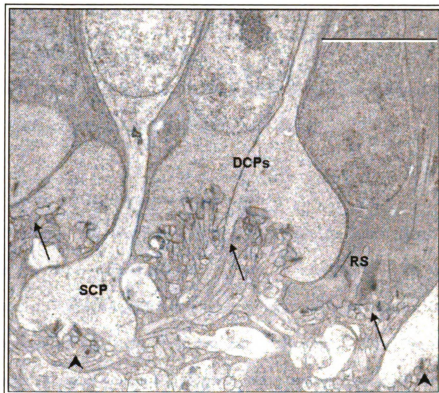


**Figure 1.4** - Ultrastructural aspect of the chick OPL. Note that the rod spherule and the double cone pedicles terminate in the outer sublayer of the OPL (arrows), whereas the single cone pedicle terminates in the inner sublayer (arrowheads). Key: SCP - Single Cone Pedicle; DCPs - Double Cone Pedicles; RS - Rod Spherule. Bar - 3  $\mu$ m.

#### 1.2.2.iv. Inner nuclear layer (INL)

The INL is composed of various nuclei and cell bodies of second order neurons such as horizontal, bipolar, amacrine and Müller cells (Figure 1.3).

##### *1.2.2.iv.a. Horizontal and amacrine cells*

The horizontal and amacrine cells serve to mediate the lateral spread of visual activation in the retina. Horizontal cells perform this modulation in the OPL. The anatomist Ramon Cajal distinguished two types of horizontal cells common to birds and reptiles; brush-shaped and stellate (summarized by Rodieck, 1973). The number of horizontal cells is similar among fish, reptiles, birds, and mammals. However, Cajal noted a correlation of rod structure and density to the size of the horizontal cells (summarized by Rodieck, 1973). In mammals and teleost fishes, the rods are somewhat thin and associated with large horizontal cells, while in birds and reptiles the rods are wide and tend to be associated with smaller horizontal cells. Amacrine cells function similarly to horizontal cells in transferring information laterally across the retina mainly at the inner plexiform layer. Historically, they were not considered neurons. By the middle of the 20th century, their neuronal nature was confirmed, and their enormous diversity established. Amacrine cells have been most successfully subdivided into morphological categories based on two parameters: diameter of the dendritic field and ramification pattern in the inner plexiform layer. There are over 20 morphological types of amacrine cells already identified in the vertebrate retina, which use several different neurotransmitters, such as glucagon, substance P, glutamate, dopamine, gamma-

aminobutyric acid (GABA), serotonin and glycine . Works combining anatomy, physiology, and neurochemistry of these cells are scarce, therefore the exact functions of all the different amacrine cell subtypes are not completely understood .

#### *1.2.2.iv.b. Bipolar cells*

Bipolar cells exist in the retinas of all vertebrates. The bipolar cells of birds, reptiles, and amphibians are very similar, consisting of two types as first recognized by Cajal (summarized by Rodieck, 1973): outer (or large) and inner (or small) bipolar cells. The defining characteristic of bipolar cells is their dendritic contact with the photoreceptors.

#### *1.2.2.iv.c. Müller cells*

The Müller cell is often referred to as the radial glial cell, it is spread out radially between the external and internal limiting membrane of the retina, which are formed by the proximal and distal endfeet of the cells. The avian retina is completely devoid of astrocytes. Thus, Müller cells constitute the only astrocyte-like cell population in avian retinæ, whereas mammalian retinæ also contain astrocytes in close association with blood vessels . Müller cells are key mediators of nerve cell protection, especially via release of basic fibroblast growth factor, via uptake and degradation of the excitotoxin glutamate, and via secretion of the antioxidant glutathione . Like other glial cells of the CNS, Müller cells undergo reactive gliosis following acute retinal injury or chronic neuronal stress. Virtually every disease of the retina is associated with a reactive Müller cell gliosis. Müller cell gliosis is characterized by proliferation, changes in cell shape due

to

se

a

c

o

b

s

h

c

f

a

r

a

d

n



to alterations in intermediate filament production, changes in ion transport properties, and secretion of signaling molecules such as vascular endothelial growth factor .

#### 1.2.2.v. Inner plexiform layer (IPL)

The more internal area of synaptic contact of the retina is the IPL, and it functions as a relay station for the vertical-information-carrying nerve cells, the bipolar cells, to connect to ganglion cells (Figure 1.3). The IPL of birds is very thick compared to the other vertebrates . It contains numerous conventional vesicular synapses made primarily by amacrine cell terminals that phasically release the inhibitory neurotransmitters gamma-aminobutyric acid (GABA) or glycine , and ribbon synapses made by bipolar cell terminals, which rapidly release glutamate , to the synaptic terminals of the ganglion cells.

#### 1.2.2.vi. Ganglion cell and nerve fiber layer (GCL+NFL)

Retinal ganglion cells are the output neurons that encode and transmit information from the eye to the brain. The axons of ganglion cells form the optic nerve, which is the anatomical link between the eye and the brain. The signals transmitted via the optic nerve represent the integration of all retinal processing that is then conveyed to higher centers along the visual pathways.

In birds, it has long been known that the intraretinal portions of ganglion cell axons are myelinated . Oligodendrocytes (a form of macroglial cell) are absent in most mammalian retinas, except in the rabbit. The bird retina, however, contains a large

numbe

respon

avian

distrib

ONL.

gangli

densiti

cones.

man co

in gan

were p

pattern

13. C

nerve

with g

within

synaps

human

chick

number of oligodendrocytes. These latter cells, along with Müller cells, are believed to be responsible for the myelination of the ganglion cell axons and optic nerve head in the avian retina . However, microglia in the bird retina show a very similar pattern of distribution to that of mammalian counterparts . Microglia are distributed in the OPL, ONL, IPL, GCL and NFL.

There is a great difference in the number, types, and distribution of retinal ganglion cells between birds and mammalian species. As mentioned previously, high densities of ganglion cells are typically correlated with high densities of their associated cones. There are about 1 million ganglion cells in the retina of the rhesus monkey and in man compared to 2 million or more in chick, pigeon, and quail . The large variations seen in ganglion cells make them challenging to classify. However, accepted classifications were performed in the past on the basis of soma size, dendritic field size and branching patterns within the inner plexiform layer.

### **1.3. Central visual pathways**

The basic route that information from photoreceptors is conveyed to the optic nerve is as follows: the photoreceptor synapses with bipolar cells which in turn synapse with ganglion cells, the axons of which form the optic nerve. Modification of the signal within the retina occurs via the action of horizontal and amacrine cells. The former cells synapse with photoreceptors and the latter with bipolar cells.

As in mammals, 100% of the optic nerve axons of the chick are myelinated. In humans the total axon count of the optic nerve is about 101-102 million, whereas in the chick it is 423,000 . In the chicken, optic nerve fiber decussation in the chiasm is

complete . There are two major visual pathways in the nervous system of reptiles, birds, and mammals, which show a high degree of anatomical similarity. These two pathways arise from retinal efferent fibers, which travel to either the optic tectum in birds (equivalent to the superior colliculus in mammals) or the optic thalamic complex in birds (equivalent to the dorsal lateral geniculate nucleus in mammals). The retino-collicular pathway of mammals is known as the tectofugal pathway or collothalamic pathway in birds. From the tectum, there are efferents to the thalamus (nucleus rotundus in birds and pulvinar in mammals). The thalamic nuclei send projections to different areas of the telencephalon: the visual wulst in birds (striate cortex in mammals), which is the primary visual pathway, or to the entopallium (previously called the ectostriatum) in birds (extrastriate in mammals), which is a secondary visual pathway. This retino-thalamo-striate pathway of primates has been called a thalamofugal or lemnothalamic pathway in birds . In the avian visual system, the temporal (posterior) retina is connected to the rostral (anterior) optic tectum, nasal (anterior) retina to the caudal (posterior) tectum, and likewise dorsal and ventral retina are connected to the ventral and dorsal tectum, respectively.

#### **1.4. The visual transduction pathway**

Photoreceptor cells are highly specialized for the capture of light and for phototransduction, the conversion of light into a biochemical signal. Phototransduction takes place in a series of membranous discs comprising a unique structure: the photoreceptor OS. Basically, phototransduction is the process by which a photon of light captured by a molecule of visual pigment generates an electrical response in a

photoreceptor cell. The stimulated photoreceptor increases its potential difference across the cell membrane (hyperpolarizes), reducing the amount of neurotransmitter released at the synaptic cleft. The photoreceptor potential produces a graded potential (not an action potential) in the bipolar cells with which it synapses. As discussed above, rods, which comprise the majority of photoreceptors in rodents and in humans, and the minority in chickens, are the most light-sensitive photoreceptor cell type. Cone photoreceptors, which comprise the majority of photoreceptors in chickens, are much less sensitive to light, but are active in the light intensities typical of daylight (natural or artificial). Many types of birds have a need for high-acuity vision during the day . Retinal rods and cones share a similar phototransduction pathway involving cyclic guanosine monophosphate (cGMP). Some differences are known, such as that cones are typically 100 times less photosensitive than rods and their response kinetics are several times faster, but the fine underlying mechanisms of cone phototransduction still remain largely unknown. It is generally accepted that the process in both cells is similar but almost all proteins involved in phototransduction have distinct rod and cone variants. Specific differences in properties between rod and cone pigments have been described, such as a 10-fold shorter lifetime of the meta-II state (active conformation) of cone pigment and its higher rate of spontaneous isomerization, but their contributions to the functional differences between rods and cones remain speculative .

Since vertebrate rod phototransduction is one of the best-studied G protein signaling pathways, it is described here in detail to serve as a model for studying the general phototransduction mechanism. In this pathway the photoreceptor-specific G protein, transducin, mediates the relation between the visual pigment, rhodopsin, and the

effector enzyme, cGMP phosphodiesterase. Rhodopsin is a visual pigment (photopigment) specifically localized in the rod OS. Visual pigments are members of the superfamily of G protein-coupled receptors (GPCRs) whose natural ligand, the small-molecular-weight chromophore 11-*cis* retinal, is already covalently attached in darkness (in its inactive conformation) . The 11-*cis* isomer acts as a powerful antagonist, and it is only when a photon of light isomerizes the chromophore to its all-*trans* form, which acts as a powerful agonist, that the visual pigment becomes active . The active form of the photopigment rhodopsin is called metarhodopsin II or Rh\* , and it is this form of the pigment that activates the G protein transducin. This triggers the transduction cascade. Transducin consists of  $\alpha$ ,  $\beta$  and  $\gamma$  subunits. Upon activation transducin releases a GDP and combines with GTP. The combined  $\alpha$  subunit of transducin and GTP split from  $\beta$  and  $\gamma$  subunits . Two  $\alpha$  transducin subunits interact with the phosphodiesterase (PDE) complex (which consists of excitatory  $\alpha$  and  $\beta$  subunits and two inhibitory  $\gamma$  subunits) to release the inhibitory  $\gamma$  subunits of the holoenzyme. Activated PDE  $\alpha$  and  $\beta$  subunits catalyzes the hydrolysis of cGMP to 5' GMP. In darkness, cGMP keeps a small proportion of the cationic channels, present in the plasma membrane of the OS, open . The decrease in intracellular cGMP concentration causes the cGMP-gated channel in the cell membrane to close and the rod cell hyperpolarizes. Intracellular  $\text{Ca}^{2+}$  levels decrease as the Na/Ca-K exchanger continues to extrude  $\text{Ca}^{2+}$  from the OS .

Rh\* is inactivated by two sequential processes: first the phosphorylation of rhodopsin by rhodopsin kinase, reducing its affinity to transducin , and then the binding of arrestin to the phosphorylated photopigment.

The inactivation of the entire visual cascade requires hydrolysis of the GTP on the  $\alpha$ -subunit of transducin to GDP, a reaction activated by a protein named regulator of G-protein signaling (RGS). PDE also returns to its inactive state as a result of this reaction. Additionally, to complete the inactivation of the visual cascade reassociation of the  $\alpha$ -subunit of transducin with its  $\beta$  and  $\gamma$  subunits is required to form the inactive transducin heterodimer. Low intracellular  $\text{Ca}^{2+}$  concentration results in 1) the activation of guanylate cyclase, a process mediated by the calcium-binding protein GCAP; and 2) an increase in the sensitivity of the cGMP-gated channel to cGMP as a result of the dissociation of calmodulin from the channel. As cGMP concentration increases, the cGMP-gated channels reopen and the cell is returned to its resting depolarized state. The increase in  $\text{Ca}^{2+}$  also converts guanylate cyclase to its inactive or basal level of activity . See Figure 1.5 for a simplified diagram of the visual transduction cascade.

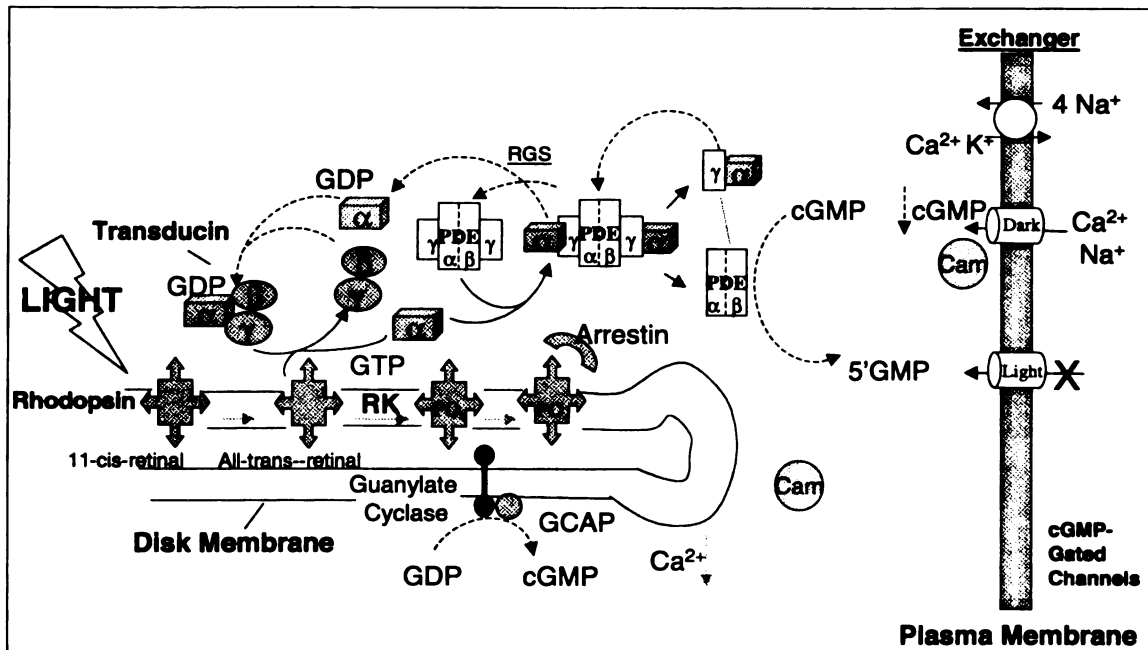


**Figure 1.5** - Diagram of rod phototransduction cascade. Key: GCAP-Guanylate Cyclase Activating Protein; PDE – cGMP Phosphodiesterase;  $\alpha$ ,  $\beta$  and  $\gamma$  - subunits of transducin; RK – Rhodopsin Kinase; RGS - Regulator of G-protein Signaling; Cam - Calmodulin

### 1.5. Electroretinogram (ERG)

Electroretinography, a technique in which light-induced trans-retinal voltage response is measured, is an extensively used and widely accepted method that is reasonably sensitive and quantitative for the assessment of retinal function. Its clinical value has been clearly established, not merely for the diagnosis of hereditary degenerative diseases, but also for evaluation of their progression and prognosis . The bioelectrical potential of the retina originates from its various cellular layers, and represents a compounded mass response . A flash ERG is a recording of the transient change in the standing potential of the eye in response to light stimulation induced by a brief illumination of the eye. A Ganzfeld sphere is often used to deliver the flash



stimulus. The term *ganzfeld*, meaning “full field” in German, implies that the stimulus reaches practically all parts of the retina and its intensity is approximately equal across that area. Full-field illumination is more advantageous for electroretinographic studies than a simple strobe-light stimulus because the former allows for an assessment of the homogeneous summation of electrical activities from the entire retina while the latter stimulus does not evenly illuminate the retina. Recording of a single flash intensity, full-field electroretinogram may not be sensitive enough to allow detection of early changes in retinal function such as those that occur in the early stages of some forms of retinal dystrophy. Therefore stimulus of different intensities, different wavelengths and under retinal dark- or light adaptation are commonly used to gather more information about retinal function.

The first widely accepted analysis of the ERG stems from the investigations of Ragnar Granit (1933). Granit studied the ERG components in a cat retina using corneal recording electrodes. He observed that as the level of ether anesthesia was deepened, different components, named P (process) components of the ERG disappeared. Granit termed the different components or processes in sequence of their disappearance: P-I, P-II and P-III. The P-I component is a slow cornea-positive wave. P-II is also a corneal-positive wave that rises relatively fast to a peak amplitude and then recovers to an intermediate potential while the light stimulus is still on. The last component, P-III, which was the most resistant to the level of ether anesthesia, is a cornea-negative wave that develops faster than the other two and remains as a negative potential for as long as the light stimulus is present. He noticed that the magnitude of P-II altered the magnitude of P-I. Additionally, another positive waveform, sometimes called the d-wave, is

generated at stimulus offset . The component analysis of Granit has been modified slightly over the years but remains the basis for our understanding of the ERG. For his work on the ERG, Ragnar Granit won the Nobel Prize for Physiology and Medicine in 1954. See Figure 1.6 A for a diagrammatic representation of the different components of the ERG.

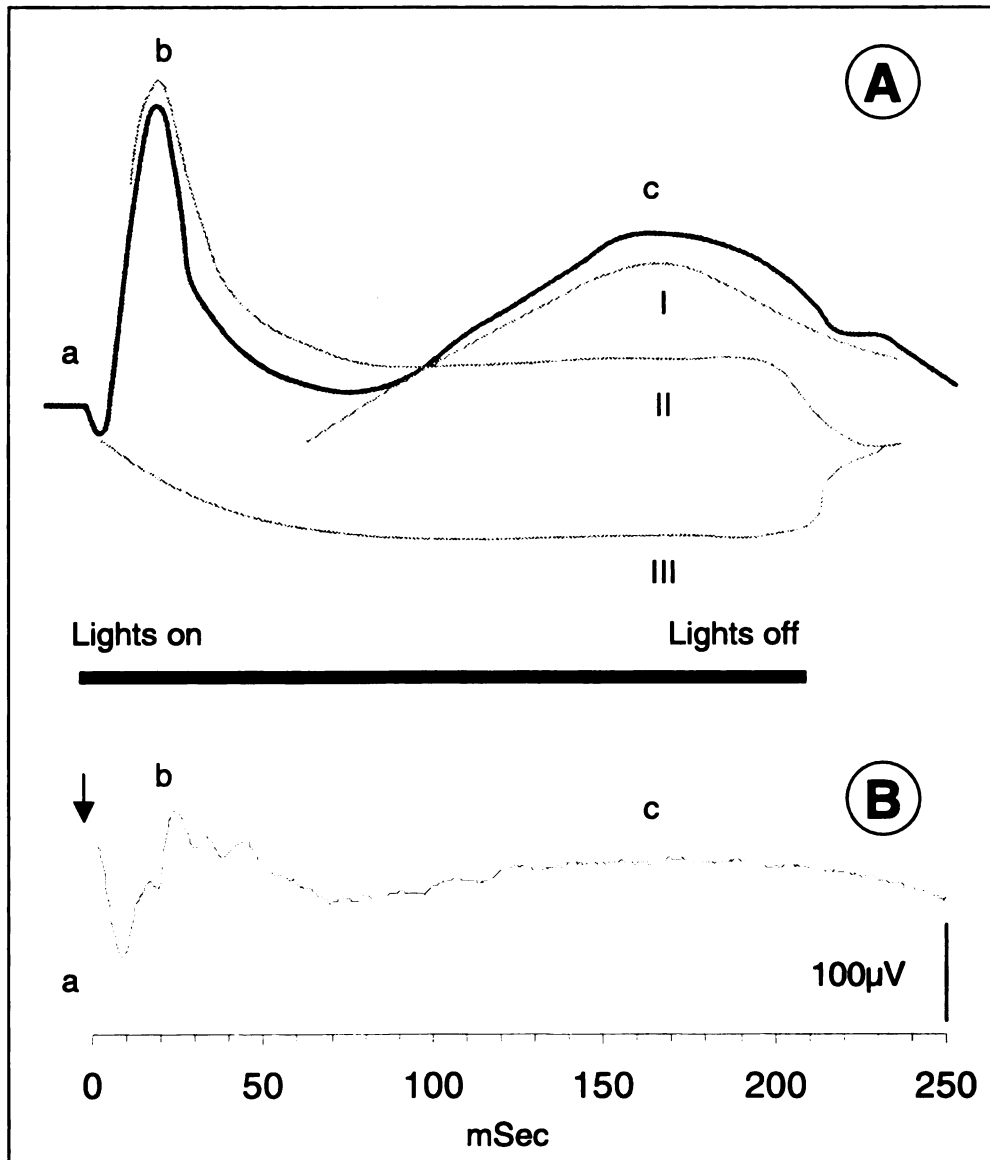


**Figure 1.6 - A)** Diagrammatic representation of the Granit waveforms (I, II and III) which make up the electroretinogram (ERG). Note the superimposed representation of a-, b- and c-waves correlating with the waveforms III, II and I, respectively. **B)** An actual ERG from a 90- day-old chicken. The arrow indicates the timepoint at which the eye was stimulated by a flash. Note the chicken ERG has the same basic components of a mammalian ERG. The a-, b- and c-waves are marked.

The use of chemicals and microelectrodes has contributed greatly to an understanding of the cellular origin of the various components of the ERG. The evidence from such studies has shown that the negative a-wave is produced by the photoreceptors (rods and cones). It is visible until overwhelmed by a larger positive response from the Müller and bipolar cells. The Müller cell component is induced by changes in extracellular potassium ion concentration as the electrical response is conveyed to the inner retina. This corneal positive response contributes the majority of the b-wave. Furthermore, drugs that block transmission from photoreceptors to bipolar cells, almost completely remove the b-wave. Noell (1953) showed that systemic injection of sodium azide elicited an electrical potential from the retina similar to the ERG c-wave. The azide-induced potential was not influenced by iodoacetic acid, which is known to destroy photoreceptors, or by cutting the optic nerve, which causes degeneration of the ganglion cells. This interpretation of the c-wave origin was proven directly when intracellular recordings were made from pigment epithelial cells in response to light stimuli (identical in shape and temporal properties to the ERG c-wave). When the retina is separated from the sclera and pigment epithelium, the ERG response consists of only the a- and b-waves. There is an additional layer of complexity in the formation of the c-wave of the ERG. The RPE basal membrane (choroidal side) is less permeable to potassium ions than the apical membrane (retinal side). This asymmetry causes a constant potential difference between the retina and the choroid. The retinal side is more positively charged relative to the choroidal side. This is also called the standing potential of the eye. A reduction in the extracellular concentration of potassium ions near the apical membrane of the pigment

epithelial occurs due to light-induced electrical activity in the photoreceptors. This is expressed as an increase in the trans-epithelial potential with the retinal side becoming even more positive relative to the choroidal side. There is a high correlation between peak amplitude of the c-wave and peak reduction in extracellular potassium concentration. This is the ERG c-wave when recorded with a corneal electrode . See Figure 1.6 A for a diagrammatic representation of an electroretinogram and a comparison with Granit waveforms (I, II and III).

As mentioned previously, a single intensity flash-ERG provides limited information about retinal function. Nevertheless, it is possible to utilize the different physiological features of rods and cones to differentially stimulate them. Methods used include varying the intensity of the light stimulus, altering stimulus wavelength with color filters, dark or light adapting the patient, or using a flickering light of differing frequencies. Additionally, carefully measured intensity-response functions combined with explicit models, such as the Naka-Rushton function for ERG analysis, can provide the possibility of identifying sites and mechanisms of disease action for specific diseases and individual patients .

In chicks, the ERG waveform is comparable to an adult one already at hatch. However, a- and b-wave amplitudes increase as the bird matures. Most of this increase in amplitude occurs during the first 14 days . See Figure 1.6 B for an example of a typical chicken electroretinogram.

## 1.6. Inherited retinal dystrophies

Retinal dystrophies are the major causes of incurable blindness in the Western world, currently affecting about 1.5 million individuals. Our insight into their etiology has improved remarkably over the past decade and a number of key genes important for retinal function have been identified . In fact, more than 80 genes associated with human photoreceptor degenerations have been identified .

Phenotypically, the inherited retinal dystrophies can be divided into different categories. For example, in some forms there is a failure in phototransduction resulting in a lack of development of normal retinal function, as assessed by ERG, followed by rapid loss of photoreceptors (e.g. *rd1* mouse, *rcd1* dog and *rcd3* dog) . Other gene mutations result in a progressive loss of photoreceptors, which up until their death, function relatively normally. Photoreceptor loss is reflected in a progressive reduction in ERG amplitudes (e.g. *prcd* dog) .

Some gene mutations result in a profound abnormality in retinal function as shown by vision testing and ERG testing and yet they cause either no obvious retinal degeneration or merely a slow retinal degeneration. Examples include the congenital stationary night blindnesses where rod function is severely affected and yet the retina does not degenerate (e.g. *nob* mouse) and mutations in RPE65 where rod and cone vision is severely affected and the ERG responses grossly abnormal and yet there is only a slow degeneration of the retina .

A unique form of inherited retinal degeneration is the enhanced S-cone syndrome (ESCS) in humans and *rd7* in mice. ESCS patients and *rd7* mice lack rod photoreceptor

function, like other inherited retinal degenerations such as retinitis pigmentosa, but are unique because their S (blue) cones, normally the least numerous cone type, are greatly increased in numbers. ESCS and *rd7* are caused by a mutation in a transcription factor named *NR2E3*, which plays an important role in differentiation of photoreceptors. Lack of *NR2E3* function leads to a reduction in the number of rod cells and a twofold increase in the total number of cone cells. It is speculated that when photoreceptor progenitor cells normally fated to become rods lack the normal signal to become rods they end up differentiating into S-cones. Besides the abnormally high number of S-cone cells, *rd7* retinas have Müller cell gliosis, and RPE migration to the inner retina. Despite evidence of slow degeneration there is a lack of cells undergoing apoptosis, which is the common pathway for photoreceptor loss in retinal dystrophies .

Growing evidence indicates that a mutation expressed in a particular retinal cell type may affect not only these cells autonomously, but also may affect retinal cells that do not express the mutated gene . A clear example of non-cell-autonomous effects is that mutations of genes expressed uniquely in rods also result in cone and RPE degeneration . The mechanisms underlying these non-cell-autonomous degenerations remain unknown. However, they may involve trophic or toxic interactions mediated either by diffusible factors or by contact-mediated cell interactions .

Several forms of retinal degenerations have been reported and characterized in the chicken (*Gallus gallus*). These include the following conditions: *retinal dysplasia and degeneration* (*rdd* strain) , *retinal degeneration* (*rd* strain) , *blindness, enlarged globe* (*beg* strain) , and finally the *delayed amelanotic* (*dam* strain) . Histological and ERG changes are reported for the *rdd* , *rd* and *dam* chicken strains . The *rdd* chicken

phenotype is sex-linked and characterized by a progressive degeneration of the retina, culminating in blindness. Morphologically, the condition is recognizable by abnormalities in both the RPE and the neural retina. Gaps in the RPE which are first detected macroscopically at nine days of incubation become larger and more numerous at the time of hatching, then disappear during the subsequent week. After hatching, the thickness of the retina decreases with age, primarily due to loss of photoreceptors and cells from the INL. Detachment of the atrophic retinas generally occurs in adults, and is followed in some adult birds by granulation and ossification of the posterior segment . At three weeks of age, homozygotes have a flat ERG indicating severe loss of visual function. Linkage analysis mapped the *rdd* locus to a small region of the chicken Z chromosome with homologies to human chromosomes 5q and 9p .

The *rd* phenotype is caused by a *null* mutation in the photoreceptor guanylate cyclase (*Gucy1\*b*) gene and is therefore a model of Leber Congenital Amaurosis type 1 in humans . The photoreceptor cells of *rd* birds undergo degenerative changes after about 7 days of age. A decrease in the number of OSs, spaces between ISs and large spaces in the ONL occur by 10 days of age. By 21 days of age, most of the ISs appeared swollen and there is a decrease in the abundance of OSs and photoreceptor nuclei. By 60 days of age, no OSs remain and the majority of identifiable ISs are from cones with many of the surviving cones being double cones. By six months of age, very few photoreceptor ISs and nuclei remain. ERGs are not recordable either under light- or dark-adapted conditions in affected chicks from the time of hatch .

The *dam* chicken is characterized by a postnatal, spontaneous cutaneous amelanosis and a high incidence of blindness. Cutaneous pigment loss is accompanied by



a destruction of the choroidal melanocytes. The presence of blindness correlates with the histopathologic finding of severe degenerative changes in the RPE and neural retina first seen near the base of the pecten and progressing radially in irregular patterns . The main ERG change observed in this phenotype is a generalized decrease in a- and b-wave amplitudes .

Only preliminary observations are available for the *beg* phenotype . The *beg* chicks are blind at hatch, have vestibular abnormalities and develop globe enlargement .

The GSN/1 chicken, recently described, also presents a hereditary form of visual impairment. Nevertheless, the histopathological findings suggest that the visual impairment observed in GSN/1 affected individuals is related to developmental defects in the visual pathways, especially in the optic tectum, which, in affected birds, show a pronounced atrophy .

#### 1.6.1. Globe enlargement in chicks with retinal disease

The eyes of chicks have been extensively used for research into ametropies since they are large, compensate for defocus rapidly, and are capable of color vision . Alterations in chick globe dimensions are readily induced by alterations in the retinal image, including vision deprivation, defocus and constant light exposure . For instance, myopia or hyperopia can be experimentally produced in chicks by defocusing the eye using goggles fitted with negative or positive diopter lenses, respectively , and both can alter the axial or radial globe length, respectively, in a matter of days . It is well established that the signaling mechanism for globe growth and, thus, the resulting changes in the refractive state of chicks are restricted to the retina itself . It has been shown that experimentally induced globe growth occurs despite optic nerve section and destruction of the Edinger-Westphal nucleus, responsible for accommodation in the central nervous system .

#### 1.7. Position of the field when the work started

A unique phenotype, caused by an autosomal recessive mutation, was identified as causing blindness and globe enlargement in some birds in flocks of commercial layer chickens in the UK. A retinal origin for the blindness was suspected on the basis of preliminary electroretinographic investigations. The name *retinopathy, globe enlargement (rge)* was selected to reflect the characteristics of the disorder. All the

available information about *rge* chicks was derived from two published papers written by a veterinary ophthalmologist named Roger Curtis from England, who first recognized the condition . In these papers he described that impaired vision was present usually by eight weeks of age and that the condition had an autosomal recessive hereditary basis. He noted that affected birds developed globe enlargement and were unable to perceive food particles on a flat surface, although apparently able to discern large objects and to respond to bright light. Curtis performed preliminary ERGs in two affected birds and observed that they were abnormally low in amplitude. In addition, he noticed that some affected birds developed linear fundus lesions that correlated with abrupt thinning of the retina histologically.

## **CHAPTER 2**

### **CLINICAL FEATURES OF THE RETINOPATHY, GLOBE ENLARGED (*rge*)**

### **PHENOTYPE**

#### **2.1. Introduction**

A flock of *rge* chickens was established at Roslin Institute (Edinburgh) by crossing a single carrier bird from Dr. Roger Curtis' original flock with a white leghorn. Subsequently a second flock was established at Michigan State University from hatching eggs imported from the Roslin Institute. This chapter reports the initial clinical characterization of the *rge* phenotype by general physical examination and necropsy. Assessment of vision and detailed eye examination, including ophthalmoscopy, tonometry, corneal pachymetry and globe dimension measurements, were performed.

#### **2.2. Material & Methods**

Breeding was performed to produce homozygous affected (*rge/rge*), heterozygous carrier (*rge/+*) and homozygous normal (*+/+*) chicks. Birds were group housed under 12 hour light/dark cycles and fed a commercial chicken diet (Home Fresh Poultry Feed, Kent Feeds, Inc.).

All procedures using chicks were conducted in accordance with the ARVO Statement for the Use of Animals in Ophthalmic and Vision Research and approved by the Institutional Animal Use Committee.

### 2.2.1. General examination, observation of behavior, ophthalmic examination and necropsy and preliminary histological examination

Twenty one birds, of which 9 (6 males and 3 females) were *rge* and 12 were carriers (4 males and 8 females), were examined at hatch, then at 7, 14, 21, 28, 42, 49, 70, 77, 84, 98, 280, 308, 336 days of age. A general physical examination was performed at the time intervals listed. The ability of the birds to locate and peck at food particles on the floor was evaluated. An ophthalmic examination was performed using a transilluminator, hand-held slit lamp (Kowa SL-14) and indirect ophthalmoscope (Heine). Comparative gross necropsies and histopathological examination were performed on *rge* and control birds at hatch, 14, 60 and 180 days of age. A minimum of 2 *rge* and 2 control birds, per age group were analyzed. Tissue samples from the central nervous system (CNS), liver, muscle and heart were collected, fixed in 10% buffered formalin, embedded in paraffin, processed routinely for histologic slide preparation, and stained with hematoxylin-eosin. Sections from the liver, heart and muscle were also stained with periodic acid-Schiff (PAS). CNS sections were stained with PAS and with Weil and luxol fast blue stains, for myelin. Eyes from 2 *rge* and 2 control birds at 13, 90 and 270 days of age were routinely processed for histology. In brief, immediately after euthanasia the globes were enucleated and injected with 10% buffered formalin, then plunged into the same fixative for 48 hours, embedded in paraffin, processed routinely and stained with hematoxylin-eosin.

### 2.2.2. Vision testing with an optokinetic device

Visual acuity was assessed by the use of an optokinetic device. This consisted of a drum with a diameter of 38 cm, which could be lined with different sets of alternating black and white vertical stripes, and could be rotated, in alternating directions around the bird at a velocity of 48 degrees/second. The widths of black and white stripes stimulus used in this study were 4.5, 7, 13 and 25 mm with a spatial frequency of 0.37, 0.23, 0.13 and 0.06 cycles per degree, respectively. The head of the test bird was approximately 19 cm from the stripes. Vision was assessed under both dim and bright light, 0.22 and 24.5 cd/m<sup>2</sup> respectively, as measured by a photometer (Research Radiometer IL 1700 with SED033 silicon light detector, International Light, Inc.). Birds were tested at 1, 14, 30, 60, 150 and 270 days of age. The response of the chick was observed and classified as positive response (head and neck turned to follow rotating stripes), partial response (head sometimes followed the rotation of the stripes but not every time) or negative response (the head never turned to follow the rotating stripes).

### 2.2.3. Tonometry, central corneal pachymetry and eye dimension measurements

Central corneal thickness (CCT), intraocular pressure, and axial globe length were measured following application of a topical anesthetic (proparacaine hydrochloride 0.5% ophthalmic solution USP – Alcon Laboratories). In each case three readings were taken and averaged for each eye of each bird. These measurements were repeated on the same

21 birds, of which 9 (6 males and 3 females) were *rge* and 12 were carriers (4 males and 8 females).

Central corneal thickness (CCT) was measured using an ultrasonic pachymeter (Pachette™, Ultrasonic Pachymeter Model DGH 500) with the speed of sound in the cornea pre-set at 1,640 m/sec. The axial globe length was measured by A-mode ultrasonography (Humphrey - A/B Scan System 835).

Intraocular pressure (IOP) was measured by applanation tonometry using a Tonopen (Mentor). Additionally, more detailed A-mode ultrasonographic measurements of the eyeball, including lens thickness, anterior and vitreous chamber depth were performed in another group of 16 *rge* and 17 carrier chicks at 13 days of age (6 *rge* and 5 carriers), 33 days of age (7 *rge* and 9 carriers) and 92 days of age (3 *rge* and 3 carriers), using an ophthalmic A-mode ultrasonic biometer (Echorule - Phakosystems Inc.). Following euthanasia of these birds the weight of the enucleated globe trimmed of extraocular tissues was recorded.

The radial globe diameter (dorsal equator to ventral equator) of both eyes was measured using Castroviejo calipers immediately following enucleation of 15 *rge* and 15 carrier birds terminally anesthetized at 13, 33, 92, 200 and 270 days of age.

#### 2.2.4. Refraction and measurement of corneal curvature

Infrared photoretinoscopy and photokeratometry were performed at 13 days of age (6 *rge* and 5 carriers), 33 days of age (7 *rge* and 9 carriers) and 92 days of age (3 *rge* and 3 carrier). The infrared photoretinoscopy technique was calibrated against

conventional retinoscopy in chickens and agrees with the results of the latter within a fraction of a diopter, the difference being due to the difference in wavelengths employed and the chromatic aberration of the chick eye (Howland, personal communication, 2003).

#### 2.2.5. Statistical Analyses

Statistical analyses of the clinical measurement results were performed by repeated measures analysis of variance (ANOVA), one-way ANOVA (radial globe diameter) and t-test (when comparing any one time-point data between two groups). Data from the vision testing using the optokinetic device was analyzed using an ordinal model for multinomial data. The tests were all run in two different statistical analysis softwares (StatView and SAS 2001 - version 8.2. SAS Institute Inc.). If any statistically significant difference was found the data were further analyzed using *post hoc* comparisons with Fisher's or Tukey-Kramer tests. Data were deemed significant when  $P < 0.05$ .

### 2.3. Results

A summary of the statistically significant differences in ocular dimensions, refraction and intraocular pressure of *rge* chicks compared to controls is shown in Table 1. There was no significant difference between carrier and normal birds for any of the morphological measurements (data not shown).



**Table 2.1 – Summary of the main clinical features observed in chicks presenting the *rge* phenotype. \*\*  $P<0.05$ ; \*\*\*  $P<0.001$ ; \*\*\*\*  $P<0.0001$ .**

| <i>rge</i> Phenotype             |   | Mean<br>Result and SD for <i>rge/rge</i> | Mean<br>Result and SD for <i>rge/+</i> |
|----------------------------------|---|--|--|
| <b>Corneal Radius</b>            | Increased at 33 days of age****         | 4.68 ± 0.17 mm                           | 3.90 ± 0.19 mm                         |
| <b>Central Corneal Thickness</b> | Increased at 42 days of age**           | 258.75 ± 10.50 µm                        | 243.83 ± 3.55 µm                       |
| <b>Axial Globe Length</b>        | Increased at 92 days of age****         | 14.41 ± 0.16 mm                          | 12.55 ± 0.97 mm                        |
| <b>Radial Globe Diameter</b>     | Increased at 33 days of age**           | 1.62 ± 0.96 cm                           | 1.38 ± 0.12 cm                         |
| <b>Anterior Chamber Depth</b>    | Decreased at 13 days of age***          | 0.858 ± 0.68 mm                          | 0.980 ± 0.42 mm                        |
| <b>Vitreous Chamber Depth</b>    | Increased at 33 days of age***          | 7.56 ± 0.32 mm                           | 6.58 ± 0.34 mm                         |
| <b>Eyeball Weight</b>            | Increased at 33 days of age***          | 1.42 ± 0.10 g                            | 1.14 ± 0.90 g                          |
| <b>Refraction</b>                | Hyperopia (higher at 33 days of age)*** | 12.00 ± 2.30 D                           | 4.44 ± 1.60 D                          |
| <b>Intraocular Pressure</b>      | Decreased at 49 days of age**           | 17.60 ± 1.26 mmHg                        | 20.25 ± 1.57 mmHg                      |

### 2.3.1. Physical examination, post mortem and preliminary histopathologic examinations

*Rge* chicks appeared less active than carrier and normal chicks immediately after hatch, although this was not quantified. The *rge* birds sporadically exhibited a characteristic slight lateral nodding movement of the head and some “pecking at the air” behavior starting at 2 weeks of age. This characteristic behavior continued for the duration of the study. Affected and control birds responded similarly to sound stimuli produced by hand clapping.

It was noticed from the histological examination of eye globes that the anterior chamber appeared progressively shallower in *rge* globes than in controls (Figure 2.3). Cataracts were a common finding in *rge* birds by 270 days of age. Thinning of retinal layers was evident in the sections from the 90 and 270 day-old birds. Additionally, ossification of the posterior segment was noticed in one bird at the same age. A detailed characterization of the retinal histopathological changes is described in Chapter 5. Neither gross lesions nor any non-ocular abnormalities were observed in *rge* birds on necropsy or light microscopy histopathologic examination of liver, muscle and heart. No specific differences could be detected among the six brains that were processed regarding the structure or myelination of the components of the visual system.

### 2.3.2. Vision testing

From hatch *rge* chicks were less efficient than carrier and normal chicks at pecking food particles placed on the floor, spending an average of 3 attempts before actually picking up the particle. By 30 days of age the *rge* chicks did not attempt to peck at food particles placed on the floor. Once the *rge* chicks were familiar with their environment they were able to consistently locate feed and water containers. From approximately 30 days of age *rge* chicks failed to show an “escape response” to the visual stimulus produced by the approach of a person, making the *rge* chicks easier to catch than the carrier and normal chicks. Visual menace response was absent in the *rge* chicks by about 30 days of age but present in all the age-matched carrier and normal chicks.

An assessment of visual acuity using the optokinetic device showed that the percentage of *rge* chicks showing a response (partial or complete) to the rotating stripes decreased with age (Figure 2.1). At each time-point, and for each width of stripe, the percentage of chicks showing any response was lower under the dimmer room lighting. Although at 150 days of age 60% of *rge* chicks showed some response to the widest stripe under bright lighting conditions (Figure 2.1) they were not able to peck at food particles, and lacked the menace and “escape” responses.

The reduction in response to stripes of smaller widths, with increasing age and with lower light levels in comparison to carrier or normal chicks was statistically significant ( $P<0.001$ ).

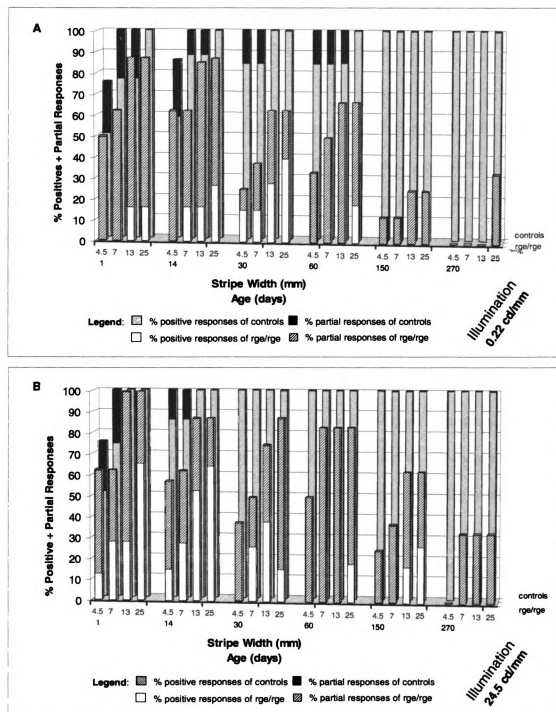


**Figure 2.1** – Results from vision testing with an optokinetic device. Comparison of the percentages of control and *rge* birds that responded positively or partially to the optokinetic device, under two different light intensities, (A) 0.22 cd/m<sup>2</sup> and (B) 24.5 cd/m<sup>2</sup>. 1 day of age n= 4 controls and 8 *rge*; 14 days of age n= 7 controls and 8 *rge*; 30 days of age n= 6 controls and 8 *rge*; 60 days of age n= 6 controls and 6 *rge*; 150 days of age n= 6 controls and 8 *rge*; 270 days of age n= 2 controls and 3 *rge*.

### 2.3.3. Ophthalmic examination and globe biometry findings

Globe enlargement developed in the *rge* chicks (Figure 2.2 A & B) resulted in a mild lateral strabismus causing a characteristic exposure of the sclera at the medial canthus region, bilaterally. The area exposed increased with age to some extent. Clinical examination showed that the cornea was flatter and the anterior chamber shallower in the older *rge* chicks compared to carrier and normal chicks (compare Figure 2.2 C with D and see Figure 2.3). In the older *rge* birds the anterior surface of the lens was almost in contact with the posterior corneal surface (Figure 2.2 D and 2.3 D). The pupillary light reflex became increasingly sluggish in the *rge* chicks, although it did not disappear completely during the time of the study. Fundoscopy revealed that about half the *rge* chicks, at approximately 45 to 49 days of age, had a number of white to gray linear fundus lesions, typically extending from the pecten to the periphery. By approximately 70 days of age, most of the fundi of the *rge* chicks that were originally pigmented had some reduction in pigmentation. In all fundi the pecten appeared to atrophy to a certain extent as the disease progressed. *Rge* birds commonly developed anterior subcapsular and cortical cataracts by 4 to 6 months of age (Figure 2.4). The development of cataracts in some birds interfered with visualization of the fundus.

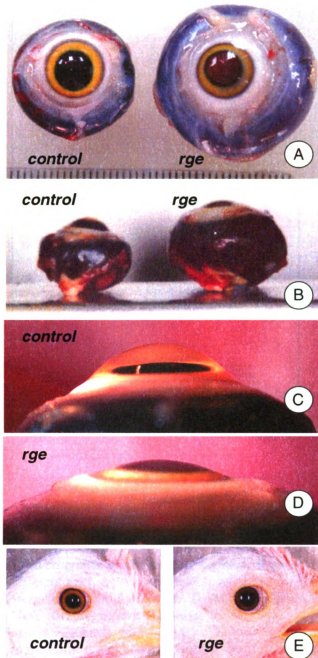


**Figure 2.2** - Series of age-matched gross ophthalmic photographs from representative *rge* and control birds. **A)** Appearance of freshly enucleated eye globes of a control and an affected (*rge*) chick, at 180 days of age. Note the difference in radial diameter of the globes. **B)** Freshly enucleated eye globes of a control and an *rge* chick, at 270 days of age. Note the difference in axial length of the globes. **C)** Profile view of the cornea and anterior chamber of a control (**C**) and an *rge* chick (**D**), at 180 days of age. Note the flatter cornea and very shallow anterior chamber of the *rge* eye. **E)** Detail of the eye position inside the orbit of a control and an *rge* bird at 45 days of age. Note the mild lateral strabismus causing greater exposure of the sclera at the medial canthus in the *rge* chick.

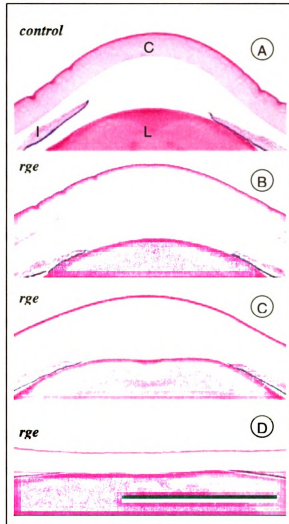


**Figure 2.3** - Series of micrographs of the anterior segment of the eye of representative *rge* and control birds at different ages. **A)** A control chick, at 13 days of age. **B)** An *rge* chick, at 13 days of age. **C)** An *rge* bird, at 90 days of age. **D)** An *rge* bird at 270 days of age. Stain – hematoxylin/eosin. Note the progressive flattening of the cornea, and shallower anterior chamber that develops in *rge* birds with age. By 270 days of age (D) the anterior lens capsule is adjacent to the corneal endothelium surface. Key: C = cornea; I = iris; L = lens. Bar – 2 mm.

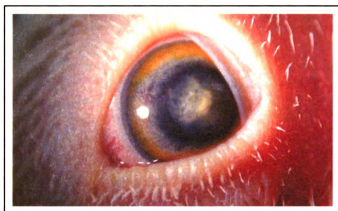


**Figure 2.4** - Gross photograph showing the detail of a hypermature cataract in an *rge* chick, at 270 days of age. Note the presence *rubeosis iridis*, which is most likely indicative of a lens-induced uveitis.

Morphometric measurements of the globe confirmed the clinical impression of a progressive globe enlargement both in the radial globe diameter (Figure 2.5 - as measured on enucleated globes) and in the axial direction (Figure 2.6 – measured by A-mode ultrasound in the living bird). The mean radial diameter of the globe of *rge* chicks was significantly greater than carrier and normal chicks by 33 days of age ( $P<0.05$ ) (Figure 2.5) and the axial globe length by 92 days of age ( $P<0.0001$ ) (Figure 2.6). Globe mass increased in parallel with globe enlargement and by 33 days of age *rge* globes were significantly heavier than the carriers ( $P<0.001$ ).



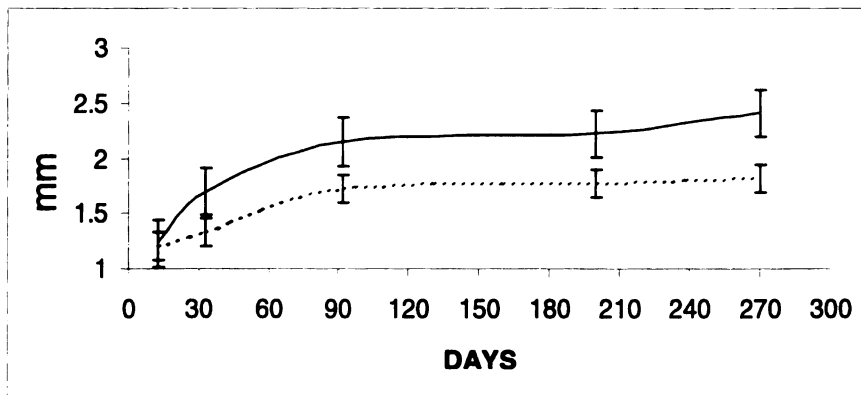


**Figure 2.5** - Radial globe diameter of *rge* (solid line) and control (dashed line) eyes, with respective standard error bars on each time-point evaluated. Note that the mean radial globe diameter of the *rge* eyes became significantly different (greater) than the controls at 33 days of age (this is before the axial length was significantly greater). 13 days of age (n= 3 *rge* and 4 control), 33 days of age (n= 4 *rge* and 4 control), 92 days of age (n= 3 *rge* and 2 control), 200 (n= 3 *rge* and 2 control) and 270 days of age (n= 2 *rge* and 3 control).

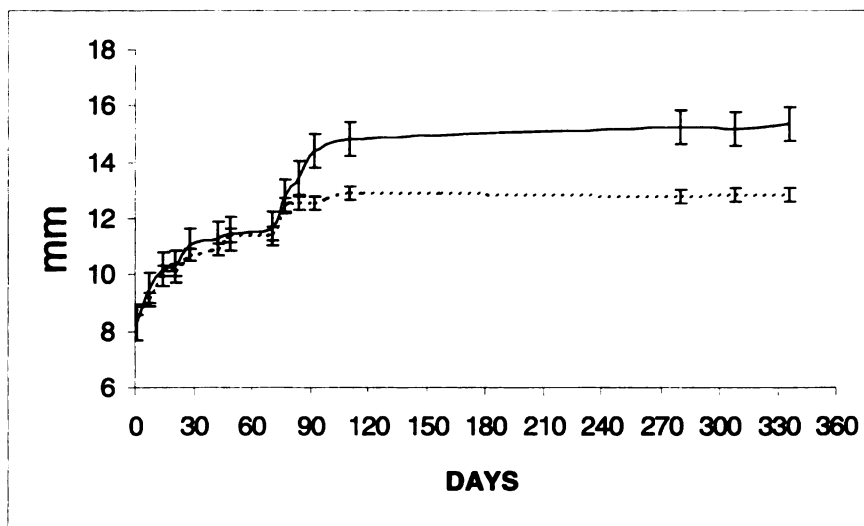


**Figure 2.6** - Mean axial globe length of *rge* (solid line) and control (dashed line) eyes with respective standard error bars on each time-point evaluated. Note that the mean axial globe length of the *rge* eyes became significantly greater than the controls at 92 days of age. n= 21 birds, 9 were *rge* and 12 were controls. Examined at 1, 7, 14, 21, 28, 42, 49, 70, 77, 84, 92, 98, 280, 308, 336 days of age.

To investigate the possibility that globe enlargement was secondary to an increase in intraocular pressure (IOP) tonometry was performed. There was no significant difference in IOP between *rge*, carrier and normal chicks until 49 days of age, at which time the IOP of *rge* chicks was lower than carrier and normal chicks ( $P<0.05$ ) (Table 2.1) and remained lower for the duration of the study (data not shown). Furthermore, no morphological abnormalities of the iridocorneal drainage angles were detected histologically in the *rge* birds at any age.

A detailed ultrasound study of axial globe measurements showed that the anterior chamber of *rge* chicks was significantly shallower than that of carriers from the first time point measured (13 days of age,  $P<0.05$ ) and continued to become shallower with age ( $P<0.001$ ), confirming the slit-lamp observations. This feature is also shown in the histological sections (Figure 2.3). The increase in axial globe length in *rge* chicks was due primarily to an increase in the vitreous chamber depth, which was significantly different from the carriers by 33 days of age ( $P<0.001$ ). The axial thickness of the lens was not significantly different from carrier and normal chicks at any time-point measured ( $P = 0.34$ ).

Pachymetry revealed that CCT development occurs in two phases. The first phase corresponds to an initial decrease in CCT with the lowest point being reached at around 12.5 days of age. The second phase of corneal maturation is characterized by a gradual increase in thickness. CCT in control chicks reaches a plateau at 70 days of age and does not continue to increase. Conversely, CCT in *rge* chicks was significantly thicker than controls by 42 days of age ( $P<0.05$ ) (Figure 2.7), this statistical difference between the 2 groups was maintained for the duration of the study.

Corneal curvature (radius) was measured by infrared photokeratometry to investigate the change in radius detected by ophthalmoscopic and biomicroscopic examination. The mean corneal curvature (corneal radius) of *rge* and carrier chicks was not significantly different at 13 days of age ( $3.4 \pm 0.1$  and  $3.4 \pm 0.08$  mm, respectively,  $P=0.79$ ), but by 33 days of age the cornea of *rge* chicks had flattened resulting in a significantly greater corneal radius than that of the carrier chicks ( $4.68 \pm 0.17$  and  $3.9 \pm 0.19$  mm, respectively,  $P<0.0001$ ). By 92 days of age there was further flattening of the cornea in the *rge* chicks (corneal radius in *rge*  $6.8 \pm 0.4$ , and in carrier chicks  $4.8 \pm 0.2$  mm,  $P=0.0015$ ).

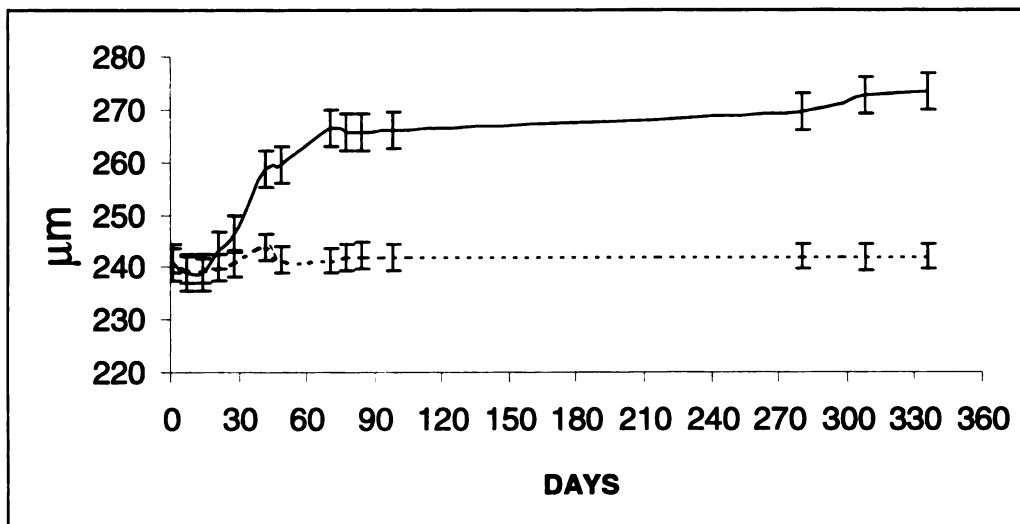


**Figure 2.7** - Mean central corneal thicknesses (CCT) of *rge* (solid line) and control (dashed line) eyes with respective standard error bars on each time-point evaluated. Note that the mean CCT of the *rge* eyes became significantly different (thicker) than the controls at 42 days of age.  $n=21$  birds, 9 were *rge* and 12 were controls. Examined at 1, 7, 14, 21, 28, 42, 49, 70, 77, 84, 98, 280, 308, 336 days of age.

Infrared photoretinoscopy was performed to investigate the effects of the abnormal globe morphology of *rge* chicks on refraction. The *rge* and control chicks had

a similar degree of hyperopia at 13 days of age ( $10.8 \pm 2.5$  and  $10.4 \pm 1.7$  diopters, respectively), by 33 days of age the degree of hyperopia of carrier chicks had decreased to  $4.4 \pm 1.6$  diopters ( $P < 0.001$ ) while that of *rge* chicks remained significantly greater at  $12.0 \pm 2.3$  diopters ( $P < 0.001$ ). Measurements taken at 92 days of age showed that the degree of hyperopia of control chicks was  $4.3 \pm 0.57$ , while that of *rge* chicks was  $9.8 \pm 7.4$  diopters.

## **2.4. Discussion**

The results obtained in this clinical study confirm that the *rge* phenotype differs from those of previously described chick retinal dystrophies such as *rd*, *rd**d* and *beg*. The vision of *rge* chicks deteriorates over the first few weeks after hatch and is worse under lower lighting conditions. They become unable to peck at small crumbs of food and lose vision related responses such as menace and escape responses progressively during the first month of life. Some *rge* birds have no visual responses as assessed by the optokinetic device at one day after hatch, whereas others retain some optokinetic responses for several weeks. However, even those that retain some optokinetic responses did not have sufficient vision to allow them to peck at food particles beyond about 30 days of age. The use of the optokinetic device for vision testing has shown to be a valuable method for vision testing and was used to assess the progressive loss of vision in the *dam* chicken

The *rge* chicks, in addition to vision loss, develop marked changes in globe morphology. The dimensions of the globe of *rge* chicks are not different from control or normal chicks at 1 day of age but they subsequently develop a marked increase in globe

size not associated with a change in IOP. A decrease in anterior chamber depth was the earliest morphological change detected. The increased globe size is primarily due to an increase in the vitreous cavity volume, initially, causing an increase in radial globe diameter and then in axial globe length. A flattening of the cornea (increased corneal radius), and an increase in corneal thickness also developed in the *rge* chicks. The same biochemical mediators that are responsible for the globe enlargement may induce the abnormal pattern of development of CCT observed in *rge* chicks.

It was possible to document the CCT development in control chicks over the first year of life. The first phase of CCT development corresponds to an initial decrease with the lowest point being reached at around 12.5 days of age in both groups of birds. Maturation of corneal endothelial function may account for the initial decrease in corneal thickness seen in newly hatched chicks. A similar initial pattern of corneal thickness development is observed in humans and dogs. The second phase of corneal maturation was characterized by a gradual increase in thickness. This increase in CCT is probably due to general growth of the eye as the chick matures. However, unlike in dogs whose corneal thickness continues to increase into adulthood, CCT in the control group of chicks reaches a plateau at 70 days of age and does not continue to increase significantly.

The *rge* chicks had a significantly greater degree of hyperopia than controls by 33 days of age. The refractive errors of *rge* and control chicks were similar at 13 days of age (the first time point at which they were refracted), with both groups exhibiting hyperopia.

Normal chicks have previously been shown to be hyperopic at hatch and with differential ocular growth they then tend towards emmetropia. In this study the refraction of control chicks examined changed towards emmetropia as expected while the

globe of *rge* chicks failed to undergo normal emmetropization. Although the mean degree of hyperopia of *rge* chicks decreases with age, the range of refractive errors within the *rge* group appears to increase. The increase in vitreous chamber size and decrease in anterior chamber depth tend to reduce the degree of hyperopia. It is conceivable that these latter changes develop as a compensatory mechanism for the hyperopia. The early increase in the radial diameter of the globe may be responsible for the flattening of the cornea. The resulting defocus (hyperopia) would be expected to induce a compensatory increase in axial length.

In experimental ametropies the following biochemical changes take place in the retina: fall of the level of 3,4-dihydroxyphenylalanine, dopamine and 3,4-dihydroxyphenylacetic acid; rise of the level of vasoactive intestinal polypeptide (VIP); rise of the amount of VIP-specific mRNA in amacrine cells within the inner retina and, lastly, rise of the amount of transforming growth factor  $\beta 2$ . An imbalance of one or some of these mediators, secondary to the initial retinal dysfunction, might be responsible for the abnormal eye growth in the *rge* chick.

In both, mammals and birds, dopamine and melatonin play an important role in regulating eye growth. Retinal melatonin levels are higher at night in chicks and other vertebrates and are decreased following light adaptation. Melatonin levels were also shown to be decreased in the constant light exposure chick. A reduced antagonistic effect of melatonin on dopamine-induced scleral growth is believed to account for the increase in globe size in the constant light exposure chick. Further evidence to support this theory was provided by the finding that intramuscular injections of melatonin partially prevented changes in globe size in chicks exposed to constant light. The morphological globe

abnormalities that develop in *rge* chicks are similar to those seen in constant light exposure chicks (e.g. increased corneal thickness, hyperopia, radial globe enlargement and linear fundus lesions) . It is therefore conceivable that melatonin might also play a role in the morphological globe changes in the *rge* chick.

## CHAPTER 3

### ELECTRORETINOGRAPHIC FEATURES OF THE *rge* CHICK PHENOTYPE

#### 3.1. Introduction

The electroretinographic abnormalities of some of the chicken models of retinal dystrophy have been characterized. The *rd* chicken phenotype is of a congenital blindness reflected by a lack of ERG tracings at hatch . The *rdd* affected birds have an extinguished (“flat”) ERG by three weeks of age indicating severe vision loss . The main ERG changes observed in *dam* chickens are a generalized decrease in waveform amplitudes. It affects c-waves more than a-waves, and a-waves more than b-waves. Dark-adapted responses are affected more than light-adapted responses. Data from the intensity response series of several *dam* chickens were fitted using the Naka-Rushton equation, as a result decreased retinal sensitivity and decreased  $V_{\max}$  could be observed for a- and b-waves .

As previously described in Chapter 2, the *rge* mutation is a naturally occurring autosomal recessive form of blindness. The affected birds lose functional vision over the first few weeks of life and then develop secondary morphological eye globe changes.

The present work characterizes the ERG abnormalities of the *rge* chicken in more detail and shows that the *rge* ERG waveforms are abnormal from hatch, showing initial supernormal b-wave responses and then a gradual loss of amplitudes with age.



## **3.2. Material & Methods**

### **3.2.1. Animals**

A breeding flock of *rge* chicks were maintained at the vivarium of the College of Veterinary Medicine, Michigan State University under 12 hour light-dark cycles. Breedings were arranged to produce homozygous affected (*rge*), heterozygous carriers and homozygous normal birds. All procedures were conducted in accordance with the ARVO Statement for the Use of Animals in Ophthalmic and Vision Research and approved by the Michigan State University All-University Committee on Animal Use and Care.

### **3.2.2. ERG recording**

To avoid circadian rhythm-induced differences all ERGs were recorded between 9:30 AM and 5:30 PM. Scotopic and photopic white light intensity series ERGs were recorded from 36 *rge*, 44 *rge*-carriers and 6 wild type birds. Different numbers of birds (minimum of 3 and maximum of 10 birds per group) were studied at different age groups, ranging from 1 to 500 days of age. The left eye was used for ERG recording. One drop of 1% vecuronium bromide (ESI Lederle, Philadelphia, PA) was administered topically 20 minutes before the experiment to fully dilate the pupil. General anesthesia was induced and maintained with isoflurane delivered in 1 ml of oxygen per gram of body weight. A

pulse-oximeter (Vet/Ox 4400, Heska Inc) was used to record pulse rate and the oxygen saturation for the duration of the recording. Body temperature was maintained using a heated pad.

Conjunctival stay sutures of 4-0 silk (Ethicon, Inc) were used to stably position the eye in primary gaze. A Burian-Allen bipolar corneal contact lens electrode (Hansen Labs) was lubricated with 2.5% hydroxypropyl methylcellulose (Goniosol, Alcon Inc.) and placed on the cornea. A ground electrode was placed subcutaneously in the hind limb.

Full-field (Ganzfeld) flash intensity-series ERGs were recorded with a UTAS-E 3000 Electrophysiology unit (LKC Technologies Inc, Gaithersburg, MD), with the bandpass set between 1 and 500 Hz and to isolate oscillatory potentials between 100 and 300 Hz.

### 3.2.3. Electrophysiological test protocols

Scotopic intensity series ERG: Birds were dark-adapted for 20 minutes. Responses from a series of 12 white flash stimuli (-2.4, -2, -1.42, -1.194, -0.79, -0.39, -0.002, 0.394, 0.85, 1.4, 2.3, 2.8 log cdS/m<sup>2</sup>) were recorded. For intensities between -2.4 to -0.79 log cdS/m<sup>2</sup> 10 flashes were averaged and from -0.39 to 2.8 log cdS/m<sup>2</sup> 3 flashes were averaged. Inter-stimulus intervals were increased from 1 second at low intensities to 3 minutes at higher intensities to avoid light adapting the rods.

Photopic intensity series ERG: Following the scotopic intensity series the birds were light adapted to a background light of  $30 \text{ cd/m}^2$ , for 10 minutes. The same intensities used for the scotopic ERG were repeated to record the photopic responses.

30Hz flicker ERG: 30Hz flicker ERGs were recorded using white flash stimuli of  $0.4 \text{ cdS/m}^2$  superimposed on a background light of  $30 \text{ cd/m}^2$ . The flicker response was evaluated at 1, 7, 14, 28, 80, 130, 160 and 500 days of age in *rge* and control birds. The number of *rge* birds used on each time-point was 5, 8, 4, 4, 2, 2, 2, 2 and 4, respectively. The number of *rge*-carrier birds used on each time-point was 4, 9, 4, 5, 2, 3, 2, 2 and 3, respectively. Additionally, wild type birds were evaluated at 14, 28, 160 and 210 days of age. The number of wild type birds for each time-point evaluated was: 7, 2, 4 and 5, respectively.

Evaluation of response to photopically matched colored flashes: In view of the supernormal responses observed in a preliminary ERG study on the *rge* chicks, a finding shared with enhanced S-cone syndrome, we wanted to evaluate whether or not there were differential responses to different wavelengths of light. Three different gelatin color filters (Eastman Kodak Company, Rochester, NY) were used with the following peak spectral transmittances: 400-500 (blue), 540 – 560 nm (green) and 600 - 1100 nm (red) (Kodak Wratten Filter numbers 58, 29 and 47A, respectively). In order to photopically match the stimuli in control chicks, intensities of  $2.4 \log \text{ cdS/m}^2$  for the blue filter,  $2.6 \log \text{ cdS/m}^2$  for the green and  $2.8 \log \text{ cdS/m}^2$  for the red filter were used to record ERGs with

a background white light of 30 cd/m<sup>2</sup>. Control and *rge* chicks were studied at 2, 14, 30 and 150 days of age.

Visually evoked potentials (VEPs): VEPs were recorded using an exploring needle electrode inserted into the skin and anchored in the skull above the region of the right optic lobe. A piece of black tape covered the right eye and the left eyelids were sutured opened using stay sutures of 4-0 silk (Ethicon, Inc). The reference electrode was inserted in the chick's crown and the common ground electrode was placed on the same position as for the ERG recordings. 20 flashes at 0.4 log cdS/m<sup>2</sup> with a frequency of 2 Hz was used as the light stimulus. The test was performed in 4 *rge* and 5 control chicks at 1 and 45 days of age.

#### 3.2.4. Data analysis

The a- and b-wave amplitude and implicit time were measured for each averaged response. The a-wave amplitude was measured from the onset of stimulus to the trough of the a-wave; b-wave amplitude from the trough of the a-wave to the peak of the b-wave. A-wave implicit time was the time measured from the onset of the stimulus to the time when the maximal a-wave trough occurred and b-wave implicit time from the onset of the stimulus to the time when the peak b-wave was present. B-wave amplitude as a function of log stimulus luminance of each individual within a genotype and at each age was fit by non-linear regression with the 3-parameter Hill equation (Naka-Rushton

function). The 3 independent parameters are: the maximum response ( $V_{\max}$ ), slope ( $n$ ) and half-saturation constant ( $K$ ). This function is as follows:

$$V = (V_{\max} \times I^n) / (I^n + K^n),$$

where  $V$  denotes the b-wave amplitude for a given flash intensity  $I$ ,  $V_{\max}$  is the upper asymptote of the amplitude *versus* intensity function,  $K$ , the flash intensity yielding a response amplitude of  $1/2 V_{\max}$ , and  $n$ , an exponent affecting slope. In some cases,  $n$  is restricted to 1;  $n$  was allowed to vary freely in these curve-fits.  $K$  is often considered to reflect retinal sensitivity since it represents a constant criterion ( $1/2 V_{\max}$ ) that determines where the amplitude *versus* intensity function is located along the flash intensity axis. The curves were fit using SigmaPlot 2001, version 7.101 (SPSS, Inc), which employs a Marquardt-Levenberg algorithm to perform least-squares fits.

An inverse prediction technique was used to obtain the mean b-wave threshold (defined as the log retinal illuminance necessary to elicit a 5  $\mu V$  response), i.e. a value of  $I$  that is required to attain a correspondent fixed value of  $V$ . Let  $I(x)$  be a value such that  $V = x$ . From the 3-parameter Hill equation above this value can be obtained by back-solving the equation for  $I$  as follows:

$$I(x) = K (x / (V_{\max} - x))^{1/n}$$

Similarly, a 95% confidence interval (CI) on  $I(x)$  was obtained from the limits of the 95% CI on  $V$ . Let  $x_{l95}$  and  $x_{u95}$  be, respectively, the lower and upper limits of 95% CI on  $V$ , then lower limit of 95% CI on  $I(x)$ , say  $I(x, l95)$  is given by:

$$I(x, l95) = K (x_{l95} / (V_{\max} - x_{l95}))^{1/n}$$

The upper limit  $I(x, u95)$  was calculated by replacing  $x_{l95}$  by  $x_{u95}$  in the equation above. Finally an approximate standard error on  $I(x)$  was obtained by:

$$SE(I(x)) = (I(x, u95) - I(x, l95))/4$$

To compare the maximum response obtained for a- and b-wave amplitude in the *rge* group of birds and compare to controls, scotopic maximum a-wave ( $A_{\max}$ ) and b-wave ( $B_{\max}$ ) response were obtained using the MAX function of numeric entries (Microsoft Excel version 2000).

These parameters, together with a- and b-wave amplitudes and implicit times for all flash intensities used, were compared between control and *rge* birds. Repeated measures ANOVA was performed to determine statistical significance of the difference of mean amplitude and latency between genotypes at a given fixed age and intensity, and between ages for the same genotype at a fixed intensity. If any statistically significant difference was found the data were further analyzed ( $P$  values adjusted) using *post hoc* comparisons with Fisher's or Tukey-Kramer tests. Data were deemed significant when

$P < 0.05$ . This analysis was performed using statistics computer software (SAS 2001 - version 8.2, SAS Institute Inc., Cary, NC, USA).

The relationship between the amplitudes of the b- and a-wave was used as an index for evaluating the electroretinogram according to the technique suggested by Perlman (1983).

Additionally, in an attempt to investigate whether the *rge* chicks had any rod-mediated activity, subtractions of intensity-matched photopic from scotopic a-wave responses were performed at 1, 7 and 160 days of age and compared between *rge* and control chicks using Hood and Birch's isolated rod a-wave response technique (Hood & Birch, 1997).

### **3.3. Results**

There were no significant differences between the ERGs recorded from *rge*-carriers and wild type birds for any of the parameters examined. Therefore the results from both *rge*-carriers and wild type birds were combined and considered as controls.

A comparison of the raw scotopic and photopic intensity series waveforms (Figures 3.1 and 3.2) shows that the *rge* birds have an elevated response threshold, increased a- and b-wave implicit times and a grossly abnormal waveform compared to the control birds. In particular the *rge* birds have an apparent absence of oscillatory potentials (OPs) and c-waves (Figures 3.1 and 3.2). Although OPs were not apparent on the raw waveforms narrowing the bandpass revealed the presence of markedly reduced OPs in the younger chicks (Figure 3.3). These changes are maintained at all ages tested, with a gradual deterioration in amplitudes with age (compare Figures 3.1 and 3.2). In

addition to having an abnormal waveform both the scotopic and photopic b-waves of the younger *rge* chicks have greater amplitudes than those of age-matched control birds in response to flashes of light brighter than  $0.9 \log \text{ cds/m}^2$  (Figure 3.1).

These differences are further analyzed, quantified, averaged and statistically compared below.



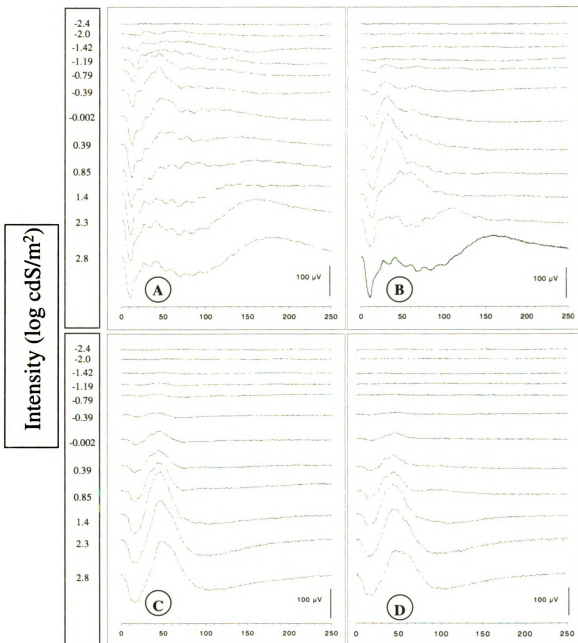


**Figure 3.1** - Representative scotopic (A) and photopic (B) ERG recordings from a control bird at 7 days of age. Light intensities (log cdS/m<sup>2</sup>) are indicated in the figure. Note the high a-wave amplitude, reduced latencies of a-wave and b-wave, high OPs and the presence of the c-wave with stronger flashes. The c-wave becomes faster with light adaptation. In the control bird there is an increase in threshold between scotopic (A) and photopic (B), which is normally observed in other species as well. C) Representative scotopic ERG recordings from an *rge* bird at 7 days of age. Light intensities as for 3.1 A & B. Note the low a-wave amplitude, increased latencies of a-wave and b-wave, low OPs and absence of a c-wave with any flash intensity. Also note the high threshold for eliciting an ERG response. D) On the photopic ERG recordings from the same *rge* bird it is possible to observe similar wave amplitudes and that apparently the ERG threshold does not change from the scotopic series. Also note the high overall threshold for eliciting an ERG response on C and D compared to the *rge* bird on A and B.

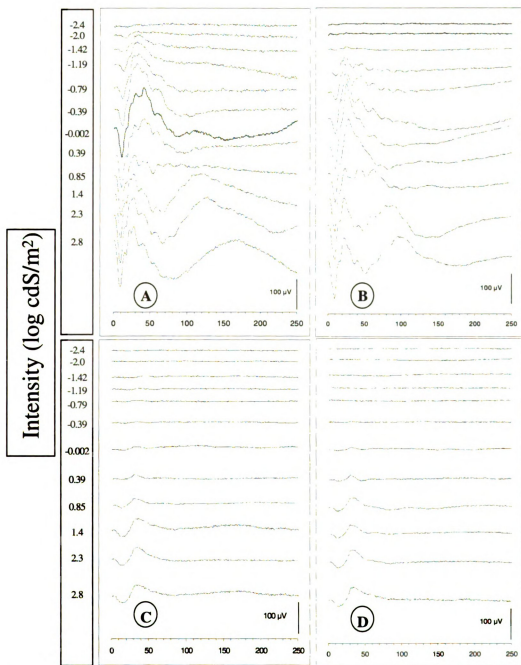


**Figure 3.2** - Representative scotopic (A) and photopic (B) ERG recordings from a control bird at 270 days of age. Light intensities ( $\log \text{cdS/m}^2$ ) are indicated in the figure. The same features observed in the control bird on Figure 3.1 are observed here. Comparing Figure 3.1 A and B with Figure 3.2 A and B it is possible to note that even higher a-wave amplitudes are observed as the birds get older. Also even more reduced latencies of a-wave and b-wave with higher OPs are noted at this age. C) Representative ERG recordings from an *rge* bird at 270 days of age. Comparing Figure 3.2 C and D with Figure 3.1 C and D, it is possible to observe the deterioration of the ERG response with even lower a-wave amplitudes, even more increased latencies of a-wave and b-wave, very low OPs and absence of a c-wave with any flash intensity. The b-wave amplitude is no longer supernormal but actually lower than the controls at this age. Note the higher threshold for eliciting an ERG response.

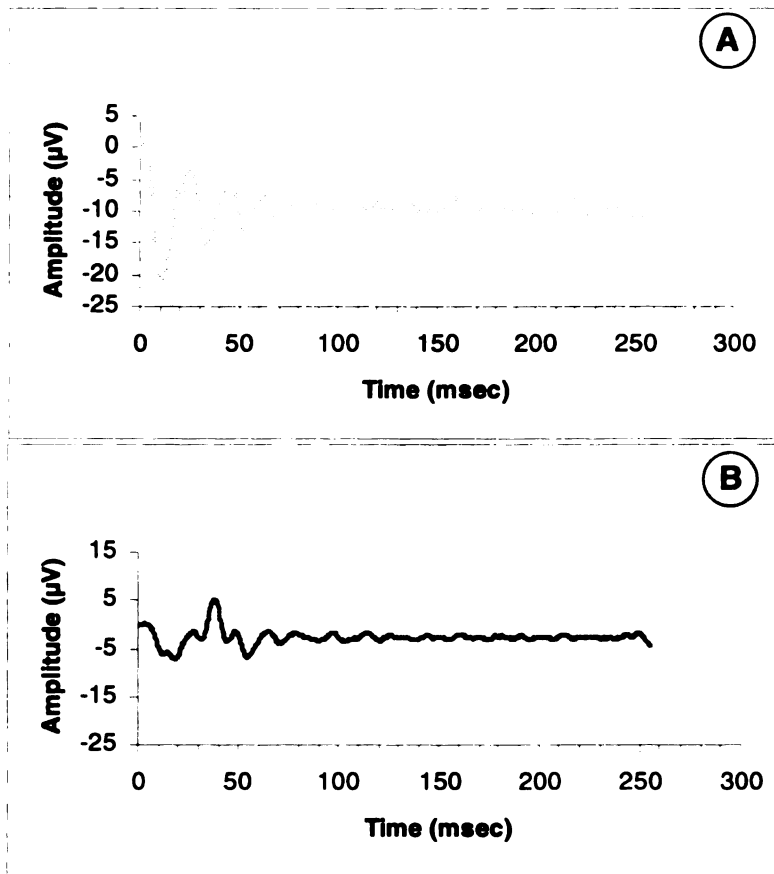


**Figure 3.3** - A) Representative scotopic isolated oscillatory potentials (OPs) of an ERG recording from a control bird at 1 day of age, using the light intensity of  $2.8 \log \text{cdS/m}^2$ . B) Representative scotopic isolated OPs of an ERG recording from an *rge* bird at 1 day of age, using the light intensity of  $2.8 \log \text{cdS/m}^2$ . Bandpass 100 and 300 Hz. Note the obvious difference in the amplitude of the OPs. This difference was observed in all the ages studied in all light intensities. On Figures 3.1 and 3.2 it is possible to observe the same difference using different light intensities.

### 3.3.1. A-wave responses

The a-wave responses were analyzed in a number of different ways: the a-wave threshold was investigated using a  $5 \mu\text{V}$  threshold criterion; the slope of the leading edge of the a-waves were compared; the maximal a-wave amplitudes were calculated; and a-wave implicit times were compared; finally a subtraction of intensity matched scotopic and photopic a-waves was performed.

### 3.3.1.i. A-wave threshold

The scotopic a-wave threshold (Figure 3.4) of *rge* birds was significantly elevated from the earliest time point (1 day of age:  $-0.32 \pm 0.12 \log \text{cdS/m}^2$  for *rge* birds and  $-1.28 \pm 0.14 \log \text{cdS/m}^2$  for control birds,  $P=0.0164$ ). It became further elevated over the first two weeks of age and then reached a plateau, over the same time period the scotopic a-wave threshold of controls decreased. The overall scotopic 5  $\mu\text{V}$ -criterion a-wave threshold in *rge* birds considering all time points was  $0.16 \pm 0.37 \log \text{cdS/m}^2$  whereas that of controls was  $-1.28 \pm 0.14 \log \text{cdS/m}^2$  ( $P<0.0001$ ).

At one day of age the photopic a-wave 5 $\mu\text{V}$ -criteria threshold of *rge* birds was greater than controls, although the difference was not significant. The photopic a-wave threshold of the control birds decreased with retinal maturation while that of the *rge* birds increased. By 7 days of age the photopic a-wave threshold of *rge* birds was significantly greater than that of controls ( $0.15 \pm 0.04 \log \text{cdS/m}^2$ , and  $-0.71 \pm 0.11 \log \text{cdS/m}^2$  respectively,  $P=0.0354$ ) and remained significantly elevated for the rest of the study.

Interestingly the mean overall photopic a-wave 5 $\mu\text{V}$ -criteria threshold of *rge* birds was not significantly different from the scotopic a-wave threshold of *rge* birds.

### 3.3.1.ii. A-wave amplitudes

The mean a-wave intensity: response curve of young *rge* chicks was shifted to the right. At the brightest intensities the a-wave of controls had reached a plateau, whereas it appeared that the a-wave responses from the affected birds was still increasing at the

brightest flash and might have increased further had brighter flashes been available (Figure 3.5).

The overall (considering a-wave amplitude at all intensities) scotopic and photopic mean a-wave amplitudes of the *rge* birds compared to controls were significantly decreased at all age points ( $P<0.0001$ ). However, the mean of the individual maximum a-wave amplitudes recorded from the scotopic and photopic intensity series studies ( $A_{\max}$ ) was not different between the *rge* and control group during the first 2 weeks of life (a plot of the scotopic  $A_{\max}$  is shown in Figure 3.6). The control chicks showed a maturation of the mean (of all intensities) scotopic and photopic a-wave amplitude and scotopic  $A_{\max}$  over the first few weeks of life; whereas the *rge* chicks showed an initial increase in the mean a-wave amplitude, but not  $A_{\max}$  from 1 to 7 days of age ( $P=0.0145$ ) after which, further maturation was halted and a slow deterioration occurred in the mean a-wave amplitude and in  $A_{\max}$  (from 14 to 500 days of age,  $P<0.05$ . Figure 3.6).

#### 3.3.1.iii. Slope of the a-wave leading edge

The slope of the leading edge of the a-wave of *rge* chicks was consistently shallower than that recorded from control birds at the same flash intensity and this difference became more apparent with age (Figures 3.1 and 3.2).

#### 3.3.1.iv. A-wave implicit times

The scotopic a-wave implicit time was increased compared to controls at 1 day of age (Figure 3.5) whereas the photopic a-wave implicit time was increased mostly at the higher intensities. However, when the overall mean a-wave implicit times were compared at 1 day of age the *rge* chicks were shown to have a greater overall mean scotopic implicit time than controls ( $16.66 \pm 1.65$  mSec and  $12.12 \pm 1.55$  mSec, respectively,  $P < 0.0001$ ). The a-wave implicit times of *rge* birds became greater with age (data not shown).

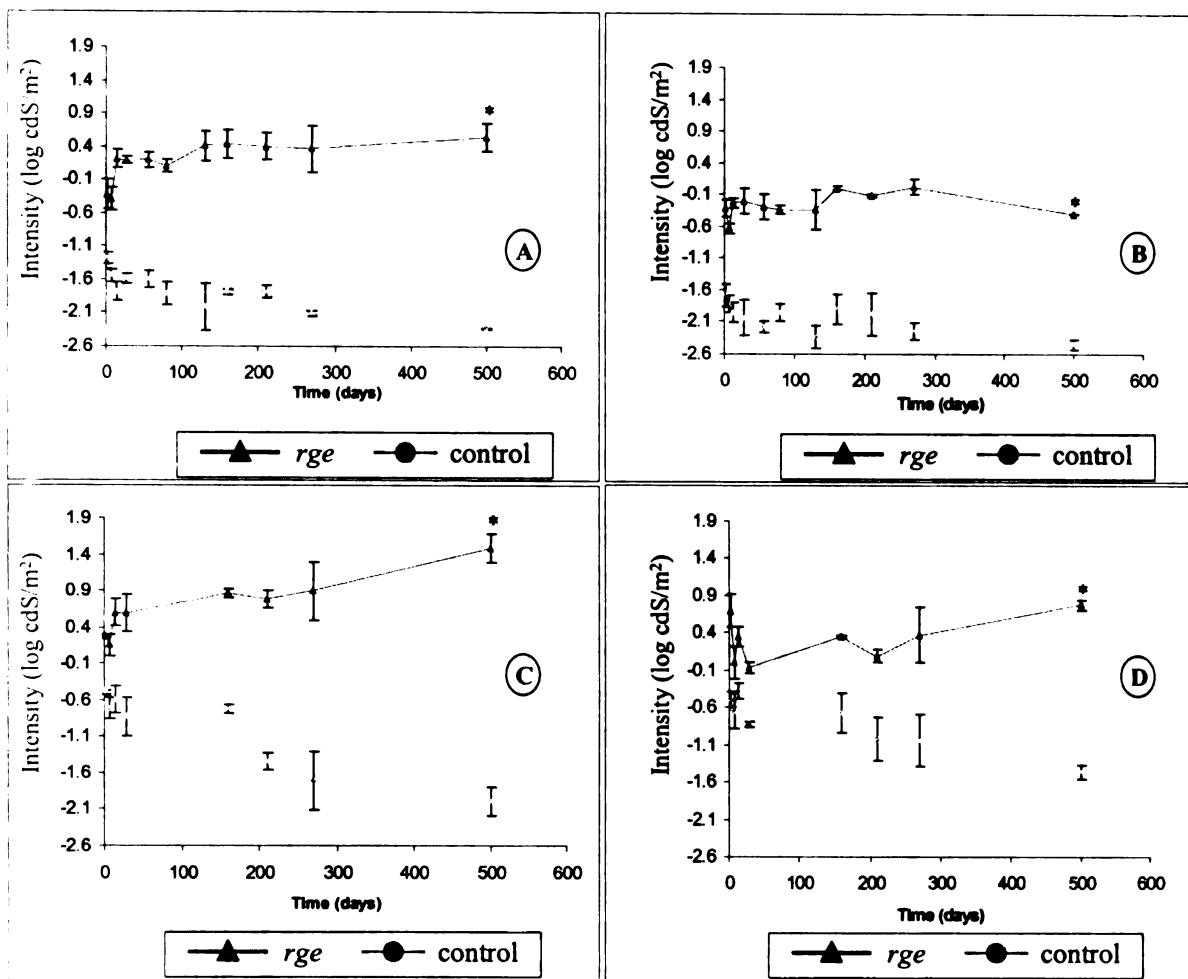


**Figure 3.4** – Scotopic and photopic threshold using a 5  $\mu$ V-criterion. Mean scotopic threshold for a-wave (A) and for b-wave (B) with respective standard error bars ( $1x \pm SEM$ ) for all the age groups studied. The black continuous line with triangles represents the mean threshold intensity (log cdS/m<sup>2</sup>) for the *rge* birds. The gray dashed line with circles represents the mean threshold intensity (log cdS/m<sup>2</sup>) for control birds. The mean photopic threshold, using a 5  $\mu$ V-criterion, for a-wave (C) and for b-wave (D) with respective standard error bars ( $1x \pm SEM$ ) for all the age groups studied is also shown. The black continuous line with triangles represents the mean threshold intensity (log cdS/m<sup>2</sup>) for the *rge* birds. The gray dashed line with circles represents the mean threshold intensity (log cdS/m<sup>2</sup>) for control birds. Note the difference in threshold between the *rge* and the control group. In the *rge* group the threshold is always higher. Also, note that in the *rge* group the mean overall difference between photopic and scotopic thresholds is not significant ( $P > 0.05$ ). When the age groups were analyzed separately, this difference was only significant ( $P < 0.05$ ) in one age group (500 days of age) (\*).

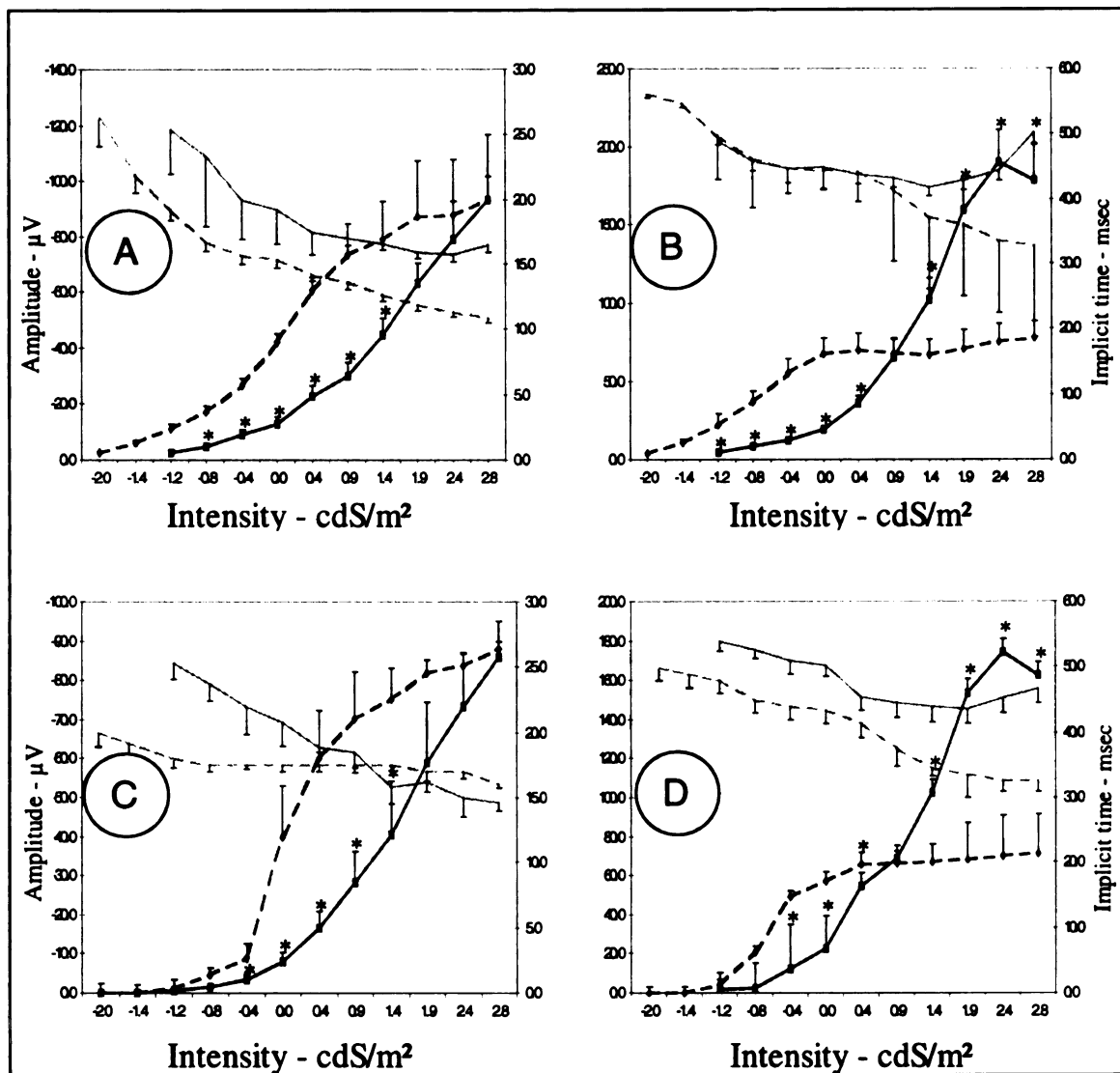


**Figure 3.5** – Scotopic and photopic intensity: response (I:R) plot. Mean scotopic (A) and photopic (C) a-wave amplitude and latency, with standard error bars ( $1x \pm \text{SEM}$ ) at 7 days of age, using an intensity-series of flashes in dark-adapted *rge* and control birds. The black solid line represents the mean a-wave amplitude curve of the *rge* birds. The black dashed line represents the a-wave amplitude curve of controls. The gray solid line represents the a-wave latency curve of the *rge* birds. Gray dashed lines represent the a-wave latency curve from controls. Note the increased latencies between *rge* and controls. Additionally, note the increased threshold and difference in a-wave amplitude with increasing intensities between the *rge* and control birds ( $n=7$  control and 7 *rge* birds). The mean scotopic (B) and photopic (D) b-wave amplitude and latency, with standard error bars ( $1x +$  and  $- \text{SEM}$ , respectively) at 7 days of age, are also shown, using an intensity series of flashes in dark-adapted *rge* and control birds. The black dashed line with markings represents the mean b-wave amplitude curve of the *rge* birds. The black solid line represents the b-wave amplitude curve of controls. The gray solid line represents the b-wave latency curve of the *rge* birds. The gray dashed line represents the b-wave latency curve from controls. Note increased latencies in the *rge* birds. Additionally, with higher light intensities (1.4, 1.9 and 2.4 log cdS/m<sup>2</sup>) b-wave amplitude is higher in *rge* than controls ( $n=7$  control and 7 *rge* birds) (\* =  $P < 0.05$ ).



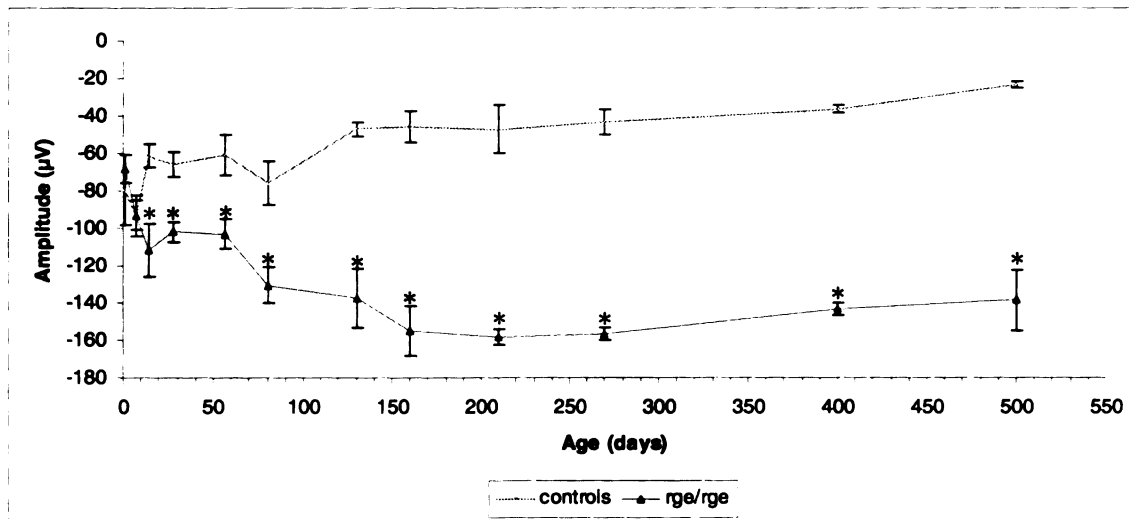


**Figure 3.6** - Mean scotopic  $A_{max}$ , with respective standard error bars ( $1x \pm SEM$ ) of all the age groups studied. The black solid line represents the mean  $A_{max}$  amplitude of the *rge* birds. The gray dashed line represents the  $A_{max}$  of the control birds. Note the decay of the  $A_{max}$  response in the *rge* group from 14 to 500 days of age. (n=6 control and 5 *rge* birds) (\*  $P < 0.05$ ).

### 3.3.1.v. Subtraction of intensity matched photopic a-wave from scotopic a-wave to reveal rod-mediated a-wave response

Subtraction of intensity matched photopic and scotopic a-waves revealed that at 7 days of age the *rge* chicks had a very low amplitude subtracted a-wave (data not shown). The amplitude of the subtracted a-wave further decreased with age until it had almost disappeared by 160 days of age (Figure 3.7).

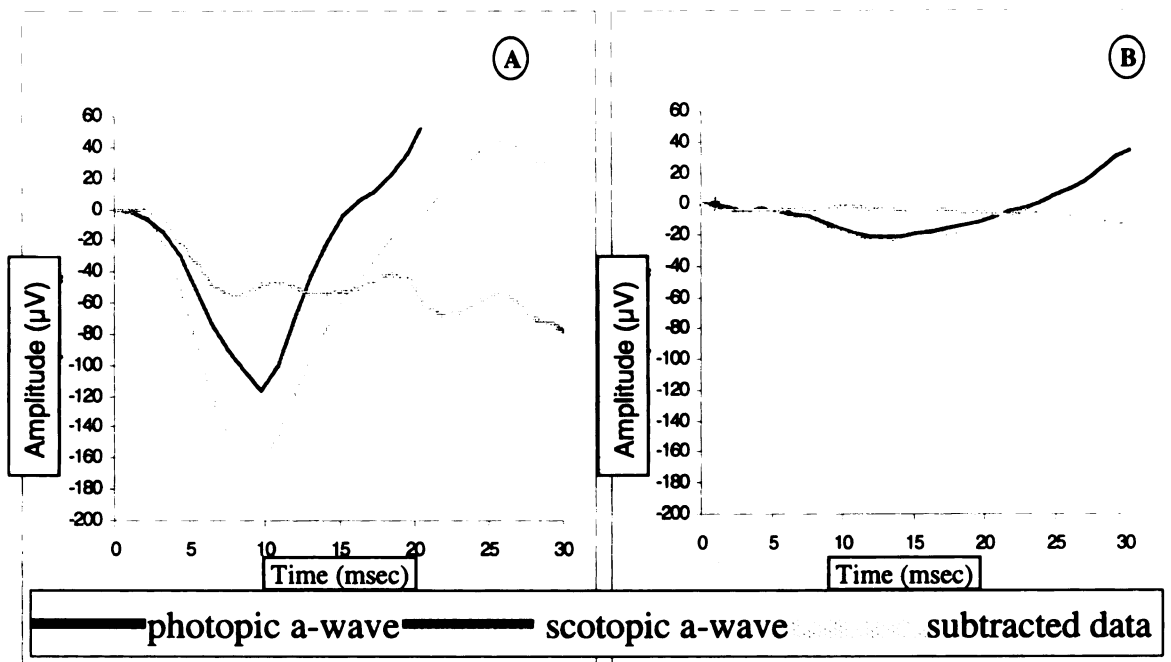


**Figure 3.7** - Intensity matched ( $2.8 \log \text{cdS/m}^2$ ) a-wave tracings from a control (A) and an *rge* chick (B) at 160 days of age. The subtraction technique was applied. The continuous gray line represents the scotopic a-wave and the continuous black line represents the photopic a-wave. The dashed line was obtained by subtracting the photopic a-wave data from the scotopic one. This results in a rod-derived hypothetical (subtracted) a-wave. Note the difference in amplitude of the subtracted a-wave between the control (A) and the *rge* chick (B). The subtracted data from the *rge* chick has very low amplitude, appearing almost like a straight line. This indicates clearly that the ERG a-wave of the *rge* chicks is mostly derived from cones.

### 3.3.2. B-wave responses

The b-waves of the *rge* birds were analyzed and compared with controls in several different ways: the scotopic and photopic b-wave thresholds were investigated using a 5 μV-threshold criterion; b-wave amplitude intensity:response (I:R) curves were plotted and the first limb of the curve analyzed using the Naka-Ruston formula, and the maximal b-wave amplitude of the second limb of the I:R curve investigated, and the b-wave implicit times were compared.

### 3.3.2.i. B-wave threshold (Figure 3.4)

The combined scotopic 5 $\mu$ V-criterion b-wave threshold of all ages of *rge* birds tested ( $0.92 \pm 1.20 \log \text{cdS/m}^2$ ) was significantly increased compared to control birds ( $0.13 \pm 0.15 \log \text{cdS/m}^2$ ) ( $P < 0.0001$ ). There was a significant difference in the 5 $\mu$ V-criterion scotopic b-wave threshold of *rge* birds ( $-0.316 \pm 0.223 \log \text{cdS/m}^2$ ) compared to controls ( $-1.69 \pm 0.33 \log \text{cdS/m}^2$ ) at 1 day of age ( $P = 0.0017$ ).

In a similar manner, the overall photopic b-wave threshold (5 $\mu$ V-criterion) in *rge* birds ( $0.36 \pm 0.35 \log \text{cdS/m}^2$ ) was also significantly greater than controls ( $-0.74 \pm 0.58 \log \text{cdS/m}^2$ ) ( $P < 0.0001$ ). There was a significant difference in the 5 $\mu$ V-criterion photopic b-wave threshold of *rge* birds ( $0.69 \pm 0.30 \log \text{cdS/m}^2$ ) compared to controls ( $-0.49 \pm 0.18 \log \text{cdS/m}^2$ ) at 1 day of age ( $P = 0.0395$ ).

Interestingly, the overall mean threshold tested was not significantly different within the *rge* birds between scotopic and photopic 5 $\mu$ V-criterion for b-wave.

### 3.3.2.ii. Naka-Rushton fitting of the first limb of the I:R curves (Figure 3.8)

The Naka-Rushton equation successfully fitted the data points below a light intensity of  $0.9 \log \text{cdS/m}^2$ , and thus below the "second limb" of the response function in both *rge* and control birds. Cone activity is thought to contribute to the second limb of the response function after the response plateau. Therefore, only b-wave amplitude data below a flash intensity  $0.9 \log \text{cdS/m}^2$  were used for fitting the Naka-Rushton function.

Thus, the data points representing the second limb of the intensity:response function were excluded.

A correlation coefficient is a number between -1 and 1, which measures the degree to which two variables are linearly related. In the regression analysis performed the correlation coefficient ( $R^2$ ), which is a measure of the goodness of fit, resulting from the selected data for each individual was kept as close as possible to 1. This was successfully accomplished for the majority of the data of the control birds, with resulting  $R^2$  values around 0.96 to 0.99. However, for the *rge* birds the correlation coefficient of the fit was still positive but usually lower, with  $R^2$ -values around 0.69 to 0.80.

$V_{\max}$  values correspond to the mean maximal amplitudes of the b-wave at the first limb of the intensity:response plot.  $V_{\max}$  was significantly lower in the *rge* chicks compared to controls at all age points (e.g. at one day of age  $V_{\max}$  was  $20.75 \pm 13.86 \mu V$  and  $82.33 \pm 24.62 \mu V$ , for *rge* and control chicks respectively,  $P < 0.001$ ). The  $V_{\max}$  values in control chicks increased by a magnitude of 2.75 times with age over the time-points studied ( $P = 0.0001$ ); whereas the  $V_{\max}$  of *rge* birds decreased with age and by 14 days of age was significantly lower than at 1 day of age ( $P = 0.007$ ).

The mean K parameter value (the intensity required to elicit a b-wave of  $\frac{1}{2}V_{\max}$ ) when considering all of the age points in the *rge* birds was elevated ( $1.05 \pm 0.25 \log \text{cdS/m}^2$ , for *rge* birds and  $0.21 \pm 0.14 \log \text{cdS/m}^2$  for controls.  $P < 0.0001$ ). The first age group studied in which the difference in K parameter value between *rge* and control birds was statistically significant was 56 days of age ( $P = 0.0053$ ) (Figure 3.8). At this age the K parameter was  $-0.79 \pm 0.30 \log \text{cdS/m}^2$  for control chicks and  $-0.26 \pm 0.13$  *rge* chicks. The K parameter of *rge* birds further increased after this age (data not shown).

The overall  $n$  parameter, which is an exponent that affects the slope of the "first limb" component of the b-wave intensity/response function curve, in the present study was  $10.78 \pm 1.07$  in the *rge* group, whereas the control group was  $1.38 \pm 0.69$ ,  $P=0.0001$ . The  $n$  parameter was statistically different between *rge* and controls at 1 day of age, when the mean  $n$  value was  $20.38 \pm 9.94$  for the *rge* group,  $1.38 \pm 0.69$  for the control group,  $P=0.0004$ .

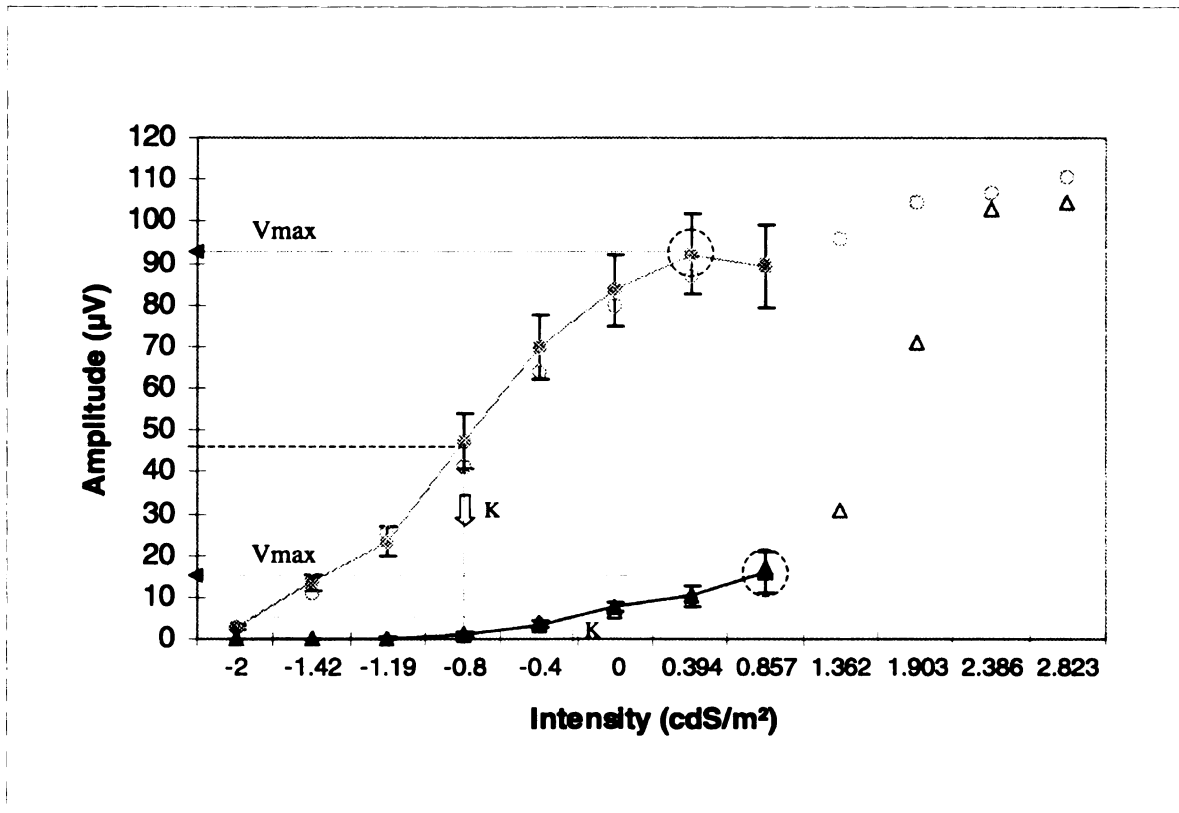


**Figure 3.8** – Naka-Rushton fit parameters. Scotopic b-wave intensity:response function from *rge* and control chicks at 56 days of age (*rge* = black open triangles; controls = gray open circles). The superimposed curves (continuous lines) represent the predicted the rod-b-wave derived from a Naka-Rushton model (*rge* = black with triangles; controls = gray with circles).  $V_{max}$  = maximal rod b-wave amplitude (dashed circles);  $K$  = log intensity at half maximal rod response ( $1/2 V_{max}$ ) (open arrow) ( $n=6$  *rge* and 9 control birds).

3.3.2.iii. Maximal amplitude of the b-wave - second limb of the intensity:response plot ( $B_{max}$ ) (Figure 3.9)

The second limb of the b-wave intensity:response plot of younger *rge* birds (responses to flashes greater than  $0.9 \log \text{cdS/m}^2$ ) shows a substantial increase in amplitudes compared to the first limb, whereas the responses of control birds plateau after the first limb (Figure 3.5). At the higher intensities in younger *rge* birds this leads to a supernormal b-wave. A plot of the mean maximum b-wave response ( $B_{max}$ ) against age (Figure 3.9) reflects this supernormal b-wave response. The value of  $B_{max}$  of *rge* birds is significantly greater than controls from 7 days of age ( $192.19 \pm 53.75 \mu\text{V}$  and  $77.81 \pm 15.93 \mu\text{V}$ , respectively,  $P=0.0079$ ) to 28 days of age ( $196.80 \pm 22.56 \mu\text{V}$  and  $114.47 \pm 28.89 \mu\text{V}$ , respectively,  $P<0.0001$ ). After that age the mean scotopic  $B_{max}$  values of *rge* birds decrease progressively until the last age group evaluated and is significantly lower than controls by 130 days of age ( $118.50 \pm 33.23 \mu\text{V}$  and  $190.60 \pm 42.86 \mu\text{V}$  respectively,  $P=0.0376$ ).

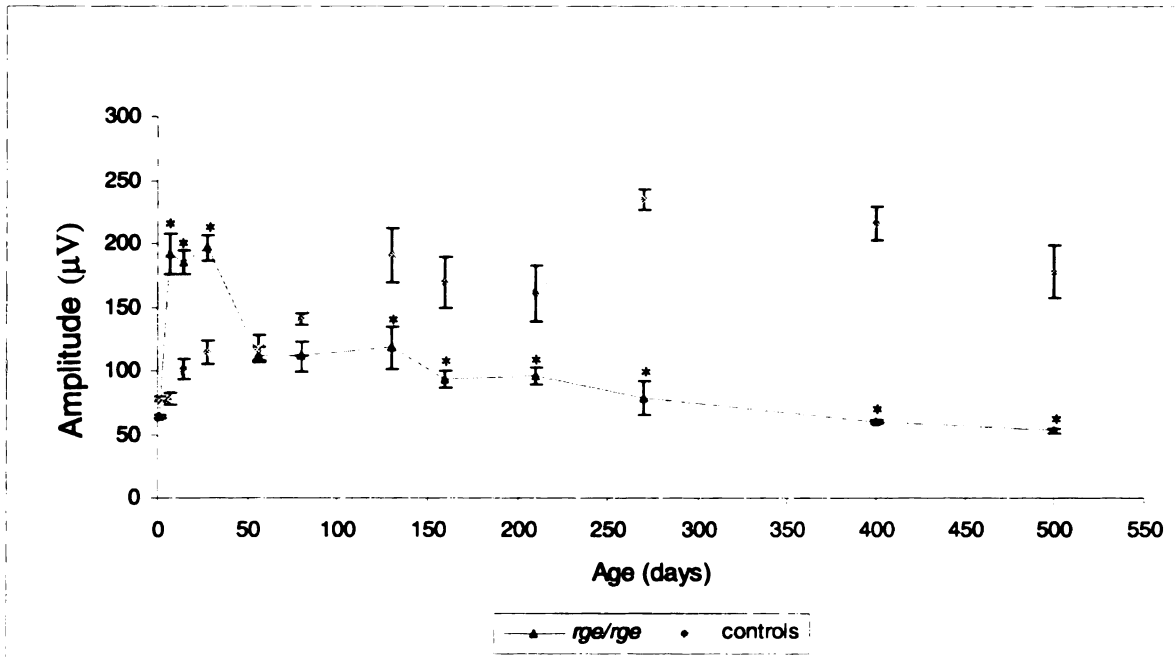


**Figure 3.9-** Mean scotopic  $B_{max}$ , with respective standard error bars ( $1x \pm SEM$ ) of all the age groups studied. The black solid line represents the mean  $B_{max}$  amplitude of the *rge* birds. The gray dashed line represents the  $B_{max}$  of the control birds. Note the supernormal  $B_{max}$  in the *rge* group from 7 to 28 days of age. Additionally, note the deterioration of the  $B_{max}$  in the *rge* group (\* =  $P < 0.05$ ).

### 3.3.2.iv. B-wave implicit times

A plot of b-wave implicit time against flash intensity in young chicks shows that at lower intensities the implicit time is similar to controls but becomes increased in parallel with the development of supernormal amplitudes in response to higher flash intensities (figure 3.5). However, the mean implicit time of the b-waves of *rge* chicks when combining the results from all light intensities used was significantly greater than controls from 1 day of age ( $52.73 \pm 6.98$  mSec and  $37.33 \pm 8.66$  mSec, respectively,  $P=0.0001$ ). The b-wave implicit times of *rge* chicks further increased with age (data not shown).

#### 3.3.2.v. Ratio of b-wave to a-wave amplitudes

The overall ratio of b- to a-wave amplitudes was greater in the *rge* birds compared to controls group ( $2.28 \pm 0.60$  compared to  $1.08 \pm 0.20$ ).

#### 3.3.3. ERG response using color filters

The a- and b-wave ERG amplitudes generated with the use of different color filters were analyzed. Control birds showed no statistically significant difference in a- or b-wave amplitudes in response to any of the different filters that had been photopically matched at any of the age groups studied ( $P>0.05$ ).

However, at 14 days of age the mean a-wave amplitude of the *rge* chicks captured with the use of the red filter,  $-75.30 \pm 6.64 \mu\text{V}$  (wavelength of 600-1100 nm), was significantly greater than the mean a-wave produced with the green filter,  $-57.92 \pm 6.08 \mu\text{V}$  (wavelength of 540-560 nm) ( $P=0.046$ ). The mean a-wave amplitude obtained with the red filter at this age was also significantly greater than the one obtained with the blue -  $-49.26 \pm 12.70 \mu\text{V}$  (wavelength of 400-500) ( $P=0.0127$ ) (See Figure 3.10).

A similar result was observed at 30 days of age. The mean a-wave amplitude of the *rge* chicks with the use of the red filter,  $-92.01 \pm 16.97 \mu\text{V}$  (wavelength of 600-1100 nm), was significantly greater than the mean a-wave produced with the green filter, -  $55.65 \pm 5.02 \mu\text{V}$  (wavelength of 540 – 560 nm) ( $P=0.0414$ ). The mean a-wave amplitude obtained with the red filter, at 30 days of age, was also significantly greater than the one



obtained with the blue  $-56.3 \pm 4.80 \mu\text{V}$  (wavelength of 400-500) ( $P=0.0434$ ) (See Figure 3.10)

At 150 days, the difference observed in the results for the red filter in the *rge* group was no longer significantly different ( $P>0.05$ ).

The ERG mean b-wave amplitudes were not significantly different within the *rge* group for any of the wavelengths tested. The same was observed in the control group ( $P>0.05$ ).

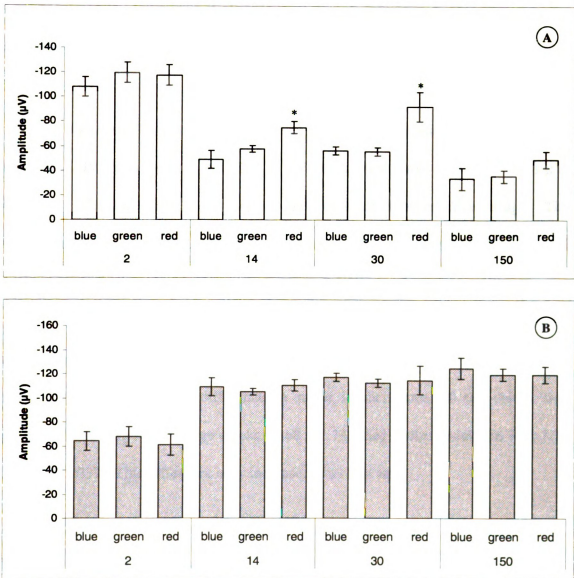


**Figure 3.10** - Mean a-wave amplitudes ( $1x \pm SEM$ ), photopically matched using stimuli of 3 different peak spectral transmittances: 400-500 (blue), 540 - 560 nm (green) and 600 - 1100 nm (red). Note that the control birds (B) showed no statistically significant difference between any of the different filters studied ( $P > 0.05$ ). Within the *rge* group (A), however, the a-wave amplitude obtained with the red filter was significantly higher than the remaining filters at 14 and 30 days of age ( $P < 0.05$ ) ( $n = 3$  *rge*; 5 control chicks).

#### 3.3.4. 30Hz flicker ERG comparison (Figure 3.11)

The mean amplitude of 30 Hz flicker of *rge* chicks was considerably lower than controls at 1 day of age ( $rge = 9.32 \pm 3.25 \mu V$  and control birds =  $39.72 \pm 10.68 \mu V$ ,  $P=0.0003$ ). The amplitude of response in the *rge* birds deteriorated with age. The overall mean amplitude of the 30Hz flicker ERG response in *rge* chicks was  $-5.60 \pm 4.20 \mu V$  compared to  $90.14 \pm 11.13 \mu V$  for controls ( $P<0.0001$ ).

The overall 30Hz flicker ERG implicit time of the *rge* group was also abnormally increased as compared to controls,  $18.86 \pm 11.44$  mSec and  $14.92 \pm 2.23$  mSec, respectively ( $P=0.0498$ ). The difference in mean implicit time of *rge* chicks was significant from 7 days of age (*rge* chicks  $19.68 \pm 1.73$  mSec control chicks  $16.78 \pm 1.74$  mSec,  $P=0.0037$ ). This difference only increased after that age.

#### 3.3.5. VEPs (Figure 3.12)

In the control chicks, the waveforms of the VEPs were composed of an initial positive wave, followed by a second negative wave followed by a few small additional wavelets (Figure 3.12) and are similar to those of a previously described study using chicks. The responses of the VEPs in the *rge* chicks were similar to those in the controls in shape but with very small amplitudes from 1 day of age (Figure 3.12). The amplitude

of the VEPs further deteriorated with increasing age, although cortical activity could still be recorded at 45 days of age (data not shown).

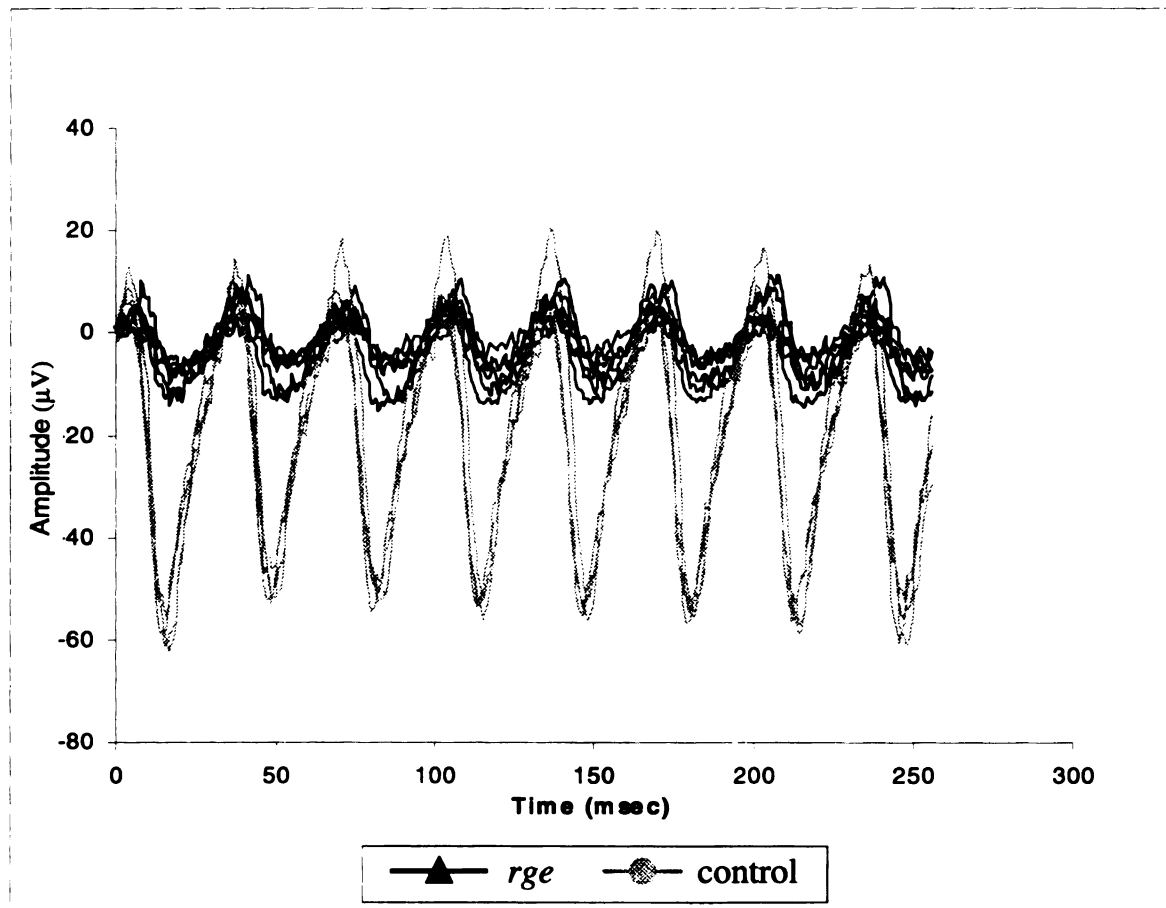


**Figure 3.11** - A comparison of 30 Hz flicker tracings using the flash light intensity of 0.4 log  $\text{cdS/m}^2$  at 1 day of age. The *rge* chicks are represented in black solid lines and the control birds in gray solid lines. The comparison reveals that *rge* chicks have lower amplitudes than the control group ( $n = 5$  *rge*; 4 control chicks).

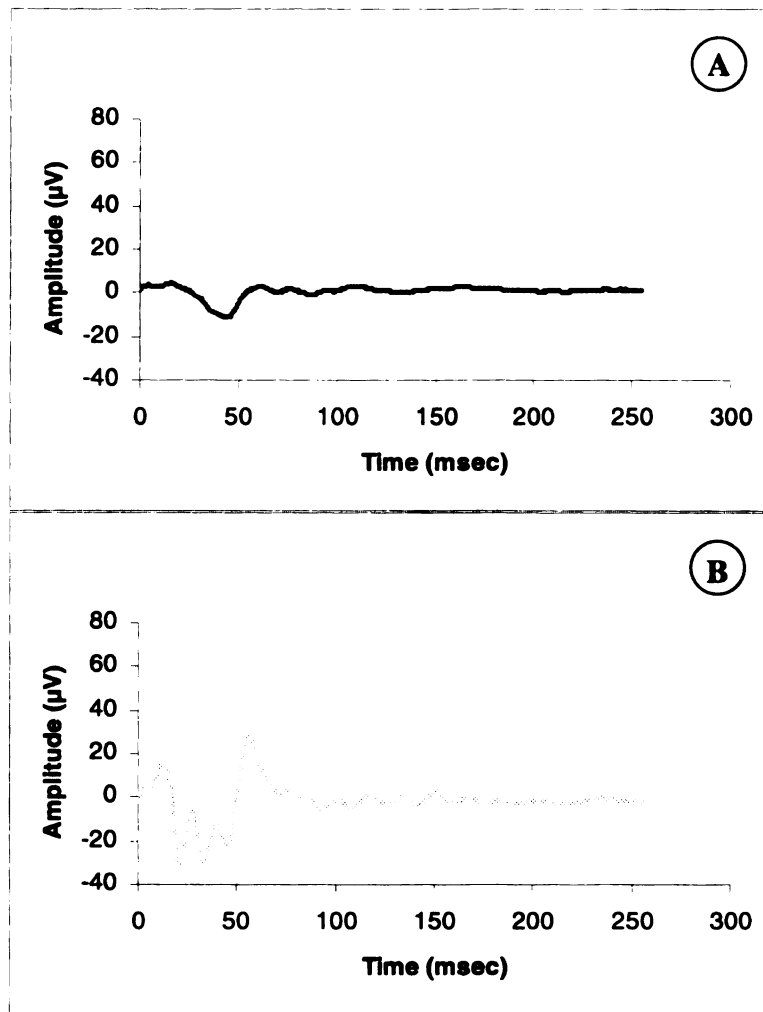


**Figure 3.12-** A comparison of the VEP response at 1 day of age in a *rge* (A) and a control (B) chick. The recording electrode was placed at the region of the right optic lobe. Note that the VEP response in the *rge* chick had very small amplitudes at that early age.

### 3.4. Discussion

The *rge* chick has unusual ERG changes, with an abnormal shape of ERG waveform from hatch that slowly deteriorates with age but is maintained until well after the age at which vision loss occurs. These changes are very different from those

described in other chicken models of retinal dystrophy such as *rd*, *rdd* and *dam* and appear different to those reported in retinal dystrophies in other species.

The waveform of the ERG of *rge* chicks from hatch has very reduced OPs and a lack of c-waves from both photopic and scotopic responses. The slope of the leading edge of the a-wave is reduced and at lower intensities the a-wave has an increased implicit time. The normal chick a-wave intensity:response (I:R) plot shows a typical sigmoid curve, whereas the a-wave I:R plot of the *rge* chick is shifted to the right, reflecting an elevated response threshold and shows a rising phase but no plateau even with the highest intensities tested. It seems likely that brighter flashes would be required to fully saturate the a-wave in the *rge* birds reflecting the reduced photoreceptor sensitivity compared to controls. The peak recorded a-wave amplitude of the *rge* birds is not different from controls in the first week after hatch, but by 14 days of age the maximum a-wave recorded at the light intensities used is significantly lower than controls and continues to deteriorate with age. Scotopic and photopic a-wave thresholds of affected birds are very similar. Subtraction of photopic a-wave from scotopic a-wave suggests that the younger birds may have some rod-mediated responses, although these are markedly lower than controls and disappear with age. Application of the Naka-Rushton formula to the first phase of the b-wave response, which is intended to model the retinal rod driven responses, showed that  $V_{\max}$  was markedly reduced in the *rge* birds. The K value, a reflection of retinal sensitivity, was not significantly different from controls initially. These results show that the *rge* chicks have an initial loss of rod responses. The initial maintenance of the K value suggests that this may be due to a loss of function in the majority of rod photoreceptors with the remaining functional rods

having a relatively normal sensitivity. Modeling the first phase of the b-wave I:R plot has usually been applied to rod-dominated retinas. The validity of using this technique in a retina with a higher ratio of cones to rods, such as the chick retina, has not been established. Additionally, modeling scotopic b-wave responses from *rge* birds is complicated by the low amplitudes of the first phase of the I:R plot. Attempts to compare the slope of normalized photopically subtracted scotopic a-waves using the method suggested by Hood and Birch (1996), were not considered valid because of the very low amplitude of the resulting subtracted a-wave in the *rge* bird prior to normalization compared to that obtained in controls. The initial reduction in rod photoreceptor responses correlates with the results from vision testing of the *rge* birds, which showed that they have a more severe loss of visual function in the early stages of the disease under lower lighting intensities (Chapter 2).

The *rge* b-wave has a smoother and broader waveform than normal, partly accounted for by the reduction in OPs. The normal chick scotopic and photopic b-wave I:R plots have a typical sigmoid curve. In the *rge* chicks both scotopic and photopic b-wave I:R curves are sigmoid-shaped but are shifted to the right and, in the younger chicks, show an abnormally elevated b-wave amplitude with flash intensities above 0.9 log cdS/m<sup>2</sup>. However, this elevated b-wave amplitude significantly deteriorates with age. Investigation of the b-wave to a-wave ratio using the method of Perlman (1983) shows that the ratio for control chicks is 1.08 which is within the normal range of 0.8 to 1.2 reported for other species. The b-wave : a-wave ratio of the *rge* birds in the first two weeks of age was abnormally high (2.28) and is a reflection of the supernormal b-wave. There are several reports in the literature of human patients having similarly abnormally

enhanced ERG waveforms . The ERGs of these patients typically had delayed b-waves that were supernormal in amplitude to brighter flashes but lower in amplitude and markedly delayed in response to weaker flashes. Further studies of some patients with supernormal b-waves and animal models showed that this can result from an alteration in the ratios of photoreceptor types. Examples include humans and animals with mutations of genes coding for transcription factors important in determining the fate of photoreceptor progenitor cells, such as mutations of the *NR2E3* and *Nrl* genes. The former is responsible for enhanced S-cone syndrome in humans and the *rd7* mouse phenotype . Affected humans and mice have increased numbers of S-cones and reduced rod function . Other inherited diseases such as Best's macular dystrophy , cystinosis , albinism , and non-inherited conditions such as hyperthyroidism , corticosteroid administration , optic atrophy , optic nerve hypoplasia and central retinal vein occlusion can cause supernormal b-waves. To investigate whether the *rge* chick had an alteration in the ratio of different cone types, as seen in animals with *NR2E3* and *Nrl* gene mutations, ERGs were performed using a series of different colored flashes that were photopically matched in normal control chicks. None of the responses to colored light flashes showed increased amplitudes compared to controls and the only difference seen was that flashes of long wavelength light produced differentially larger a-wave amplitudes than the other colors in young *rge* chicks, but this effect was lost with increased age. As the short-wavelength flashes of light did not result in increased amplitudes that would be typical of *NR2E3* and *Nrl* mutations this suggests that the *rge* phenotype has a different pathogenesis. The differential response to the long wavelength flashes of light may be due to slower loss of function from the long wavelength cones compared to other cone



types rather than a developmental abnormality in ratios of cone types. The responses of the *rge* chicks to brighter flashes decrease with age showing loss of cone photoreceptor mediated function as well as rod responses. However, marked reduction in responses does not coincide with the clinical loss of vision that was previously shown (Chapter 2). Investigations of the VEPs of *rge* chicks showed that transmission to the visual cortex was markedly reduced from an early age even though the ERG responses to bright lights are well maintained in the early stages of the disease. The VEP changes appeared to more closely correlate our previous study of vision loss using an optokinetic device (Chapter 2). Reduced inner retinal function is reflected by the markedly reduced OPs and the very reduced amplitude and increased implicit time of the 30Hz flicker responses. Thus the ERG changes in the *rge* chick suggest that from an early age there are markedly abnormal responses from all retinal layers.

The obvious absence of c-waves may reflect an abnormality in retinal pigment epithelium-generated electrical fields. The photoreceptor responses are abnormal, with rods being more severely affected than cones initially. The abnormal b-wave shape may reflect abnormal transmission from photoreceptors to the second order neurons or abnormalities in the cells responsible for generation of the b-wave. Additional evidence of inner retinal dysfunction is provided by the lack of OPs and abnormal flicker responses and lack of central transmission of visual information.

Previous histopathological examination of the central visual pathways of *rge* chicks did not reveal any abnormalities. This observation supports a retinal origin for the blindness (Chapter 2). Further studies to investigate the abnormally shaped and supernormal b-wave in the *rge* chick would require pharmacological dissection studies to

se

ch

re

see which cells are responsible for the generation of the abnormal waveform in the *rge* chick. Such investigations may shed light on the pathogenesis of this apparently unique retinal dystrophy.

## CHAPTER 4

### PHARMACOLOGICAL DISSECTION OF THE *rg* ELECTRORETINOGRAM

#### 4.1. Introduction

As discussed in Chapter 1, the electroretinogram (ERG) is widely used to assess sensory retinal function. Its clinical value has been clearly established, not merely for the diagnosis of hereditary degenerative diseases of the retina, but also for evaluation of their progression and prognosis . This has been further enhanced by greater knowledge of the retinal processes underlying the different components of the ERG, mainly when different techniques, such as the use of drugs (pharmacological dissection) and intracellular recordings, were introduced. Since then, it has been commonly assumed that cells in the distal part of the sensory retina (photoreceptors, bipolar cells and Müller cells), are the main contributors to the ERG, while proximal processes contribute less to the response . The pharmacological dissection approach also has been used to investigate the ERG of animal models of inherited retinal disease .

APB (2-amino-4-phosphonobutyric acid), is a glutamatergic receptor agonist that has been shown to selectively block transmission from photoreceptors to ON bipolar cells in several species of animals . It also selectively blocks ON ERG responses in amacrine cells and ganglion cells , thus, removing the light responses of these cells and ON-depolarizing responses of all third-order neurons, and leaving OFF-hyperpolarizing responses intact. The effect in several different species, including the chicken , is to

remove the b-wave of the ERG. These results are consistent with the notion that activity in ON-depolarizing bipolar cells makes a significant contribution to the ERG b-wave.

The action of PDA (cis-2,3-piperidinedicarboxylic acid), a glutamatergic receptor antagonist, is less selective than that of APB. Application of PDA is associated with blockade of transmission from photoreceptors to OFF-hyperpolarizing bipolar cells and horizontal cells but not to ON-depolarizing bipolar cells . However, PDA also blocks transmission from both ON-depolarizing and OFF-hyperpolarizing bipolar cells to amacrine cells and ganglion cells . Thus, application of PDA results in relative isolation of activity in photoreceptors and ON-depolarizing bipolar cells. In the monkey, application of PDA has been shown to reduce a-wave amplitude and enhance b-wave amplitude of the photopic ERG response . These results led the investigators to propose that the b-wave represents an interaction of opposing field potentials driven by activity in ON-depolarizing and OFF-hyperpolarizing pathway cells and that the a-wave contains a significant contribution from activity in post-receptoral retinal cells.

Barium ( $\text{Ba}^{2+}$ ) reduces  $\text{K}^+$  conductance of Müller cells. Müller cells have been shown to contribute to the ERG b-wave , but attempts to understand the extent of their contribution in different species by using barium as a blocking agent have been inconsistent. Some studies have found that barium depresses the b-wave to about 35% of its control amplitude [e.g. in frogs: (Griff, 1985), whereas others find no change [e.g. in tiger salamanders: (Coleman, 1987) or an increase [e.g. in rabbits: (Lei, 1999)]. Regardless of whether there is an increase or a decrease in b-wave amplitude in response to intravitreal barium, the response is believed to be generated by the effect of the drug on Müller cells.

Ornithine aminotransferase deficiency and the consequent accumulation of ornithine results in atrophy of the choroid and retina of man. The acute effects of high levels of ornithine in the retina have been shown in the cat and in the rat . In cats ornithine is reported to cause a decrease in the c-wave but does not alter the b-wave amplitude . However, in rats, ornithine reduces the maximum amplitude of the b-wave by half . The selective toxic action of ornithine and consequently its effects on the ERG seems to depend upon the levels of activity of ornithine aminotransferase in the different retinal cells. Cells with higher ornithine aminotransferase activity appear to be more affected by an overwhelming dose of ornithine due to a higher affinity for the compound .

Very little information is available about ornithine aminotransferase activity levels in specific retinal neurons. From studies in bovine and murine retinas it is known that retinal pigment epithelium and the neuroretina, as a whole, show high specific activity for this enzyme . One immunohistochemical study in humans showed that ganglion cells, amacrine cells and photoreceptors are immunoreactive to an antibody raised against ornithine aminotransferase . Another immunohistochemical study, performed on rat retinas, localized ornithine aminotransferase to Müller cells and pigment epithelium of the retina . In chickens, the levels of enzyme activity in the retina are 80% of that found in the liver . These observations suggest strongly that ornithine aminotransferase activity might be important in maintaining the structure and/or function of the retina.

In the present study, in an effort to determine the origin of the abnormal waveforms observed in the ERG of *rge* birds, we have attempted to separate the contribution of different retinal neurons to the ERG of *rge* birds by means of

pharmacological alterations of the retinal network with glutamate analogues (APB and PDA), ornithine and barium chloride.

## **4.2. Materials & Methods**

### **4.2.1. Animals**

For the APB and PDA injections 6 *rge* birds and 6 control 120 day-old chickens (*rge/+*) were used in the experiment. For the ornithine injections 3 *rge* and 3 control chickens at 120 days of age were used. In addition, in order to see if the effect of the drugs would be the same on the supernormal b-waves, observed in younger *rge* chicks, ornithine, APB and PDA injections were performed in two 14 day-old *rge* and one 14-day-old control chick. For the barium chloride injections, 2 *rge* and 2 control chickens, at 14 days of age were used.

### **4.2.2. Pharmacological agents**

APB (2-amino-4-phosphonobutyric acid); PDA (cis-2, 3-piperidinedicarboxylic acid); ornithine hydrochloride and barium chloride- Sigma (St. Louis, MO, USA).

### **4.2.3. Intravitreal injection**

A single dose of PDA, APB, ornithine, and barium were injected into the vitreous chamber of one or both eyes using a Hamilton syringe equipped with a 30 G disposable needle. Additionally, the effect of a combination of drugs, APB + PDA, was also tested. The maximum volume injected for any drug was 0.02 ml. The target concentration was calculated using the mean vitreous volume as a parameter to achieve an effective intravitreal concentration, as previously described, of 0.1 mM APB and 5 mM PDA. The final intravitreal concentration of ornithine was 0.5 M and was based on previously described ERG studies performed in other species. The final intravitreal concentration used for barium chloride was 1 mM, which had previously been used to investigate the ERGs of frogs and salamanders.

For the calculation of the amount of drug that had to be injected to achieve the desired final vitreal concentration, the volume of the vitreous body was measured. The vitreous body was aspirated into a 1ml-syringe in freshly enucleated eye globes from age matched control and *rge* birds.

#### 4.2.4. ERG recording

All ERG recordings were performed from 9:30 AM to 5:30 PM on all occasions to avoid diurnal variations. Scotopic white light intensity series ERGs were recorded as described in Chapter 3.

Birds were dark-adapted for 20 minutes, and then the responses from a series of 7 white flash stimuli (-0.4, -0.002, 0.4, 0.85, 1.4, 2.3, 2.8 log cdS/m<sup>2</sup>) were recorded. Three flashes were averaged from -0.4 to 2.8 log cdS/m<sup>2</sup>. Inter-stimulus intervals were



increased from 30 seconds (-0.4, -0.002, 0.4 and 0.85 log cdS/m<sup>2</sup>) at low intensities to 3 minutes at higher intensities (1.4, 2.3 and 2.8 log cdS/m<sup>2</sup>) to avoid light adapting the rods. The same protocol was repeated 1 hour after the intravitreal injections of APB and PDA, 2 hours after barium and 5 hours after ornithine injections.

#### 4.2.5. Statistical Analysis

Statistical analysis to compare the ERG data between pre and post intravitreal injection of each drug was performed by paired *t*-tests, (StatView - SAS Institute Inc., Cary, NC, USA). If any statistically significant difference was found the data were further analyzed using *post hoc* comparisons with Fisher's or Tukey-Kramer tests. Data were deemed significant when  $P < 0.05$ .

### 4.3. Results

#### 4.3.1. Results after the intravitreal injection of PDA (Figure 4.1)

In the control group, after the intravitreal injection of PDA, the ERG showed significantly smaller mean overall a-wave amplitude (pre-injection =  $-87.94 \pm 43.15 \mu\text{V}$ ; post-injection =  $-46.18 \pm 19.44 \mu\text{V}$ ,  $P=0.0001$ ) with a higher but not significantly different mean implicit time (pre-injection =  $12.66 \pm 2.3 \text{ mSec}$ ; post-injection =  $13.22 \pm 2.4 \mu\text{V}$ ,  $P=0.38$ ). However, the slope of the second half of the a-wave was consistently less steep after the injection. The mean overall b-wave amplitude tended to be slightly lower after the injection but was not significantly different (pre-injection =  $137.37 \pm 20.18 \mu\text{V}$ ; post-injection =  $124.20 \pm 33.84 \mu\text{V}$ ,  $P=0.106$ ). It was also possible to observe a change in shape of the b-wave, which became broader (wider). The mean overall implicit time for the peak of the b-wave was not significantly different after the injection (pre-injection =  $34.19 \pm 7.1 \text{ mSec}$ ; post-injection =  $31.26 \pm 4.6 \mu\text{V}$ ,  $P=0.052$ ).

Subtle results were observed in the *rge* group after the injection of PDA. There was no statistically significant change in the mean a-wave amplitude or implicit time. The overall pre-injection mean for a-wave amplitude was  $-26.33 \pm 32.45 \mu\text{V}$  whereas the post-injection mean was  $-22.32 \pm 20.35 \mu\text{V}$ , ( $P=0.49$ ). The overall pre-injection mean for a-wave implicit time was  $15.43 \pm 3.1 \text{ mSec}$  whereas the post-injection mean was  $18.07 \pm 4.5 \text{ mSec}$ , ( $P=0.13$ ). The mean overall amplitude of the b-wave was not significantly different (pre-injection =  $56.62 \pm 48.39 \mu\text{V}$ ; post-injection =  $45.96 \pm 37.77$

$\mu\text{V}$ ,  $P=0.257$ ). The overall mean b-wave implicit time also was not significantly different (pre-injection =  $35.98 \pm 4.0$  mSec; post-injection =  $37.70 \pm 5.8$  mSec,  $P=0.36$ ).

Comparable results were also observed in younger control and *rge* chicks.

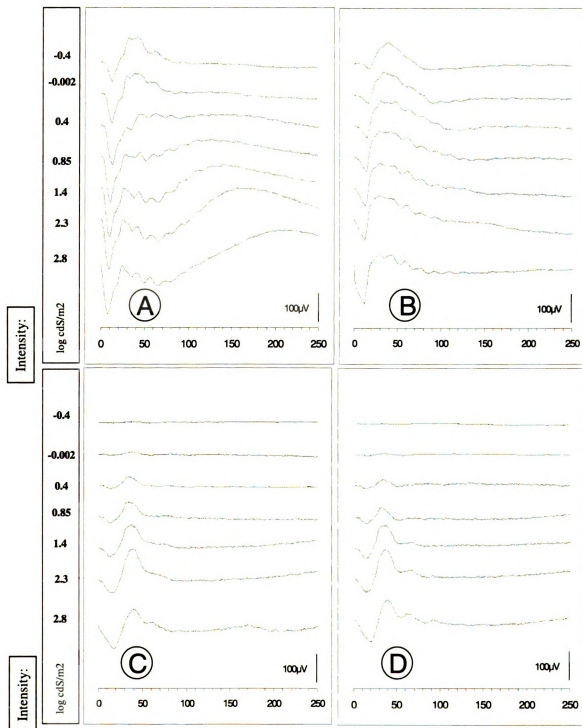


**Figure 4.1** - Representative ERGs performed before, (A) & (C), and after, (B) & (D), the intravitreal application of PDA. A & B are ERGs from a control bird while C & D are from an *rge* bird. Note that after the intravitreal injection, in the control bird (B), the a-wave became truncated, the b-wave implicit time increased and the c-wave became absent. The application of PDA in the *rge* group resulted in no changes in a- or b-wave amplitude or implicit times (D). Horizontal axis = mSec.

#### 4.3.2. Results after the intravitreal injection of APB (Figure 4.2.)

In the control group, after the intravitreal injection of APB, a complete elimination of the b-wave was observed, unmasking the a- and c-waves. The mean amplitude of the a-wave was not significantly different (pre-injection mean =  $-106.90 \pm 36.89 \mu\text{V}$ ; post-injection =  $-104.16 \pm 31.08 \mu\text{V}$ ,  $P=0.76$ ). The mean implicit time of the a-wave, on the other hand became significantly increased after the injection (pre-injection mean =  $9.57 \pm 1.12 \text{ mSec}$ ; post-injection =  $16.75 \pm 2.03 \text{ mSec}$ ,  $P<0.0001$ ).

In the *rge* group, no significant difference in the mean overall a-wave amplitude (pre-injection mean =  $-19.43 \pm 16.56 \mu\text{V}$ ; post-injection =  $-22.07 \pm 17.92 \mu\text{V}$ ,  $P=0.49$ ) and implicit time were observed (pre-injection mean =  $15.42 \pm 2.71 \text{ mSec}$ ; post-injection =  $14.92 \pm 1.90 \text{ mSec}$ ,  $P=0.33$ ). Additionally, no difference was encountered between pre- and post-injection mean overall b-wave amplitudes (pre-injection mean =  $64.86 \pm 52.92 \mu\text{V}$ ; post-injection =  $71.27 \pm 57.51 \mu\text{V}$ ,  $P=0.59$ ) and implicit time (pre-injection =  $35.65 \pm 4.4 \text{ mSec}$ ; post-injection =  $36.97 \pm 3.1 \text{ mSec}$ ,  $P=0.70$ ) in this group.

Comparable results were also observed in younger control and *rge* chicks.

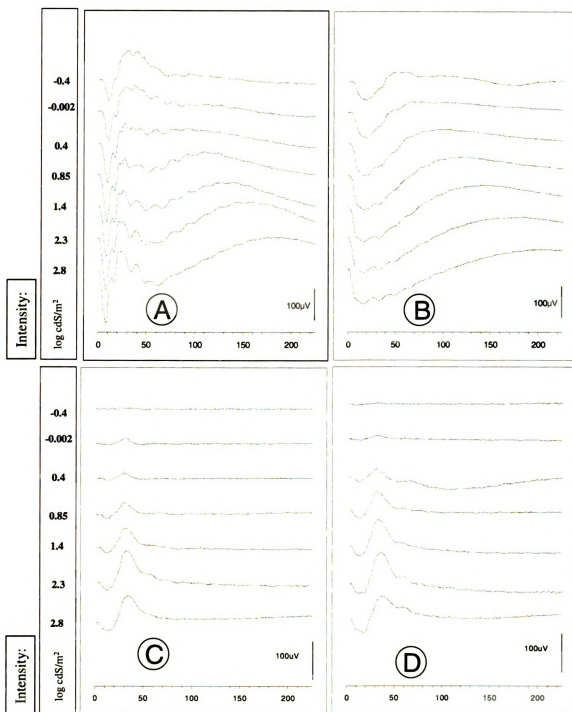


**Figure 4.2** - Representative ERGs performed before, (A) & (C), and after, (B) & (D), the intravitreal application of APB. A & B are ERGs from a control bird while C & D are from an *rge* bird. Note that in the control bird, after the intravitreal injection (B), the b-wave was eliminated and the implicit time of the a-wave increased. The remaining waveforms consisted of the a-wave and the positive c-wave. In contrast, the application of APB in the *rge* bird had no significant effect. No significant changes in a- or b-wave amplitude and implicit time (D). Horizontal axis = mSec.

#### 4.3.3. Results after the intravitreal injection of APB+PDA (Figure 4.3)

In the control group, when the combination of APB + PDA was used, all the ERG waveform components were eliminated but the a-wave and c-wave. The a-wave amplitude was not significantly different after the injection (pre-injection =  $-105.32 \pm 31.84 \mu\text{V}$ ; post-injection =  $-102.16 \pm 37.19 \mu\text{V}$ ,  $P=0.48$ ). The a-wave implicit time, however, was increased (pre-injection =  $9.12 \pm 2.20 \text{ mSec}$ ; post-injection =  $17.54 \pm 2.31 \text{ mSec}$ ,  $P<0.0001$ ).

In the *rge* group, no significant effects in the ERG waveforms were observed after a combination of APB + PDA was used. The a- wave remained present in the ERG after the injection and was not different in amplitude (overall pre-injection mean =  $-20.25 \pm 13.42 \mu\text{V}$ ; post-injection =  $-21.19 \pm 15.14 \mu\text{V}$ ,  $P=0.08$ ) and implicit time (overall pre-injection mean =  $14.94 \pm 2.16 \text{ mSec}$ ; post-injection =  $15.01 \pm 2.02 \text{ mSec}$ ,  $P=0.31$ ). The b-wave also remained present after the injection and was not different in amplitude (overall pre-injection mean =  $67.32 \pm 50.22 \mu\text{V}$ ; post-injection =  $63.42 \pm 59.10 \mu\text{V}$ ,  $P=0.16$ ) and implicit time (overall pre-injection mean =  $36.52 \pm 5.1 \text{ mSec}$ ; post-injection =  $37.74 \pm 4.6 \text{ mSec}$ ,  $P=0.24$ ).

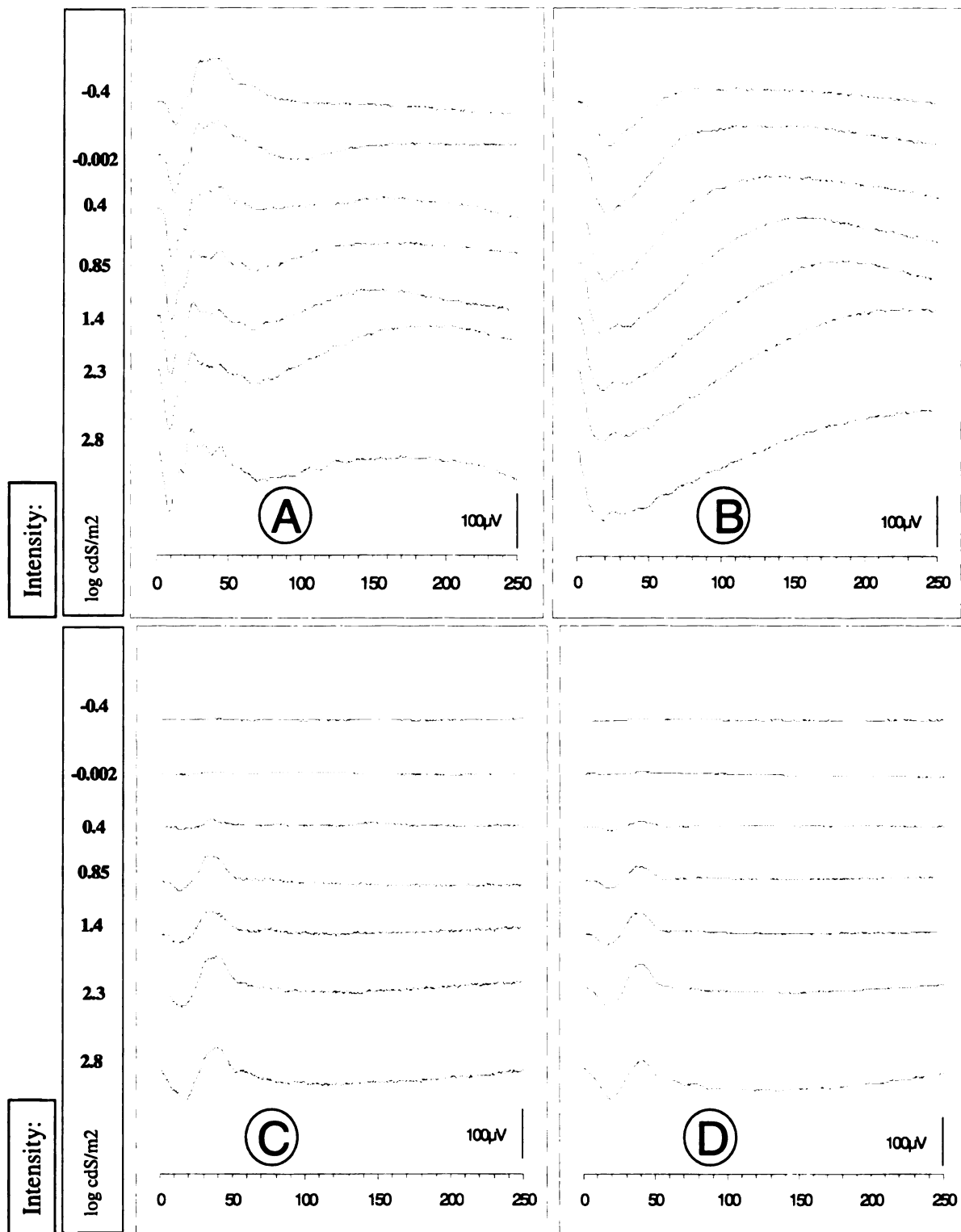


**Figure 4.3** - Representative ERGs performed before, (A) & (C), and after, (B) & (D), the intravitreal application of PDA + APB. A & B are ERGs from a control bird while C & D are from an *rge* bird. Note that in the control bird, after the intravitreal injection (B), all responses were eliminated except for the a- and c-wave. The application of APB + PDA had no significant effect on the ERG of the *rge* chicks (D). Horizontal axis = mSec.



#### 4.3.4. Results after the intravitreal injection of barium (Figure 4.4)

After the intravitreal injection of barium chloride in the control birds the overall amplitude of the a-wave when flash intensities above  $1.4 \log \text{cdS/m}^2$  were used significantly decreased (pre-injection mean =  $-146.18 \pm 32.42 \mu\text{V}$ ; post-injection =  $-102.61 \pm 20.36 \mu\text{V}$ ,  $P=0.006$ ). The mean overall b-wave also significantly decreased (pre-injection mean =  $153.03 \pm 7.68 \mu\text{V}$ ; post-injection =  $79.87 \pm 50.08 \mu\text{V}$ ,  $P=0.0039$ ). The overall implicit time of the a-wave significantly increased (pre-injection mean =  $9.13 \pm 0.51 \text{ mSec}$ ; post-injection =  $14.00 \pm 2.90 \text{ mSec}$ ,  $P=0.015$ ). The overall implicit time of the b-wave also significantly increased (pre-injection mean =  $23.78 \pm 2.19 \text{ mSec}$ ; post-injection =  $35.05 \pm 11.06 \text{ mSec}$ ,  $P=0.03$ ).

The c-wave amplitude was not significantly different in the control group after the injection when flash intensities above  $1.4 \log \text{cdS/m}^2$  were used. However, with lower intensities, the mean overall c-wave had significantly higher amplitudes (for instance, at  $0.85 \log \text{cdS/m}^2$  pre-injection mean =  $60.30 \pm 3.81 \mu\text{V}$ ; post-injection =  $85.30 \pm 37.94 \mu\text{V}$ ,  $P=0.044$ ). The overall c-wave implicit time was also significantly increased (pre-injection mean =  $168.93 \pm 32.08 \text{ mSec}$ ; post-injection =  $264.70 \pm 38.79 \text{ mSec}$ ,  $P=0.0002$ ).

In contrast, after application of barium to the *rge* retina mean overall a-wave amplitude increased significantly (pre-injection mean =  $-63.06 \pm 22.12 \mu\text{V}$ ; post-injection =  $-103.11 \pm 50.84 \mu\text{V}$ ,  $P=0.01$ ) without a significant increase in the overall a-wave implicit time (pre-injection mean =  $13.81 \pm 1.89 \text{ mSec}$ ; post-injection =  $17.25 \pm 3.90$

mSec,  $P=0.08$ ). The mean overall b-wave also significantly increased (pre-injection mean =  $209.95 \pm 66.45 \mu\text{V}$ ; post-injection =  $368.96 \pm 110.80 \mu\text{V}$ ,  $P=0.013$ ) without a significant increase in b-wave implicit time (pre-injection mean =  $39.05 \pm 4.71 \mu\text{V}$ ; post-injection =  $46.06 \pm 10.98 \mu\text{V}$ ,  $P=0.18$ ).

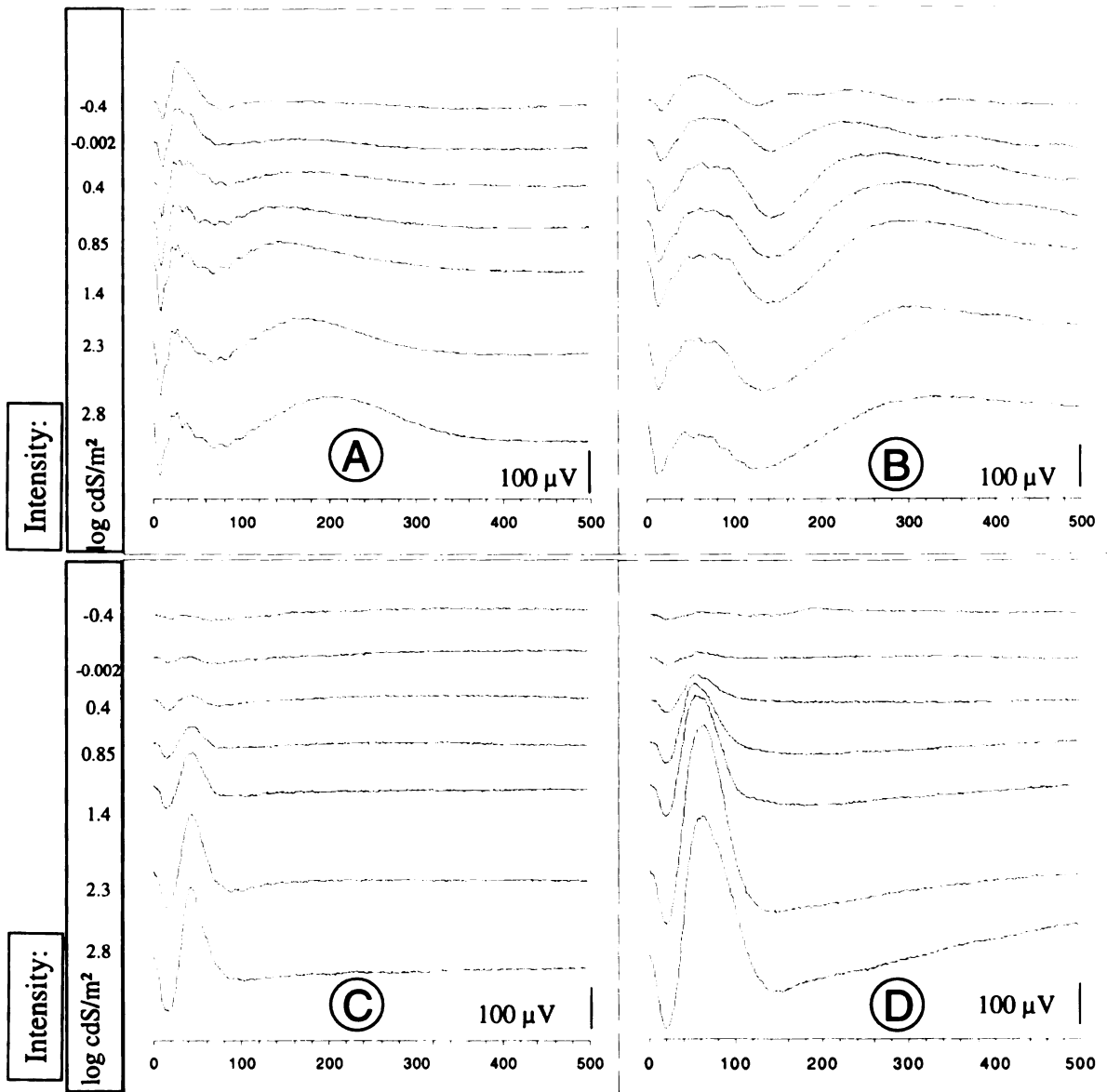


**Figure 4.4** - Representative ERGs performed before, (A) & (C), and after, (B) & (D), the intravitreal application of barium chloride. A & B are ERGs from a control bird while C & D are from an *rge* bird. Note in the control bird that after the intravitreal injection of barium (B) the amplitude of the a- and b-wave decreased. The implicit times of the a- and b-wave also increased. The c-wave amplitudes were higher when flash intensities below 1.4 log cdS/m<sup>2</sup> were used. In contrast, after application of barium to the *rge* birds (D), both a- and b-wave amplitudes increased, without an increase in a- and b-wave implicit times. Horizontal axis = mSec.

#### 4.3.5. Results after the intravitreal injection of ornithine (Figure 4.5)

After application of ornithine in the control group, the leading edge of the b-wave is depressed, resulting in a reduction in the mean overall b-wave amplitude (pre-injection mean =  $93.14 \pm 9.32 \mu\text{V}$ ; post-injection =  $22.30 \pm 27.85 \mu\text{V}$ ,  $P=0.0001$ ). The overall implicit time of the b-wave significantly increased (pre-injection mean =  $25.89 \pm 0.95 \text{ mSec}$ ; post-injection =  $30.58 \pm 3.60 \text{ mSec}$ ,  $P=0.0006$ ).

Ornithine did not significantly impact the mean overall a-wave amplitude of the control group (pre-injection mean =  $-70.15 \pm 15.24 \mu\text{V}$ ; post-injection =  $-55.60 \pm 31.98 \mu\text{V}$ ,  $P=0.19$ ) but, as expected when the b-wave is blocked or delayed, the a-wave implicit time is increased (pre-injection mean =  $8.20 \pm 0.84 \text{ mSec}$ ; post-injection =  $20.93 \pm 7.12 \text{ mSec}$ ,  $P=0.0001$ ). Ornithine also had no significant effect on c-wave amplitude (pre-injection mean =  $31.25 \pm 11.52 \mu\text{V}$ ; post-injection =  $55.40 \pm 27.29 \mu\text{V}$ ,  $P=0.36$ ) or implicit time (pre-injection mean =  $209.00 \pm 1.41 \text{ mSec}$ ; post-injection =  $190.05 \pm 39.52 \text{ mSec}$ ,  $P=0.56$ ).

In the *rge* group, the mean overall a-wave amplitude measured after the ornithine injection was numerically smaller compared to the pre-injection mean but was not significantly different (pre-injection mean =  $-28.07 \pm 19.83 \mu\text{V}$ ; post-injection =  $-24.09 \pm 19.53 \mu\text{V}$ ,  $P=0.6417$ ). The mean overall a-wave implicit was significantly increased (pre-injection mean =  $13.60 \pm 1.08 \text{ mSec}$ ; post-injection =  $18.46 \pm 1.65 \text{ mSec}$ ,  $P=0.0001$ ). The slope of the a-wave was also less steep after the injection. The mean overall amplitude of the b-wave was significantly decreased (pre-injection mean =  $79.25 \pm 14.77 \mu\text{V}$ ; post-

injection =  $42.50 \pm 5.65 \mu\text{V}$ ,  $P < 0.0001$ ) and the implicit time significantly increased (pre-injection mean =  $34.25 \pm 5.05 \text{ mSec}$ ; post-injection =  $44.35 \pm 1.78 \text{ mSec}$ ,  $P = 0.0001$ ) after the injection.

Comparable results were also observed in younger control and *rge* chicks.

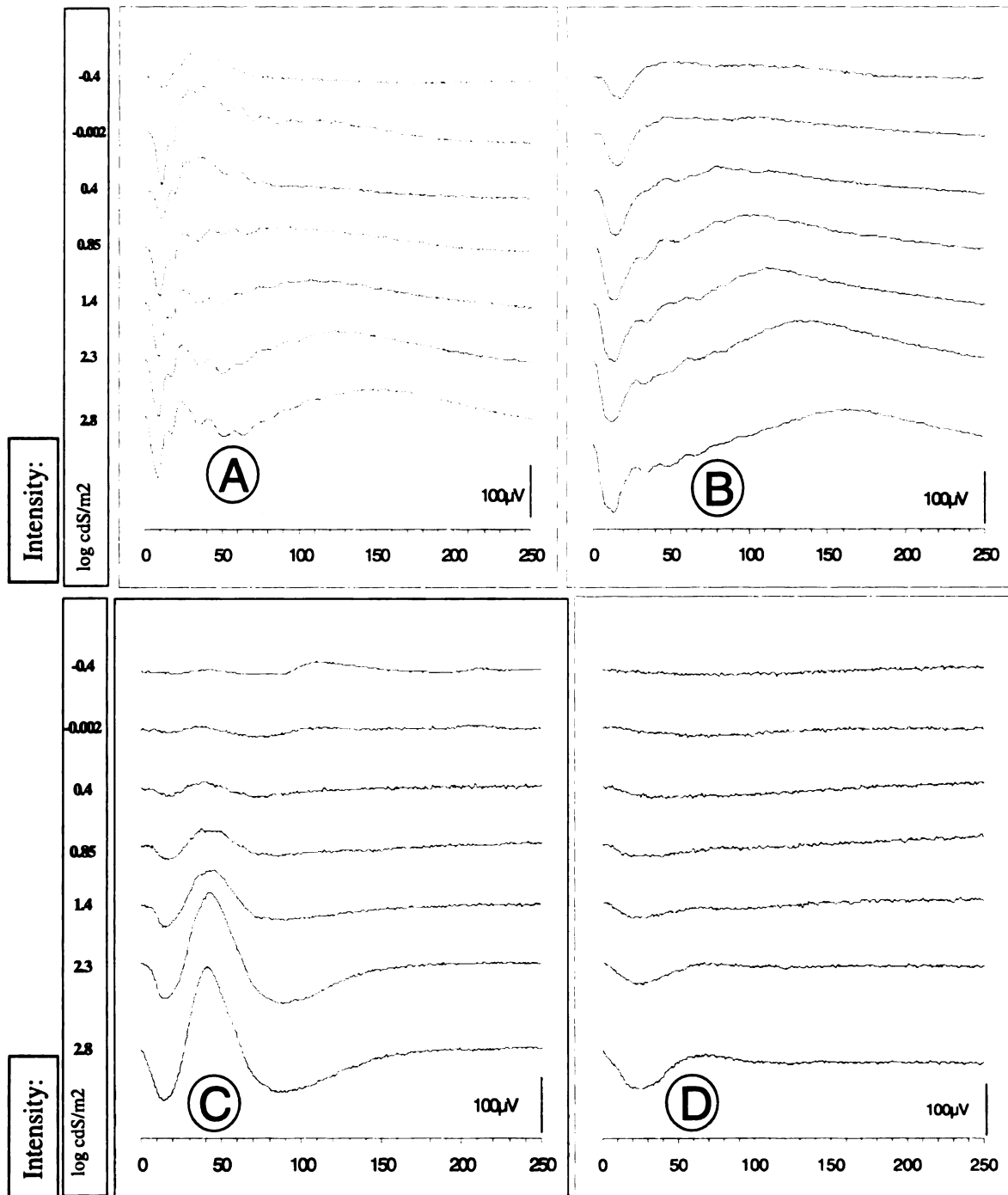


**Figure 4.5** - Representative ERGs performed before, (A) & (C), and after, (B) & (D), the intravitreal application of ornithine. A & B are ERGs from a control bird while C & D are from an *rge* bird. Note that in the control bird, after the intravitreal injection (B), the leading edge of the b-wave is depressed, resulting in reduced b-wave amplitude. Ornithine did not impact a-wave amplitude but, as expected when the b-wave is blocked or delayed, the a-wave implicit time was increased. In *rge* birds, the b-wave was nearly abolished after the application of ornithine (D). The mean a-wave was numerically smaller compared to the pre-injection values but was not statistically different. Horizontal axis = mSec. A younger *rge* chick (14 days of age) is depicted (C and D).

#### 4.4 Discussion

Previous ERG studies (see Chapter 3) showed that *rge* chicks have an elevated response threshold, slower waveforms that are abnormal in shape, a decrease in oscillatory potentials and a lack of c-waves. Interestingly, a unique electroretinographic abnormality of young *rge* chicks is the presence of abnormally elevated b-wave amplitude when flash intensities above  $0.9 \log \text{cdS/m}^2$  are used. The supernormal b-wave amplitude decreases with increasing age in the *rge* group, eventually becoming smaller in amplitude than the control b-wave. The results of the pharmacological dissection of the ERG show that the positive b-wave of *rge* birds is very different from the normal chick b-wave and is probably not generated from the same cells.

The intravitreal injection of PDA resulted in ERG changes in the control group that were similar to those previously described. PDA blocks negative-going horizontal cell and OFF-hyperpolarizing bipolar cell responses, which normally counteract the positive-going depolarizing bipolar cell response. The early depolarizing bipolar cell response is unmasked and alters the shape of the latter part of the a-wave and truncates it. This results in lower a-wave amplitudes. Due to the absence of horizontal cell and hyperpolarizing bipolar cell components, the unopposed depolarizing bipolar cell component results in a broader b-wave peak. The c-wave was abolished in the control group after the injection. A possible explanation is that when PDA is used, the b-wave is not pulled in a negative direction by horizontal cells and hyperpolarizing bipolar cells, the c-wave component might have been masked by the longer lasting b-wave peak. Alternatively, the implicit time of the c-wave might have increased to a degree that the c-

wave was not visualized within the recording time. The intravitreal injection of PDA in the *rge* group resulted in no significant changes in a- or b-wave amplitude or implicit time. Suggesting that the horizontal cell and hyperpolarizing bipolar cell responses do not play a significant role in generation of the ERG in the *rge* birds or, perhaps, these cells did not respond normally to the drugs.

As previously reported , intravitreal injection of APB to the control chick retina eliminated the depolarizing bipolar cell positive b-wave, which allowed the a-wave to continue its time course, resulting in an increased a-wave implicit time. The remaining waveform consisted of the photoreceptor-generated a-wave; horizontal cell and hyperpolarizing bipolar cell negative-going components and the positive c-wave. In contrast, the intravitreal injection of APB in the *rge* group had no significant effect. There were no significant differences in a- or b-wave amplitude and implicit time. Blocking with APB did not uncover an underlying c-wave component. This suggests that depolarizing bipolar cells in *rge* birds do not contribute significantly to the ERG waveform or for some reason are not blocked by APB.

Curiously, the c-wave could still be observed in the control group after the injections of PDA + APB. Perhaps the apparent c-wave present in the control after the PDA + APB injection is not a true c-wave (i.e. generated from RPE) but an exaggerated positive after-potential. Alternatively, the combined action of PDA + APB liberates the c-wave generator.

The intravitreal injection of both APB + PDA theoretically should eliminate contributions from depolarizing bipolar cells, horizontal cells and hyperpolarizing bipolar cell. After intravitreal injection of a combination of both agents in the control group, all



responses were eliminated as expected except for the photoreceptor-derived a-wave and the positive-going c-wave. The combination APB + PDA, however, had no significant effect on the ERG of the *rge* chicks. These results suggest that the large positive going b-wave present following the photoreceptor-derived a-wave in the *rge* chick does not have significant contributions from horizontal cells, hyperpolarizing bipolar cells or depolarizing bipolar cells because it is insensitive to agents that normally abolish the b-wave. As these agents act by mimicking the neurotransmitter that stimulate the second order neurons of the retina, it seems likely that these neurons are not activated in the *rge* retina after stimulation of the photoreceptors. An alternative and less likely hypothesis would be that these cells actually participate in the formation of the supernormal b-wave of the *rge* chicks but their glutamate receptors are somehow abnormal and are not blocked by the drugs used.

After the intravitreal injection of barium in the control birds, the amplitude of the a- and b-wave decreased and the implicit times of the a- and b-wave increased. Inversely, when  $K^+$  conductance of Müller cells is blocked by barium in *rge* birds; both a- and b-waves were dramatically increased in amplitude suggesting that the response is inhibited by  $K^+$  conductance.

Ornithine attenuated the b-wave in control chicks but had a much more dramatic effect in *rge* chicks, nearly completely blocking the positive-going b-wave response. This “Ornithine Sensitive Component” (OSC) of the b-wave, however, was not exclusive to the *rge* chick. Application of ornithine in the control birds resulted in a smaller reduction of the b-wave amplitude. However, the magnitude of the response of the OSC in the *rge* group seems to be very unique indeed. Ornithine must have some action to block b-wave

generators. However, in the *rge* mutant where most of the normal b-wave generators (horizontal and bipolar cells) make no contribution to the positive-going response the drug must have an effect on another cell type, perhaps the photoreceptor cells. The hypothesis that *rge* photoreceptors are affected by ornithine is partially substantiated by the observed change in slope of the a-wave and the smaller, even though not significantly different, mean a-wave amplitude.

The only two agents that affected a change in the *rge* ERG were barium and ornithine. Barium enhanced the response and ornithine nearly abolished it. Although ornithine might have an effect on amacrine cells, it seems unlikely that these cells are the origin of the supernormal *rge* b-waves because the normal electrophysiological response of amacrine cells tend to oscillate and the abnormal b-wave response in the *rge* birds is much greater than the usual amacrine responses and is consistently depolarizing. Therefore, possible sources of this large depolarization in *rge* chicks are the photoreceptors or RPE. It seems, however, that the supernormal b-wave of the *rge* chicks are too fast to be coming from the RPE. Additionally, the normal RPE response, the c-wave is a much slower response than the supernormal b-wave.

The idea that the normal b-wave generators are not involved in the formation of the *rge* b-wave is in keeping with the finding that the organization of the rod terminals and cone triads (dendritic terminals of bipolar cells and horizontal cells) and the corresponding ribbons is severely disrupted in the *rge* birds. Furthermore, the synaptic ribbons also appeared to be less numerous in the *rge* birds. Therefore, is not surprising to find abnormal transmission between photoreceptors and second order neurons.

Only exuberant Müller cell processes are abundant at the OPL/ONL level in the *rge* retinas. In fact, abnormal OPL morphology is the first recognizable ultrastructural abnormality observed in the affected chicks at the first time-point evaluated (at hatch). Müller cells could be involved with the abnormal b-wave waveform of the *rge* chicks, since the b-wave amplitude was greatly reduced by ornithine and this cell type has shown to express high levels of ornithine aminotransferase . Abnormal sprouting of Müller cells and re-wiring of retinal neurons at the OPL in *rge* retinas might underlie the reason for the different responses observed in the controls versus *rge* when K<sup>+</sup> conductance of these cells is blocked with the application of barium.

Further studies to explain the abnormal ERG waveforms in the *rge* bird are discussed in Chapter 7.

## CHAPTER 5

# DETAILED MORPHOLOGIC CHARACTERIZATION OF THE *rge* CHICK PHENOTYPE

### 5.1. Introduction

As discussed in Chapter 2, there is a variable degree of vision loss in *rge* chicks at 1 day of age with deterioration in vision over the next few weeks until all chicks are unable to see food particles on the floor and behaviorally act as if they are blind. However, optokinetic responses can still be induced in some birds until about several months of age. The affected birds develop a globe enlargement, apparently secondary to the vision deterioration. The *rge* chicken phenotype is unusual in that the ERG, although abnormal from initial development, only slowly deteriorates and is maintained for several months after functional vision loss (see Chapter 3). Therefore, in *rge* chicks loss of vision does not appear to correlate directly with a loss of photoreceptor function (as assessed by the ERG). Another unusual feature is that no outstanding light microscopic structural abnormalities of the retina were apparent initially and there was only a slow progressive thinning of retinal layers apparent after the age of functional vision loss. Thus, in order to understand the underlying structural changes of the *rge* phenotype, a detailed characterization of the histological changes was necessary. The purpose of the study reported in this chapter was to examine the histopathological changes in the retina of the *rge* birds in more detail by light microscopy (LM), immunocytochemistry (IHC) and electron microscopy (EM).

## 5.2. Material & Methods

A flock of *rge* birds was maintained at MSU and bred to produce homozygous affected (*rge/rge*), heterozygous carrier (*rge/+*) and homozygous normal (*+/+*) chicks. Progeny from *rge/rge* crossed with *rge/+* birds were phenotyped by ERG, as described previously (Chapter 3). All experiments and procedures were carried out in accordance with the ARVO Statement for the Use of Animals in Ophthalmic and Vision Research and approved by the Institutional Animal Use Committee.

Immediately following euthanasia using a CO<sub>2</sub> chamber, bilateral enucleation was performed. The eyes were hemisected at the equator, the vitreous body removed and the posterior segment of the eye immersed into one of the different types of fixatives used (see below). Samples from control and *rge* birds were studied at several different ages.

### 5.2.1. Morphometric analysis

Retinal thickness was measured on plastic-embedded histological sections at 6 consistent locations across the retina (Figure 5.1). The retinal regions analyzed were defined by measuring the ventral and dorsal retinal lengths from pecten to *ora serrata* under 10x magnification (Figure 5.1 A) using the software SPOT version 3.5 for windows (Visitron Systems, GmbH). The distance from pecten to *ora serrata* was divided by 3 (ventral) or 5 (dorsal) (Figure 5.1 B) to give the 6 locations for measurement of retinal thickness (Figure 5.1 C). Digital images were acquired under 400x magnification

and stored using the same software. Subsequently, Image Pro Plus version 4 (IP4) software (Media Cybernetics) was used to measure the histological thickness of 7 retinal layers defined as: nerve fiber layer + ganglion cell layer (NFL+GCL); inner plexiform layer (IPL); inner nuclear layer (INL); outer plexiform layer (OPL); outer nuclear layer (ONL); photoreceptor inner and outer segment layer (IS+OS) and retinal pigment epithelium (RPE). For each layer 5 replicate measurements were performed. Total retinal thickness was also measured at each of the six points. Care was taken to ensure that the sections were oriented perpendicular to the retinal surface.

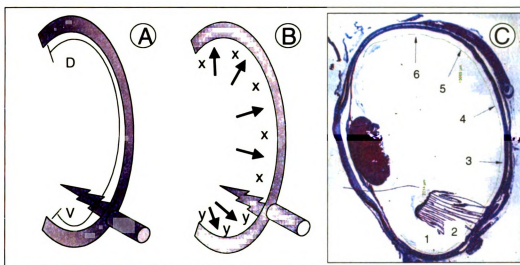


**Figure 5.1** - Graphic representation of the method used for determining the retinal regions used for retinal thickness measurement. A) Measurements were made of retinal length from the *ora serrata* (D and V - dorsal and ventral) to the pecten/optic nerve (PCT+ON). B) The value D was divided by 5, resulting in x and the value V was divided by 3, resulting in y. Starting at the center of PCT+ON, x and y values (dorsally and ventrally, respectively) were consecutively applied to determine the regions to be evaluated for retinal thickness. C) Cross section of a chick eye globe showing the 6 positions at which retinal thickness measurements were made.

Using paraffin embedded sections labeled with rhodopsin antibody (see details of the staining technique below), rod OSs were manually counted in 200  $\mu\text{m}$  segments of retinal length, using the same 6 regions described above. Additionally, the numbers of rows of cells in the INL, at each region, as well as the number of ganglion cells per 200  $\mu\text{m}$  at each of the same 6 retinal regions were measured. The number of rows of nuclei in the ONL is commonly used as a parameter of photoreceptor cell density in histological studies of retinal degeneration in other species . In the case of birds, the ONL is a bi-layered nuclei row, with rod nuclei located more internally than cone nuclei and therefore counting the number of rows of nuclei would not be a sensitive measure of photoreceptor density.

Statistical analyses for retinal thickness measurements, number of rod outer segments and ganglion cells per unit length as well as for the number of rows in the INL were performed by one-way ANOVA and *t*-test (when comparing one time-point between two groups). The tests were run in two different types of statistical analysis software (StatView and SAS 2001 - version 8.2. SAS Institute). If any statistically significant difference was found the data were further analyzed using *post hoc* comparisons with Fisher's or Tukey-Kramer tests. Differences between means were deemed significant when  $P < 0.05$ .

### 5.2.2. Conventional morphologic analysis of semi-thin and ultra-thin sections

The eyecups were fixed in phosphate buffered (0.1 M, pH 7.3) 3% paraformaldehyde + 2% glutaraldehyde solution for 3 hours at room temperature. A square shaped tissue sample (about 2 x 2 mm) per eye was collected from the central retina, subsequently post-fixed in 1% OsO<sub>4</sub> at 4°C for 2 hours, washed in distilled water, then dehydrated in acetone and finally embedded in an Araldite-based resin (Durcupan, Fluka). Semi-thin (0.5-1 µm) and ultra-thin (80 nm) sections were cut using a Reichert Jung ULTRACUT ultra-microtome, using glass and diamond knives, respectively. Semi-thin sections were stained with toluidine blue solution and examined by light microscopy and images recorded with a Polaroid DMC digital camera mounted on a Nikon Eclipse E400 Microscope. Ultra-thin sections were mounted on copper grids, stained with lead citrate and uranyl acetate, and examined and photographed in a Zeiss EM 109 transmission electron microscope (TEM). TEM photographic negative films were digitalized using a Polaroid SprintScan 35 Plus scanner.

A search for possible apoptotic nuclei was conducted using standard morphological criteria utilizing both semi-thin and ultra-thin sections.

Dr. Rafael Cernuda at the Institute of Cellular Signaling (University of Nijmegen, Netherlands), performed part of the TEM analysis.



### 5.2.3. Immunocytochemistry studies on paraffin-embedded material

For conventional staining as well as for IHC analyses at the light microscopic (LM) level, retinal samples were fixed in 4% paraformaldehyde, 3% sucrose in 0.1 M phosphate buffer for 48 hours at 4°C and then dehydrated in ethanol and embedded in paraffin blocks prior to sectioning. Eight-µm thick sections were cut and mounted on double-gelatinized glass slides. After deparaffination in xylene, sections were rehydrated gradually in ethanol and, finally in distilled water. IHC analysis was carried out by single labeling with the following antisera:

- Mouse opsin monoclonal antibody at 1:1000 (Lab Vision)
- Rabbit anti-glial fibrillary acidic protein (GFAP) at 1:2000 (Dako)
- Tyrosine hydroxylase at 1:1000 (Chemicon International)
- Guanylate cyclase-activating protein (GCAP1) at 1:400 (a gift from Dr. Palczewski, University of Washington)

The peroxidase-conjugated Vectastain ABC (avidin-biotin complex) kit (Vector) was employed as a detection system. Labeled sections were dehydrated in ethanol, cleared in xylene, mounted in a hydrophobic medium (Entellan, Merck) and examined by LM.

#### 5.2.4. Immunocytochemistry studies on frozen sections

The retinal samples were immersed in 4% paraformaldehyde plus 3% sucrose in 0.1 M phosphate buffer, pH 7.4 or Carnoy fixative (for RCA-1) for 30 minutes at room temperature (for RCA-1). Fixed tissues were washed three times in phosphate-buffered saline plus 0.05 M phosphate buffer and 195 mM NaCl, pH 7.4, (PBS), and cryoprotected in PBS plus 30% sucrose overnight, at 4°C. Cryoprotected tissues were soaked in embedding medium (O.C.T.-compound; Tissue-Tek) for 30 minutes and freeze-mounted onto sectioning blocks. Vertical 14 µm thick sections were cut on a Reichart-Jung Fridgocut<sup>™</sup> 2500 and thaw-mounted onto Super-Frost<sup>™</sup> slides (Fisher Scientific). Sections from control and *rge* eyes were placed together in pairs on each slide to ensure equal exposure to reagents. Sections were air-dried and stored at -20°C until use.

Sections were thawed at room temperature, ringed with lubricant, and washed two times in PBS. They were then covered with primary antibody solution (150 µl of antibody diluted in PBS, plus 0.3% Triton X-100 and 0.01% NaN<sub>3</sub>) and incubated for about 24 hours at room temperature in a humidified chamber. The slides were washed two times in PBS, covered with the secondary antibody solution and incubated for at least 1 hour at room temperature in a humidified chamber. Finally, they were washed three times in PBS and a coverslip was applied in 4:1 (v/v) glycerol to water.

Working dilutions and sources of antibodies used in this study included the following:

- Mouse anti-lysosomal glycoprotein at 1:80 (LEP-100; Developmental Studies Hybridoma Bank (DSHB))
- Rat anti-glycine at 1:1000 (a gift from Dr. D. Pow, University of Queensland)
- Rabbit anti-tyrosine kinase A (TrkA) at 1:5000 (a gift from Dr. F. Lefcort, Montana State University)
- Mouse anti-neurofilament at 1:2000 (RMO270; Zymed)
- Mouse anti-vimentin 1:50 (H5; (DSHB))
- Mouse anti-Islet1 at 1:50 (39.4D5; DSHB)
- Mouse anti-Hu at 1:200 (Monoclonal Antibody Facility, University of Oregon)
- Mouse anti-rhodopsin at 1:800 (rho4D2; a gift from Dr. R. Molday, University of British Columbia)
- Mouse anti-tyrosine hydroxylase at 1:100 (DSHB)
- Rabbit anti-glial fibrillary acidic protein (GFAP) at 1:2000 (Dako)
- Mouse anti-visinin at 1:100 (DSHB)
- *Ricinus communis* agglutinin-1 (RCA-1) (produced by one of the authors SSC)
- Tfbp-transferrin binding protein (TfBP) (produced by SSC)
- Mouse anti- $\beta$ 3 tubulin at 1:2000 (TUJ-1; Babco)
- Calbindin D28 at 1:1000 (Sigma-Aldrich)
- Mouse anti-glucagon at 1:400 (a gift from Dr. M. Gregor, University of Tuebingen, Germany)
- Rabbit anti-caspase-3 at 1:1000 (R&D Systems)
- Rabbit anti-synaptobrevin (anti-VAMP-1) at 1:400-1:800 (Synaptic Systems)

- Mouse anti-synaptic vesicle protein 2 (SV2) at 1:25 (a gift from Dr. Kathleen Buckley, Harvard Medical School)
- Mouse anti-GABA-A receptor Beta subunit at 1:100-1:500 (clone 62-3G1 - Upstate Biologicals).

The same detection method described above for the paraffin embedded sections was used for the frozen sections. Secondary antibodies used for both (paraffin and frozen sections) included goat-anti-rabbit-Alexa568, goat-anti-mouse-Alexa568, goat-anti-mouse-Alexa488, goat-anti-rat-Alexa488 (Molecular Probes) and goat anti-mouse-Cy3, diluted to 1:500 in PBS plus 0.3% Triton X-100.

Fluorescence photomicrographs were taken by using a Ziess Axioplan II microscope equipped with epifluorescence, FITC and rhodamine filter combinations, and a Spot<sup>TM</sup> Slider-RT digital camera (Diagnostic). Images were optimized for color, brightness and contrast by using Adobe Photoshop<sup>TM</sup> 6.0.

Dr. Andy Fischer (Department of Neuroscience, The Ohio State University, Columbus, Ohio), performed the fluorescence photomicrographs on the immunocytochemical analysis of frozen retinal sections. Dr. Sa Sun Cho (Department of Anatomy, Seoul National University College of Medicine, Seoul, Korea), performed the immunocytochemical stainings using RCA-1 and TfBP antibodies.

#### 5.2.5. Terminal Deoxynucleotidyl Transferase-mediated dUTP Nick End Labeling (TUNEL) Staining

TUNEL staining was performed to identify cells undergoing apoptosis, following previously described techniques in retinal sections from *rge* and control birds at 13 and 30 days of age. In brief, slides were warmed to 20°C and washed once in PBS, followed by one wash in PBS plus 0.3% Triton X-100, and two more washes in normal PBS. Sections were then covered with 100 µl of incubation medium (0.5 nmol Cy3-conjugated dCTP, 20 units of 38-terminal deoxynucleo-tidyl transferase, 100 mM sodium cacodylate, 2 mM CoCl<sub>2</sub>, and 0.25 mM beta-mercaptoethanol in sterile saline, pH 7.2) and incubated for 1 hour in a humidified chamber at 37°C. The sections were then washed three times in PBS, mounted in 4:1 (v/v) glycerol to water, and coverslips were added for observation by epifluorescence with a rhodamine filter combination.

#### 5.2.6. Detailed examination of the linear fundus lesions in semi-thin and ultra-thin sections

In their preliminary description of the *rge* phenotype noted the presence of white streaks extending from the base of the pecten in some affected birds. In our detailed description of the phenotype (Chapter 2) we also noted the development of these lesions in some of the affected birds. With the objective of better characterizing these lesions, a

more detailed histopathological study focusing only on the retinal portions displaying these lesions was performed using the same LM and EM techniques described above. Selected *rge* birds identified with fundus lesions were sacrificed at the following ages: 2 birds at 49 days of age, 1 at 84 days of age and 1 at 336 days of age. The globes were processed for histological examination as described above. Histological changes in the retina, Bruch's membrane, and choroid were examined by LM and EM.

### 5.3. Results

No significant differences were observed between heterozygous carrier (*rge/+*) and homozygous normal (+/+) chicks on light and electron microscopy analysis as well as by immunocytochemistry techniques using several cell type-specific markers. Thus these two groups were treated as one single control group in the study.

#### 5.3.1. Morphological measurements of the retina

At 2 days of age there was no difference in retinal thickness of *rge* chicks compared to controls but by 14 days of age the retina had significantly thinned ( $P < 0.05$ ) ( $574.51 \pm 13.47 \mu\text{m}$  compared to  $672.81 \pm 11.35 \mu\text{m}$ ) (Figure 5.2). From this age point onwards, a slow thinning of the retina continued in the *rge* birds. There was a geographic difference in the rate of thinning. The ventral regions (#1 and #2) and the far dorsal peripheral region (#6) were the ones that presented the greatest initial reduction in thickness (Figure 5.3 B). At 14 days of age the thickness (mean of all 6 retinal regions

measured) of the NFL+GCL ( $109.84 \pm 48.71 \mu\text{m}$  versus  $175.23 \pm 9.40 \mu\text{m}$ ), IPL ( $193.24 \pm 3.80 \mu\text{m}$  versus  $202.61 \pm 3.80 \mu\text{m}$ ) and INL ( $177.48 \pm 3.60 \mu\text{m}$  versus  $190.34 \pm 3.80 \mu\text{m}$ ) layers of the retina were significantly lower ( $P < 0.0001$ ) in *rge* birds than in controls. By 56 days of age, most retinal layers became significantly thinner ( $P < 0.001$ ) in the *rge* birds, except the OPL, ONL and RPE. The difference in the above mentioned layers became even greater in older birds (Figures 5.2 & 5.3). By 270 days of age all retinal layers with exception of the RPE of all six retinal regions became significantly thinner compared to controls ( $P < 0.0001$ ) (Figure 5.3 C & D).

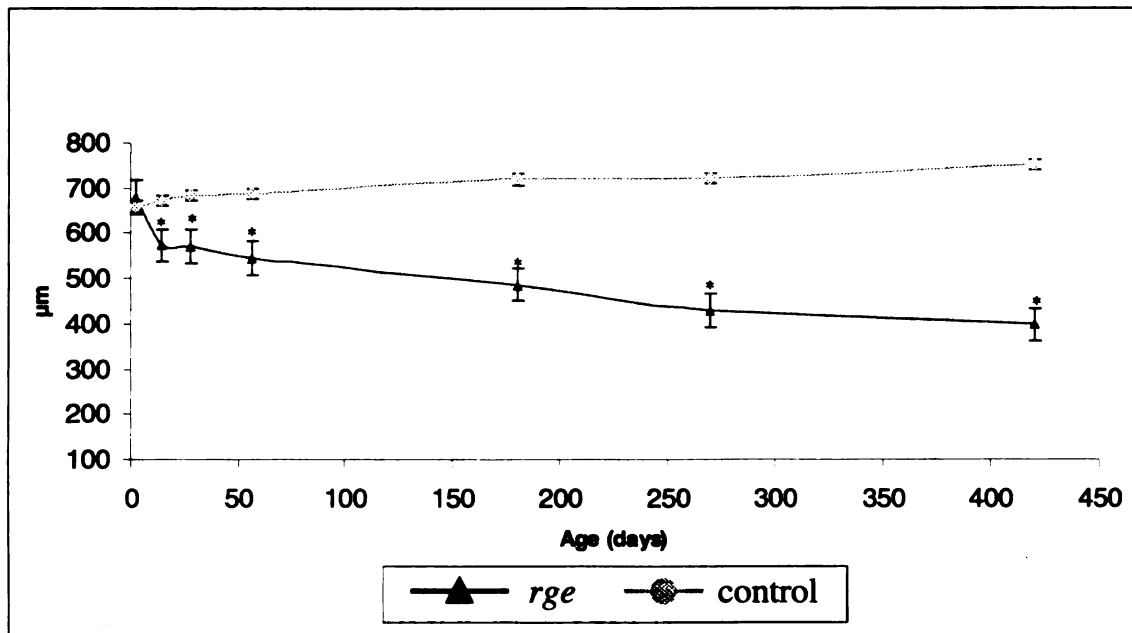


**Figure 5.2** - Total retinal thickness of *rge* (continuous black line with triangles) and control birds (continuous gray line with circles) at 2, 14, 28, 56, 180, 270 and 420 days of age. Note that the mean retinal thickness decreases with age in the *rge* group. The retinal thickness of *rge* chicks ( $574.51 \pm 13.47 \mu\text{m}$ ) was significantly thinner ( $P < 0.05$ ) than controls ( $672.81 \pm 11.35 \mu\text{m}$ ) by 14 days of age ( $n = 4$  for each group; \* =  $P < 0.05$ ).

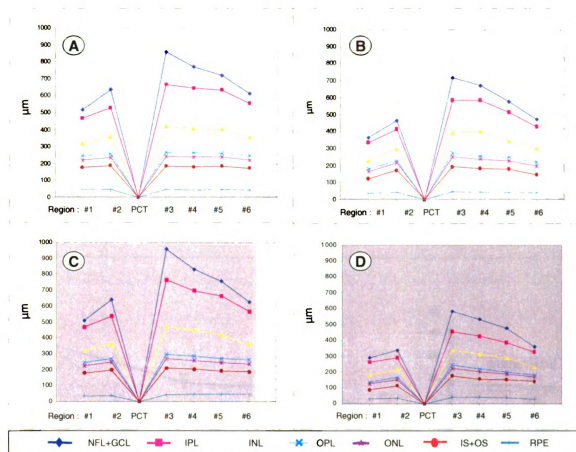


**Figure 5.3** - Mean retinal thickness of each of the different retinal layers from *rge* (B & D) and control (A & C) birds at two representative age groups. By 56 days of age (A & B), mean thickness of NFL+GCL, IPL, INL and also OS+IS layer were already decreased. Note that the ventral regions (#1 and #2) as well as the far dorsal peripheral region (#6) were the ones that presented the greatest reduction in thickness. In retinas from birds at 270 days of age (C & D), the thickness of the NFL+GCL, IPL and IS+OS retinal layers were remarkably smaller. At 56 days of age  $n = 6$  *rge*, 4 controls at 270 days of age  $n = 4$  *rge* and 5 controls. Key: RPE – retinal pigment epithelium; IS+OS – inner segments + outer segments; ONL – outer nuclear layer; OPL – outer plexiform layer; INL – inner nuclear layer; IPL – inner plexiform layer; NFL+GCL – nerve fiber layer + ganglion cell layer.

A progressive and significant ( $P < 0.01$ ) overall decrease in the number of rod OS per 200 μm length of retina occurred in the *rge* birds with age. By 21 days of age the overall mean rod OS number in *rge* retinas ( $26.30 \pm 5.14$ ) became significantly lower ( $P < 0.05$ ) than controls ( $33.25 \pm 5.91$ ) (Figure 5.4).



Additionally, the mean number of nuclei rows of the INL in the *rge* group decreased with age but only became significantly lower at 270 days of age ( $P=0.0058$ ). At this age the mean number of nuclei rows in the INL was  $2.95 \pm 0.94$  and for controls it was  $6.67 \pm 1.59$  (Figure 5.4).

The mean number of ganglion cells per 200 $\mu$ m of retinal length of both *rge* and controls tended to decrease with age, however there was no significant difference between *rge* and control groups at the ages assessed (up to 720 days of age) (Figure 5.4).

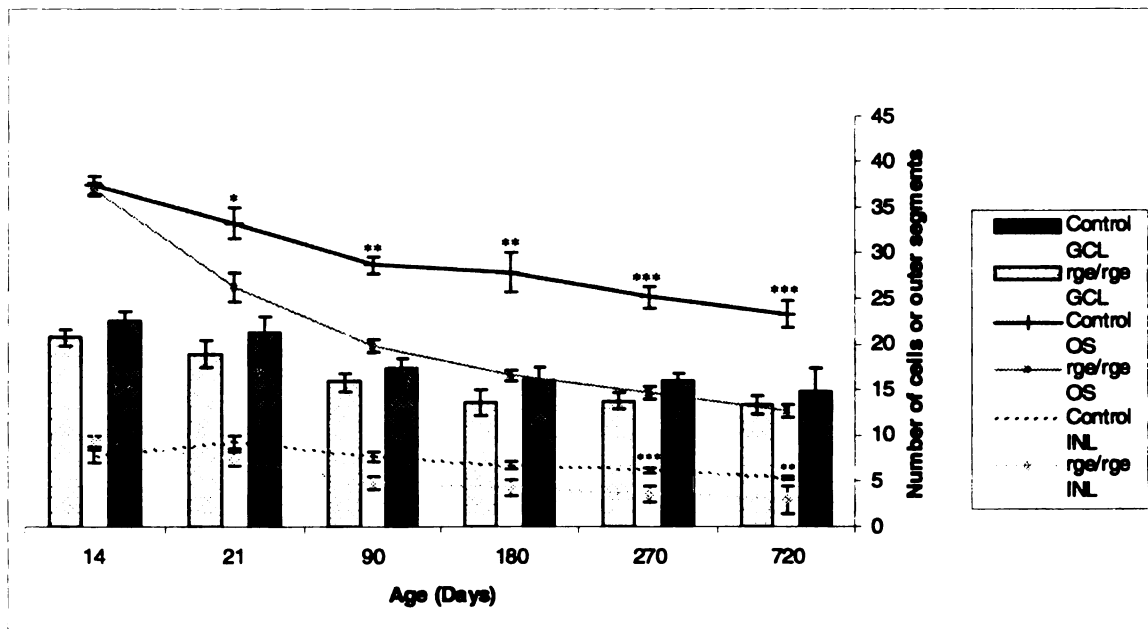


**Figure 5.4** - Number of rod OSs and ganglion cells per unit length and number of rows in the INL in cross sections (average of all retinal regions) in cross sections at 14, 21, 90, 180, 270 and 720 days of age. Note the progressive and significant ( $P<0.01$ ) overall decrease in number of rod OSs per 200  $\mu$ m of retina tissue length in the *rge* retinas. At 21 days of age the difference is already significant. Additionally, the mean number of INL cells per column in the *rge* group became significantly smaller at 270 days of age ( $P<0.0001$ ) ( $n = 4$  *rge*, 3 controls). The mean number of ganglion cells per 200  $\mu$ m of retinal length was not statistically significant between the two groups. A mean number of 4 retinal samples from *rge* and control birds were analyzed from each age group. Asterisks indicate significance:  $*=P<0.01$ ,  $**=P<0.001$  and  $***=P<0.0001$ . Key: OS – mean number of rod outer segments (immunocytochemically labeled for rhodopsin) per 200  $\mu$ m length of retina; INL – mean number of nuclei rows of inner nuclear layer; GCL – mean number of ganglion cells per 200  $\mu$ m length of retina.

### 5.3.2. Observations on semi-thin and ultra-thin sections, light and electron microscopy

No ultrastructural evidence for apoptotic nuclei was found in *rge* sections using the standard morphological criteria in semi-thin or ultra-thin sections in any of the age groups studied.

#### **5.3.2.i. Retinal sections at 1 day of age**

Semi-thin sections from *rge* chicks at 1 day of age (Figure 5.5 B) revealed that the basic morphological retinal features were similar to the controls (Figure 5.5 A). However, the cell bodies within the ONL of the *rge* sections appeared consistently somewhat dilated and less fusiform shaped compared to the controls. The most striking difference was observed in the OPL. In the control chicks the photoreceptor terminals formed two distinct layers (Figures 5.5 A & C). This regular stratification was not present in the *rge* retinas (Figure 5.5 B & D). Furthermore, the photoreceptor pedicles appeared distorted in *rge* sections (compare Figure 5.5 D with 5.5 C). There also appeared to be an abnormal positioning of the smooth endoplasmic reticulum (SER) in some cone photoreceptor cells of *rge* birds. In the accessory cones of control birds SER containing some glycogen granules was present in the ISs of rods (as part of the hyperboloid) and accessory cones (as part of the paraboloid) whereas in the *rge* retinas the SER of the accessory cones were located internal to the outer limiting membrane, close to the nucleus (Figure 5.6).

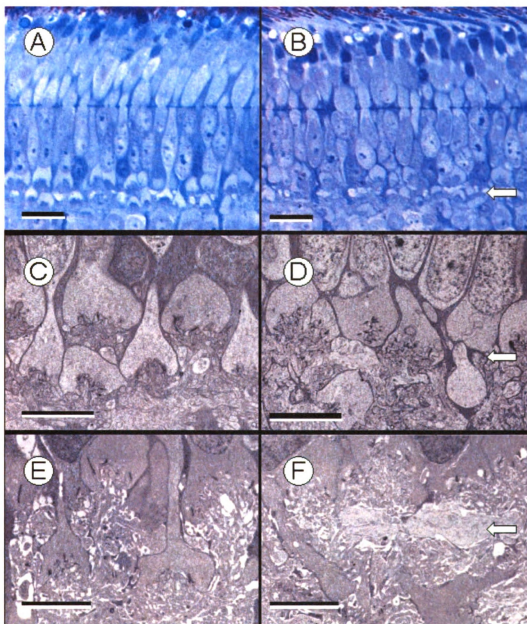


**Figure 5.5** - Semi-thin (A & B) and ultra-thin (C & D) retinal sections of a control (A & C) and of an *rge* chick (B & D), respectively, at 1 day of age. E & F are ultra-thin sections of a control (E) and an *rge* chick (F) at 60 days of age. A) Semi-thin section of a control chick demonstrating the detail of the well organized outer OPL. Stain = Toluidine blue (A & B). Bar = 10  $\mu$ m. B) Note the dilated photoreceptor cell bodies and the disorganization of the OPL architecture in the sample from an *rge* bird. Bar = 10  $\mu$ m. D) Note the disruption of the photoreceptor pedicles and spherules. The 2-layer arrangement of the photoreceptor pedicles is lost. Bar = 5  $\mu$ m. Note that there are fewer synaptic ribbons in the *rge* section (F) compared to control (E). The 2-layer arrangement of the photoreceptor pedicles and spherules is even further disorganized in the *rge* section at this age. Bar = 5  $\mu$ m.

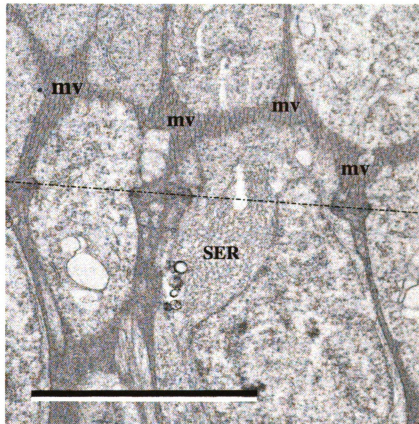


**Figure 5.6** - Ultrastructural features of the ONL/IS interface of an *rge* chick, at 1 day of age. Note the displacement of the SER (marked as SER), which in this sample, appear to be located at the perinuclear cytoplasm of an accessory cone, internal to the level of the outer limiting membrane (dashed line). At this age accumulation of glycogen is not apparent (compare with Figures 5.7 & 5.10). Müller cells microvilli are marked as “mv”. Bar = 5  $\mu$ m.

### **5.3.2.ii. Retinal sections at 7 days of age**

By 7 days of age the OPL of the *rge* chicks was more disorganized than at 1 day of age (Figure 5.7 A). Cone pedicles were increased in size compared to controls (Figure 5.8 A). These abnormally wide terminals were not as electron-dense as those of controls and often contained sets of numerous flattened (tubuliform) small vesicles, and

multivesicular bodies (Figure 5.8 C). The number of synaptic ribbons observed in the cone pedicles and rod spherules also appeared to be reduced in all sections from *rge* birds examined. At the IPL, however, no apparent difference in ribbon numbers between *rge* and controls could be appreciated. Additionally, exuberant electron-dense glial processes were observed around the photoreceptors. The organelles of the *rge* photoreceptors also showed further changes. In control retinas the ISs of the accessory cells had well-arranged SER, with small glycogen granules present among the cisterns. There was a geometrical arrangement of the cisternae, as well as a close relationship with the rough endoplasmic reticulum (RER). By comparison, *rge* retinas had larger glycogen deposits in the ISs of the accessory cells of double cones and a displacement of these deposits toward the nucleus in some cases (Figure 5.7). Large glycogen deposits were also found in EM sections at abnormal locations in the accessory cells of double cones, i.e. ISs, supranuclear cytoplasm (Figure 5.7 A & B), and in the subnuclear cytoplasm, close to the synaptic regions and associated with SER and RER (Figure 5.7 C & D).

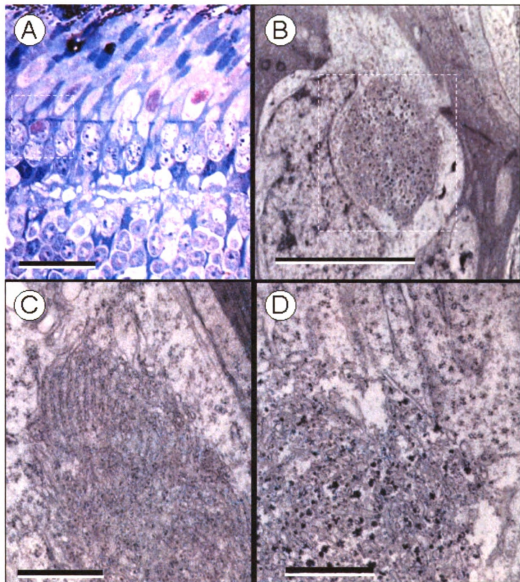


**Figure 5.7** - Semi-thin (A) and ultra-thin (B, C & D) sections of *rge* (A, B & D) and control (C) retinas at 7 days of age. A) Semi-thin section showing the detail of a large glycogen deposit (dashed white square) in the perinuclear cytoplasm. Note the disrupted OPL. Bar = 20  $\mu\text{m}$ . B) Ultrastructural detail of a deposit in the perinuclear cytoplasm of an accessory cell of double cone of an *rge* bird where it is possible to observe the abnormal accumulation of glycogen (dashed white square). Bar = 5  $\mu\text{m}$ . C) Control retina showing evenly-arranged SER in the IS (paraboloid). Small glycogen granules can be seen among the cisternae. Bar = 1  $\mu\text{m}$ . D) Abnormal glycogen accumulation associated with SER & RER in an *rge* retina at 7 days of age (same as in Figure B). Bar = 1  $\mu\text{m}$ .

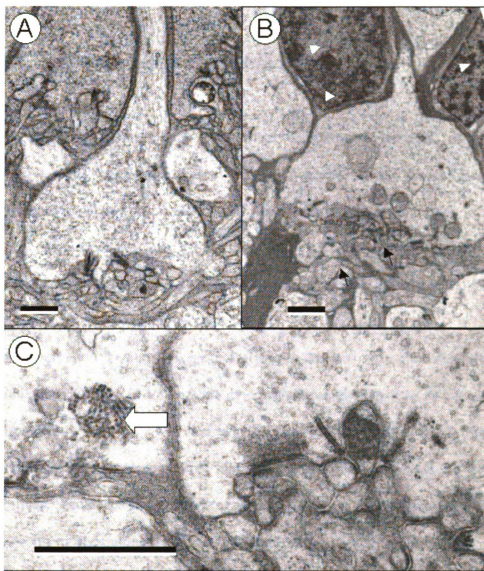


**Figure 5.8** - A) Synaptic terminal of a cone pedicle of a control chick at 7 days of age. B) A typical example of a synaptic terminal of a cone pedicle of an *rge* chick at 7 days of age. The cytoplasm is less densely stained. Note the disruption in the architecture of the synaptic terminals (small black arrows). Also note the presence of electron-dense glial processes separating the photoreceptors (white arrowheads). C) Higher power detail of an *rge* retinal section at 7 days of age demonstrating one of the sets of numerous flattened (tubuliform) small vesicles, and multivesicular bodies (wide white arrow) in a cone pedicle. Bars = 1  $\mu$ m.

### **5.3.2.iii. Retinal sections at 60 to 90 days of age**

At 60-90 days of age there was further disruption of the OPL of *rge* birds compared to younger age groups. Large Müller cell processes were present in the OPL and occasionally separated the somata of the photoreceptor cells in *rge* retinas. Abundant Müller cell processes and microvilli could also be seen among the ISs of the photoreceptor cells (Figure 5.9 A). The numbers of discernible ribbons at the OPL was also even more decreased (see Figures 5.5 E & F).

As observed in previous age groups, glycogen deposits were often displaced from the normal position in the IS towards the cytoplasmic perinuclear areas of the accessory cells of double cones, as well as of the rod cells (Figure 5.9 B). The glycogen deposits in rods of *rge* birds were larger than those that could occasionally be seen in the rod ISs of control retinas. Some occasional whorls of membranes (myelinoid figures) could be seen in the rod cells, most commonly in the subnuclear cytoplasm (Figure 5.9 C).

### **5.3.2.iv. Retinal sections at 270 days of age**

By this age the retinal thickness of *rge* birds was markedly decreased compared to controls (Figure 5.2, also compare Figure 5.3 C with D and 5.10 A with B). Both rod and cone photoreceptors could still be readily identified, although the OSs were considerably shorter (Figure 5.10 B & C). The spaces occupied by Müller cell processes were



progressively wider and the photoreceptor cells seem to be further separated at this age (Figure 5.10 D). In addition, cone OSs appeared disorganized, shorter than controls with disruption of the discs (Figure 5.10 C). The abnormal photoreceptor glycogen deposits were larger than in the other stages and often displaced internal to the outer limiting membrane (in the perinuclear cytoplasm) in many of the accessory cells and rod cells (Figure 5.10 B & D). As they were larger, they appeared more metachromatic (pink in color) in toluidine blue-stained semi-thin sections (Figure 5.10 B). In contrast, control retinas only had glycogen deposits in the ISs of the accessory cones and rod cells, as normally expected (Figure 5.10 A). In *rge* sections, photoreceptor synapses in the OPL were even more disorganized than at earlier ages. The numbers of discernible ribbons at the OPL in the *rge* sections were also even more reduced compared to the younger *rge* birds but a few could still be observed, sometimes very close to the displaced glycogen deposits.

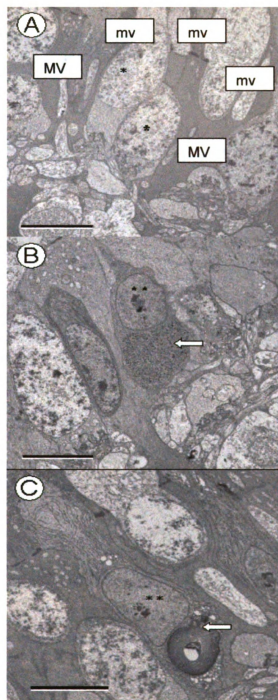


**Figure 5.9** - Ultra-thin sections of retinal samples from *rge* birds at 60 days of age. Cone cell nuclei (\*) and rod cell nuclei (\*\*) are labeled. A) Gaps between photoreceptor cell bodies were occupied by Müller cell processes (MC). Abundant long microvilli (mv) of Müller cells were present between the ISs of the photoreceptor cells. B) Large glycogen deposits can be observed in abnormal locations (arrow). Normally, glycogen can only be found in the ISs. C) Occasionally whorls of membranes forming densely packed stacks of coaxial cylindrical bilayers (myelinoid figures) (arrow) were observed in rod cell bodies in the ONL of *rge* birds. Bars = 5  $\mu$ m.

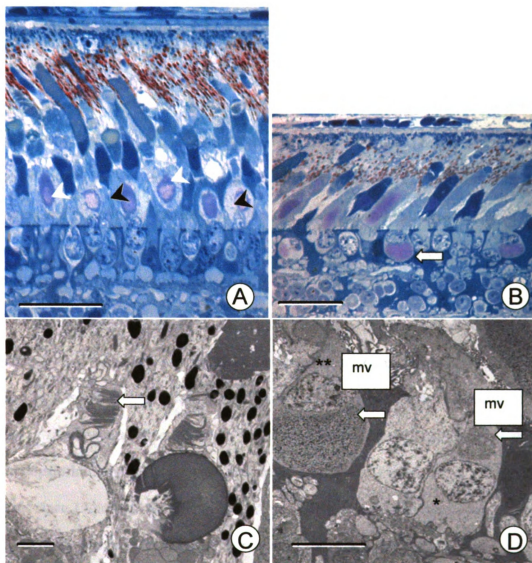


**Figure 5.10** - Semi-thin sections of retinal samples from *rge* and control birds at 270 days of age. A) Control retinas show glycogen deposits only in the ISs, external to the outer limiting membrane, associated with the rod hyperboloid (white arrowheads) and with the cone accessory cell paraboli (black arrowheads). Bar = 20  $\mu$ m. B) Larger glycogen deposits were observed at this age in retinas from *rge* birds, that quite often were displaced internal to the outer limiting membrane of the accessory cells of the double cones (arrow). These glycogen deposits are metachromatic in toluidine blue-stained semi-thin sections, appearing pink in color. The OSs are shorter and the total retinal thickness is obviously decreased. Bar = 20  $\mu$ m. C) Ultra-thin section of a retinal sample from an *rge* bird demonstrating finer detail of the very short and disorganized cone OSs (arrow). Bar = 1  $\mu$ m. D) Ultrastructural detail of glycogen deposits (arrows), present in the supranuclear cytoplasm of an accessory cone cell (\*) and in the subnuclear cytoplasm of a rod cell (\*\*) of an *rge* bird. Long microvilli (mv) of Müller cells were abundant between the ISs of the photoreceptor cells of this age group. Bar = 5  $\mu$ m.

### 5.3.3. Immunohistochemistry results (paraffin-embedded and frozen sections)

Tyrosine hydroxylase (TH) staining of control retinas was similar to previous reports . With TH-positive neurites being concentrated at the distal border of the IPL and at lesser density at 30% and 70% from the IPL-INL interface. In *rge* retinas, the basic amacrine cell morphology revealed by TH staining was intact at all ages examined (up to 730 days of age). However, in older *rge* birds there was an obvious decrease in the density of TH-positive dendrites (Figure 5.11 E, F & G).

Staining using the monoclonal antibody against mouse opsin (Lab Vision) or the mouse anti-rhodopsin antibody (rho4D2) was specific for rod photoreceptors and weakly stained the ISs and strongly stained the OSs in *rge* and control birds (Figure 5.12). The pattern of rhodopsin labeling, however, was abnormal in *rge* birds. An increased amount of rhodopsin-immunoreactivity was present in the ISs of *rge* sections, compared to controls since 13 days of age (Figure 5.12 A versus B). This pattern of labeling was more pronounced in peripheral regions of the retina. In sections from older *rge* birds (e.g. 180 and 270 days of age) rod OSs appeared swollen, with loss of the normal architecture and organization, this was also more pronounced in the periphery of the retina. Immunoreactivity to both these antibodies was localized (abnormally) to the ONL/OPL region in retinal sections from older *rge* birds (Figure 5.12 D & F).

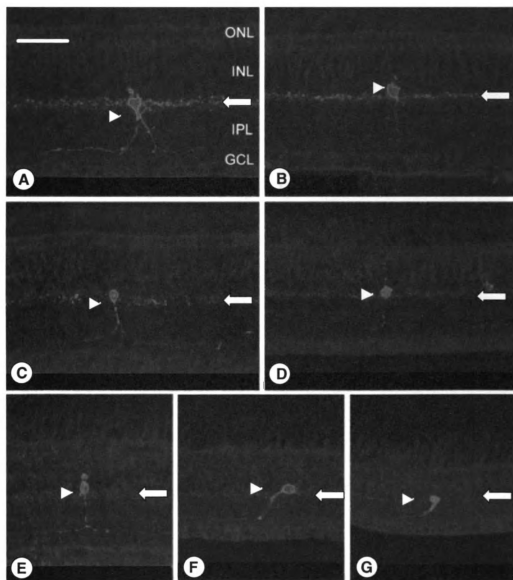


**Figure 5.11** - Immunocytochemistry sections using tyrosine hydroxylase (TH) antibody performed on samples from *rge* and control birds at 30, 180 and 730 days of age. Bar = 50  $\mu$ m. Sections from the following retinal samples are shown: A) control bird at 30 days of age; B) Control bird at 180 days of age; C) *rge* bird at 30 days of age; D) *rge* bird at 180 days of age; E) *rge* bird at 730 days of age – central retina, F) peripheral retinal and G) far peripheral retina. Note that in control retinas TH-positive neurites are found concentrated at the outer border of the IPL and at lesser density at 30% and 70% IPL-depth. At later stages of development (180 and 730 days of age) there is an obvious decrease in the density of TH-positive neurites in retinal samples from *rge* birds (compare A & B with C & D - arrows). However, no loss of TH-positive somata was observed even at very late stages of the disease (E, F & G - arrowheads). Key: ONL – outer nuclear layer; INL – inner nuclear layer; IPL – inner plexiform layer; GCL – ganglion cell layer.

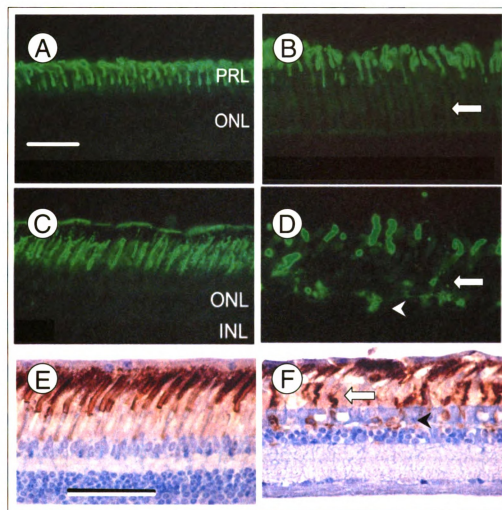


**Figure 5.12** - Fluorescence photomicrographs (A to D) and conventional photomicrograph using brown chromogen (E & F) from immunocytochemistry sections using mouse anti-rhodopsin (A to D) (rho4D2; a gift from Dr. R. Molday, University of British Columbia) and monoclonal antibody against mouse opsin (E & F) (Lab Vision), respectively. Bars = 50  $\mu$ m. Sections from the mid-periphery of the retina from a control (A) and an *rge* bird (B), at 13 days of age; from a control (C) and *rge* bird (D), at 180 days of age and from a control (E) and *rge* bird (F), at 270 days of age. Note the presence of increasing amounts of rhodopsin-immunoreactivity in the ISs of the *rge* samples (white arrows). Note that the opsin labeling in the ISs of control samples is minimal (A, C & E). Also, note that, compared to controls (C & E), the rod OSs in the *rge* retinas of older birds (D & F) appear swollen, with loss of the normal architecture and organization. The OSs of *rge* chicks also appeared more widely spaced in comparison to the controls. Mislocalization of opsin was present in *rge* retinas samples at the ONL/OPL level (arrowheads). Key: ONL – outer nuclear layer; INL – inner nuclear layer.

RCA-1 is a lectin that labels activated microglia in the avian retina. The distribution and morphology of microglia positive for RCA-1 observed in the retina of control birds was similar to that previously described (Navascues et al. 1994; Won et al 2000). In brief, the majority of RCA-1 positive microglia in the normal retina is present in the IPL and OPL, although some microglial bodies were also seen in the NFL, and GCL. In the case of the NFL, microglia appeared more often in the area adjacent to the optic disc. Microglia were ramified through the width of these layers, bearing radial and horizontal processes (Figure 5.13 A). No microglia were found in the photoreceptor layer (Figure 5.13 A). There was no detectable morphological change in the microglia at 13 days of age in *rge* retinas (Figure 5.13 B). However, by 33 days of age, there were activated microglia present in the IPL and OPL. They were amoeboid-shaped cells with enlarged somata (Figure 5.13 C). By 92 days of age, many somata of amoeboid microglia were present in the NFL and INL. These cells had short, stout processes extending from the somata, suggesting that they were highly activated at this time. Furthermore, RCA-1-labeled cells, similar to microglia or macrophages, were seen in the photoreceptor layer of *rge* birds at 92 days of age, suggesting that microglia were highly activated in most retinal layers at this age (Figures 5.15 D, E & F).

Staining using the LEP-100 antibody showed differences between *rge* and control retinas. The LEP-100 antibody recognizes a lysosomal glycoprotein that is only present in cells that are actively phagocytic. In *rge* retinas only, activated phagocytes were detected in all layers of the retina at 180 days of age, while these cells were not detected at other ages (Figure 5.14).

Glycine-immunoreactive “blobs” were detected mainly in the ISs of some photoreceptors in the *rge* retinas (Figure 5.15). Müller cells appeared to have increased levels of expression of GFAP in *rge* retinas by 30 days of age, indicating that these glial cells were reactive (Figure 5.16). However, by 730 days of age no difference was observed between *rge* and control retinas for GFAP-positive cells.

Transferrin binding protein (TfBP) is expressed by oligodendrocytes in the avian retina. These latter cells, along with Müller cells, are believed to be responsible for the myelination of the intraretinal portions of the ganglion cell axons and the optic nerve head in the avian retina . No difference in the amount of TfBP-positive oligodendrocytes was seen in the *rge* samples, compared to controls, at any age examined.



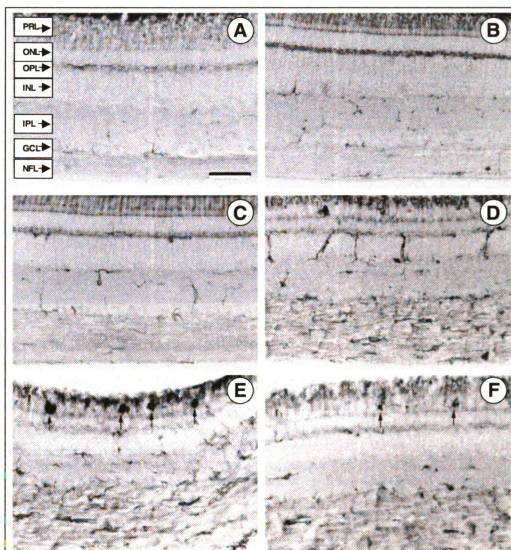


**Figure 5.13** - Immunocytochemical stained retinal sections using RCA-1 antibody of control (A) and *rge* chicks at 13 (B), 33 (C), and 92 days (D, E & F) of age. A) Most ramified microglia are located in the nerve fiber layer (NFL) inner plexiform layer (IPL), and outer plexiform layer (OPL). There was no significant difference in microglial morphology between control and *rge* retinas at 13 days of age. C) In *rge* retinas from chicks at 33 days of age, some microglia in IPL and OPL showed amoeboid-shape indicating activation of these cells. D, E & F) retinal samples from *rge* birds at 92 days of age. Note many amoeboid microglia with stout processes are seen in INL and NFL (D) and RCA-1-labeled cells similar to macrophages (E) or microglia (F) were present in the photoreceptor layer. Bar = 50  $\mu$ m. Key: PRL – photoreceptor layer; ONL – outer nuclear layer; OPL- outer plexiform layer; INL – inner nuclear layer; IPL – inner plexiform layer; GCL – ganglion cell layer; NFL – nerve fiber layer.

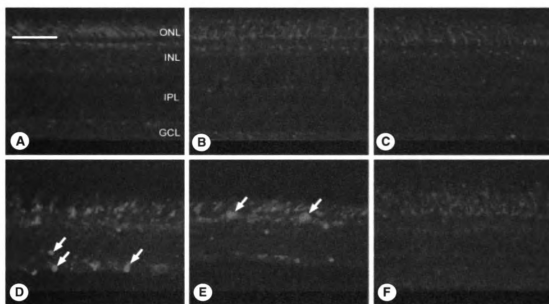


**Figure 5.14** - Immunocytochemistry of retinal sections using LEP-100 antibody. Sections from the following retinal samples are shown: A) retinal section from a control bird at 180 days of age; B) control chick at 30 days of age; C) *rge* chick at 30 days of age; D) mid-peripheral retinal section of an *rge* bird at 180 days of age; E) far-peripheral retina of an *rge* bird at 180 days of age and F) central retinal section of an *rge* bird at 730 days of age. Note the difference between *rge* (C, D & E) and control (A & B) samples. Several retinal layers of the *rge* retinas, mainly ONL, OPL, INL, IPL and GCL at 30 and 60 days of age were positively stained for this antibody. At 730 days of age no difference could be detected between *rge* and control samples. Bar = 50  $\mu$ m. Key: ONL – outer nuclear layer; INL – inner nuclear layer; IPL – inner plexiform layer; GCL – ganglion cell layer.

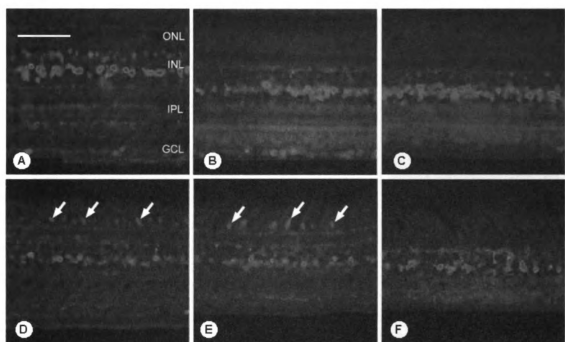


**Figure 5.15** - Immunocytochemistry of retinal sections using anti-glycine antibody. Sections from the following retinal samples are shown: A) control bird at 180 days of age; B) control chick at 30 days of age; C) *rge* bird at 180 days of age; D) *rge* chick at 30 days of age; E) retinal section from an *rge* bird at 730 days of age F) peripheral retina of an *rge* bird at 730 days of age. Note the glycine-immunoreactive "blobs"(arrows) detected in the ISs of some photoreceptors in retinas from older *rge* birds (D & E). Bar = 50  $\mu$ m. Key: ONL – outer nuclear layer; INL – inner nuclear layer; IPL – inner plexiform layer; GCL – ganglion cell layer.

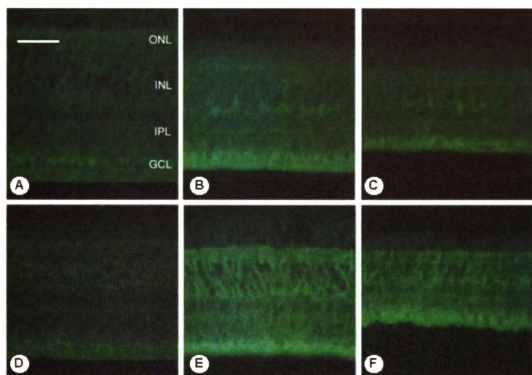


**Figure 5.16** - Immunocytochemistry of retinal sections using anti-GFAP antibody. Sections from the following retinal samples are shown: A) control bird at 30 days of age; B) *rge* chick at 30 days of age; C) peripheral retina of an *rge* chick at 30 days of age; D) control bird at 180 days of age; E) *rge* bird at 180 days of age F) peripheral retina of an *rge* bird at 180 days of age. Note the *rge* retinas appear to have a progressive increase of GFAP expression, indicating that glial cells (Müller cells) are reactive. Bar = 50  $\mu$ m. Key: ONL – outer nuclear layer; INL – inner nuclear layer; IPL – inner plexiform layer; GCL – ganglion cell layer.

The anti-calbindin and GCAP1 antibodies stained the numerous cone cells in both *rge* and control retinal samples. No difference between *rge* and control samples was observed between the amounts of positive cone cells for both these antibodies at any age examined. Furthermore, no obvious differences in labeling patterns for Vamp1, GABA-A receptor and SV2, were seen between control and *rge* birds or between sections of the two different ages of *rge* bird studied (7 and 14 days of age). The pattern observed with VAMP-1 staining was similar to the one described in mice. The antibody against the  $\beta$  subunit of the GABA-A receptor stained both, *rge* and control chick retinas in a similar

pattern, comparable to that previously described in normal chicken retinas . No differences in labeling pattern for caspase 3 were observed, comparing retinal sections from controls and *rge* birds.

The staining for synaptic vesicle protein 2, a ubiquitously expressed synaptic vesicle protein, revealed abnormalities in the stratification of the OPL in the *rge* birds compared to controls, substantiating the results observed ultrastructurally. Analyzing samples that were immunocytochemically stained for visinin, only a mild distortion in the normal arrangement as well as a mild loss of reactivity could be observed at 180 and 730 days of age in *rge* retinas (data not shown).

Additionally, no differences could be noted when comparing retinal samples from *rge* chicks with controls labeled with antibodies against  $\beta$ 3-tubulin and glucagon. Also, there was no obvious difference between *rge* chicks and controls in the distribution of retinal neurons that express the neurofilament, vimentin, Hu, Islet1, or TrkA (horizontal cells).

#### 5.3.4. TUNEL Staining

No TUNEL-positive cells were detected in retinal sections from *rge* or control birds.

#### 5.3.5. Detailed examination of the linear fundus lesions in semi-thin and ultra-thin sections

The fundic lesions present in the retinal cups from 2 *rge* chicks at 49 days, 1 at 84 days and 1 at 336 days of age were examined macroscopically in enucleated eye globes. Similar lesions were present in all four birds. They occurred bilaterally and were linear, pale-colored (white to gray) and sometimes branching. They ranged from approximately 0.5 mm to 1 mm in width and from 2.5 to 12 mm in length (Figure 5.17). The number of lesions found in the retinal cups varied from one to 8. The linear lesions most commonly had a vertical orientation, however, horizontal branches were also found occasionally. Linear lesions appeared to radiate from the pecten and optic nerve area.

Microscopically, the retina of the *rge* birds adjacent to the lesions had a relatively normal retinal architecture with a normal appearing and continuous Bruch's membrane-retinal pigment epithelium-choriocapillaris complex and normal photoreceptor-retinal pigment epithelium interface (Figure 5.18 A). Sections through the fundic lesions showed that there was a mild focal fibrosis at the level of the inner choroid and a focal absence of the retinal pigment epithelium and an accumulation of eosinophilic, hyaline material in the subretinal space. The overlying photoreceptor inner and outer segments were disorganized and there was thinning and displacement of the inner and outer nuclear layers (Figure 5.18 B).

Semi-thin sections from the retina adjacent to the lesions showed a normal Bruch's membrane lined on the retinal side by retinal pigment epithelium and on the choroidal surface by choriocapillaris (Figure 5.18 C). Semi-thin sections of the lesion

itself revealed a focal absence of the retinal pigment epithelium layer, rupture of Bruch's membrane with scar formation, deposition of collagen fibers and abnormal presence of retinal pigment epithelium cell melanosomes external to the ruptured Bruch's membrane (Figure 5.18 D).

Ultrastructural examination of the Bruch's membrane- retinal pigment epithelium-choriocapillaris complex from an area adjacent to the retinal lesions showed a normal intact Bruch's membrane with normal relationship to the retinal pigment epithelium (Figure 5.19 A). The affected area had a loss of the normal architecture of the Bruch's membrane- retinal pigment epithelium-choriocapillaris complex. There was a complete rupture of Bruch's membrane and along the inner surface fibroblasts formed an almost continuous layer that separated the outer retina from the choroid. The choriocapillaris was replaced with a pronounced deposition of collagen, debris from retinal pigment epithelium (necrotic cells containing dispersed melanosomes) and photoreceptor cells (Figure 5.19 B).

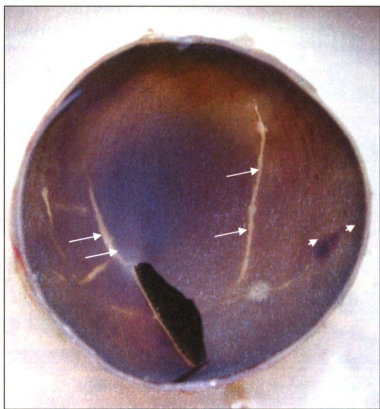


**Figure 5.17** - Photograph of the posterior eyecup from a 49-day-old *rge* bird showing lacquer cracks. The lacquer crack lesions appear as multiple white to gray linear lesions (white arrows), extending from the pecten to the periphery. Additionally, an area of subretinal hemorrhage (white arrowheads) is present.



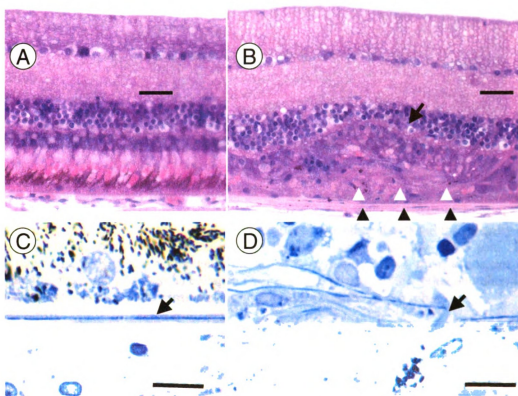


**Figure 5.18** – Plastic and resin-embedded retinal sections from *rge* birds demonstrating morphologic details of the lacquer crack lesions. A) Eye of an *rge* bird at 49 days of age. Cross section through a region of retina adjacent to the lesion shown in B. The retinal architecture is relatively normal with a normal retinal pigment epithelium layer and normal photoreceptor-retinal pigment epithelium interface. However, there is a mild dilation of the photoreceptor inner and outer segments, which is typical of early stage changes observed in the *rge* phenotype. B) Cross section through one of the lesions shown in Figure 5.17 from the central retina. Note the mild focal fibrosis at the level of the inner choroid (black arrowheads) and the absence of retinal pigment epithelium (white arrowheads). There is an accumulation of eosinophilic material in the subretinal space. The overlying photoreceptor inner and outer segments are disorganized and there is thinning and displacement of the outer and inner nuclear layers (black arrow). Stained with H&E. Size bar = 150 μm. C & D) Eye of an *rge* bird at 336 days of age. C) This shows the region adjacent to the lesion that is shown in D. Bruch's membrane is intact (arrow) and is lined by the RPE layer on one side and the choriocapillaris on the choroidal side. D) Details of a linear lesion showing an absence of the normal retinal pigment epithelium layer, rupture of Bruch's membrane (arrow), scar formation with deposition of collagen fibers and the abnormal presence of retinal pigment epithelium cell melanosomes on the choroidal side of Bruch's membrane. Stained with toluidine blue. Size bar = 20 μm.

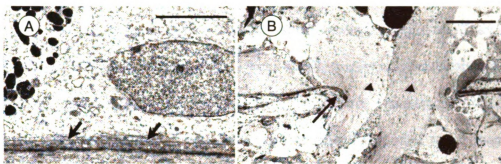


**Figure 5.19** – Ultra-thin section from the eye of an *rge* bird at 336 days of age. A) This section shows the Bruch's membrane- retinal pigment epithelium interface from a region adjacent to the lesion shown in B. Notice the detail of a normal retinal pigment epithelial cell and the integrity of the Bruch's membrane (arrows). Transmission electron microscopy. Size bar = 2.5 µm. B) Section through a LCL. Bruch's membrane in the lesion is ruptured (arrow), there is absence of retinal pigment epithelium, and there is collagen fiber deposition between the retina and choroid, forming a scar (arrowheads). Transmission electron microscopy. Size bar = 5 µm.

#### 5.4. Discussion

The vision of *rge* chicks deteriorates over the first few weeks after hatch and is worse under lower lighting conditions and by approximately 30 days after hatch vision has deteriorated to such an extent that they are functionally blind. Intriguingly, under light microscopy examination, retinal morphology in the *rge* retinal sections is remarkably preserved despite of the loss of vision.

The results from this study, including a detailed morphological examination, ultrastructural analysis, and immunocytochemistry, revealed several abnormalities in different retinal regions of the *rge* birds, particularly the OPL where the earliest morphological changes were noted. The photoreceptor pedicle arrangement in the *rge* birds appeared disorganized with loss of the normal regular bi-layered structuring seen in

control birds. The photoreceptor pedicles and spherules themselves were also clearly distorted and became more severely distorted as the disease progressed. They also appeared to have fewer synaptic ribbons and were usually larger, more electrolucent and contained abnormally shaped synaptic vesicles. The smooth endoplasmic reticulum (SER) could frequently be seen within the photoreceptor cell bodies rather than the inner segments. This was particularly apparent in accessory cells of the double cones.

The morphological abnormalities in the photoreceptor synaptic terminals may indicate abnormal physiological function and could underlie the vision loss that occurs in the *rge* birds in the absence of marked photoreceptor cell loss. The vesicular changes observed in the synapses, along with the apparently less numerous ribbons, might suggest a defect in the vesicle formation machinery or a defect in the endo- or exocytosis mechanisms.

The presence of abnormal synaptic vesicles along with the morphological changes observed in the photoreceptor pedicles of *rge* birds are somewhat similar to the ones observed in the photoreceptor synapses of synaptophysin knockout mouse and in the *rdgE* (*Drosophila* retinal degeneration E) . Both exhibited a number of synaptic and vesicular defects. Some of these defects are similar to the ones observed in *rge* chicks such as a buildup of very large multivesicular bodies and an increased amount of rough endoplasmic reticulum.

Previous optokinetic and ERG studies showed that the *rge* birds had reduced visual function under low-lighting conditions suggesting that rod dysfunction preceded loss of cone-mediated vision; see Chapter 2 and 3. As the disease progressed a generalized shortening and disorganization of all photoreceptor OSs developed. Opsin

immunohistochemistry showed abnormalities in rods from 12 to 13 days of age. Initially there was increased opsin-immunoreactivity in the ISs and later mislocalization to the ONL. Furthermore there was a progressive decrease in the number of rod OSs per unit length of retina. Mis-routing of opsin is typical of damaged or abnormal rods and has been observed in other forms of inherited retinal degenerations, such as in people suffering from retinitis pigmentosa and in the *tulp1*<sup>-/-</sup> mice .

Abnormal localization and progressive accumulation of glycogen occurred in the photoreceptor perinuclear region associated with the abnormally located RER resulting in large glycogen deposits in older *rge* birds very close to the nucleus and synaptic area. This glycogen accumulation and mislocalization was not associated with lysosomal membranes as is the case with glycogen accumulation observed in retinal glycogenosis (Pompe disease), where the glycogen accumulation is present in most cell types in the retina and always associated with lysosomes . Other types of glycogenosis were ruled out by the fact that liver, heart, brain and skeletal muscle did not show any sign of glycogen accumulation, as assessed by PAS staining, at any age group of *rge* birds. Additionally in the older affected birds myelinoid bodies developed in the photoreceptors between the nucleus and the synaptic terminal. One suggestion for the development of myelinoid bodies is degeneration of ER , however the link between the myelinoid bodies and abnormal location of RER with associated glycogen accumulation is not clear. The glycine-positive "blobs", present in the *rge* retinas, were glycine accumulations in the ISs of some photoreceptors. This may indicate abnormal photoreceptor metabolism.

The results from retinal thickness measurements confirm the previous initial impression of progressive retinal thinning. Initially, the ventral regions and far dorsal

peripheral regions of the retina were the ones that presented the greatest reduction in thickness. This is possibly a direct consequence of globe stretch caused by the globe enlargement that occurs mainly at the equator of the globe. At later stages a generalized thinning occurs. In the early stages of the disease, the greatest decrease in thickness occurs in the inner retina. Ganglion cells, however, do not seem to be decreased in numbers despite the retinal stretch. Markers used for amacrine and horizontal cells also showed no significant loss in these two cell populations. The decrease in TH-positive dendrites from amacrine cells likely resulted from retinal stretch caused by the increased globe enlargement. This is consistent with previous findings that the density of TH-positive amacrine cells decreases while total cell numbers within the retina remain constant with the increased ocular growth and passive retinal stretch . In retinas from *rge* birds, the TH-positive cells do not appear to sprout additional neurites to maintain a constant density of dendrites during the retinal stretch that occurs. By contrast, the density of TH-positive dendrites is maintained in experimentally induced retinal stretch . This finding suggests that the *rge* phenotype includes the inability of some types of amacrine cells to sprout dendrites. It has previously been shown that amacrine cell death is one cause of globe enlargement and that TH and glucagon-containing amacrine cells have been implicated in regulating the overall growth of the eye . However these cell types are present in affected birds showing that globe enlargement is not secondary to their complete loss .

In the later stages of the disease marked gliosis develops. Glial processes occupy spaces in the OPL where pedicles and spherules normally would have been located, and they also fill gaps between the somata of photoreceptor cells. This glial activation is

substantiated by increased GFAP and RCA-1 staining (indicating activated glial and microglial cells). It is not clear whether the gliosis develops in response to the development of gaps between cells, triggered by the progressive retinal stretch, or due to spaces caused by a disease associated injury and loss of retinal cells. The increased immunoreactivity to LEP-100 in the *rge* retina suggests the presence of activated phagocytes. These phagocytes may have been activated by growth factors and cytokines that might be somehow elevated in the retinas from *rge* birds. Judging by the different sizes and morphology of some of the LEP-100-positive cells, these cells appear to be macrophages that have migrated into the retina, while others might be activated resident microglia. Despite this activation, no morphological (LM or EM), immunocytochemical (caspase 3) or molecular (TUNEL) evidence of apoptosis could be detected. It seems likely that cell loss in the *rge* retina occurs very gradually during several months. By 730 days of age no difference could be detected between *rge* and control sections for GFAP and LEP-100 immuno-staining, indicating that most of the glial activation and, perhaps, phagocytosis has been terminated at that time point.

The linear retinal lesions examined in this study are similar to the lesions experimentally produced by when inducing form-deprivation myopia in chicks, by in constant light exposure chicks, and lacquer crack lesion (LCL) in humans with pathologic myopia . All of these linear retinal lesions share the following characteristic histologic features: loss of retinal pigment epithelium, rupture of Bruch's membrane and disruption of the choriocapillaris. LCLs are a well-characterized pale coloured (white to gray), linear lesions of the ocular fundus that develops in human patients as a secondary manifestation of a severe form of myopia, called pathological myopia . LCLs are thought to represent

mechanical breaks in the Bruch's membrane- retinal pigment epithelium-choriocapillaris complex due to progressive posterior segment elongation . LCL is also thought to be an extremely important predisposing factor in the formation of choroidal neovascularization, which is a severe fundus alteration found in patients with advanced pathological myopia . In a recent study of human patients with pathological myopia, 29.4% of eyes with LCL developed myopic choroidal neovascularization during the follow-up period . The reported prevalence of LCL in humans with pathological myopia varies between 0.6% , 4% and 15.7% . As a general rule, the presence of these lesions implies a guarded prognosis for the retention of central vision of human patients suffering from pathological myopia .

A limited number of publications are available describing the histopathological features of human LCL, probably due to its early occurrence in the course of myopic macular degeneration . Understandably, myopia by itself is not a major cause of enucleation and consequently, represents a small percentage of samples submitted to ocular pathology laboratories.

It appears that the exaggerated internal cartilaginous layer growth in the *rge* chicks forces the remodelling or stretching of the fibrous layer of the sclera and Bruch's membrane to the point of rupture of the latter. This additionally induces mechanical breaks in the retinal pigment epithelium and choriocapillaris complex, all of which characterize classical LCLs. Posterior segment enlargement in the *rge* chick causes lesions that are histologically identical to LCL.

To our knowledge, there are no reports of other spontaneously occurring animal models of globe enlargement with LCL formation. A laboratory animal model of

spontaneously occurring LCLs, such as the *rge* chick, would greatly facilitate future research toward the complete understanding of the pathological mechanism underlying its manifestation in human patients with severe myopia.

The *rge* phenotype appears unique with morphological features quite unlike those described in the other forms of chicken retinal dystrophies such as *rd*, *rdd*, *dam* and *beg* . ERG responses in young *rge* chicks show supernormal b-wave amplitudes to brighter light stimuli (Chapter 3). A similar ERG abnormality can be seen in mice and humans with *NR2E3* gene mutations ; however, morphologically the diseases are quite different. Unlike the *NR2E3* mutant mice and humans in which S-cone photoreceptors are present at greatly increased numbers, in the *rge* chicken there were no obvious changes in photoreceptor populations. Molecular genetic studies to identify the causal gene mutation should help explain why the morphological features of the *rge* phenotype develop and clarify the association with the vision loss and the electroretinographic abnormalities.



## CHAPTER 6

### CONTRIBUTIONS TO THE MOLECULAR CHARACTERIZATION OF THE *rge* DEFECT

#### 6.1. Introduction

Prior research showed that the *rge* phenotype is inherited in an autosomal recessive fashion , but the specific gene mutation had not been characterized. The gene mutation underlying one other autosomal recessive retinal dystrophy in chickens, the *rd* chicken, had been identified however . The same mutation was also shown to be the cause of retinal dystrophy in another strain of chickens that had been thought not to be related to the *rd* strain . It was considered prudent, therefore, to ensure that the *rge* chick was not just an additional strain in which the *rd* mutation was present before spending time investigating the *rge* phenotype.

The *rd* chicken has a null mutation in the photoreceptor guanylate cyclase gene (GUCY1\*B) caused by a deletion of approximately 22 kb which spans exons 4 to 7 . Thus, our first experiment was to use an RT-PCR assay to show that the *rd* mutation was not present in the strain of chickens we were planning to study.

Once the *rd* mutation had been excluded we planned to map the *rge* locus. At the time that we had performed the breedings to produce a pedigree for mapping and were collecting the necessary DNA samples, researchers from the Roslin Institute (Edinburgh) reported they had mapped the *rge* defect to chicken chromosome 1 . We, therefore, changed our plans to build on that mapping and to try to narrow the chromosomal interval to which *rge* mapped. Once the *rge* confidence interval was narrowed we aimed

to use comparative mapping and the information from the human genome project to identify positional candidate genes for further studies.

## **6.2. Material & Methods**

### **6.2.1. Testing the *rge* chicken for the deletion of the guanylate cyclase gene present in the *rd* chicken**

#### **a) Isolation of total RNA**

Immediately following euthanasia the globes were enucleated and retinas were dissected from 3 *rge/rge*, 3 *rge/+* and 2 *+/+* birds and immediately frozen in liquid nitrogen.

RNA was prepared using sterile, disposable, RNase free plasticware and solutions prepared with 0.1% diethylpyrocarbonate (DEPC, Sigma) to minimize RNase activity. Items such as micropestles and spectrophotometer chambers were soaked overnight in 50:50 (v/v) mixture of methanol and concentrated HCl and then rinsed repeatedly with DEPC treated water.

Total retinal RNA was extracted using trizol (Invitrogen) reagent method. In brief:

- Retinal tissues were placed in 1.0 ml of ice-cold trizol in a 5 ml micropestle tube (Kontes Glass Co. Duall ® 22) and homogenized
- The homogenized retina was further sheared by several passes through a 22 gauge needle. For each 1 ml of trizol used 0.2 ml chloroform was added

- The solution was mixed by repeatedly inverting the microcentrifuge tube for 5 seconds and then incubated for 3 minutes at room temperature. The solution was then centrifuged for 15 min at 8500 rpm
- The aqueous layer was then transferred to a clean-RNase free tube and 0.5 ml isopropanol was added
- The tube was incubated at room temp for 10 min, then spun for 10 min at 8500 rpm. The RNA pellet could then be seen
- The isopropanol was removed and the pellet washed with 1 ml (per ml of Trizol) of 75% ethanol then spun for 5 min at 8500 rpm
- The ethanol was then carefully removed leaving the pellet inside the tube
- The tube was air dried for 10 minutes and 50 µl of RNase free water was then added
- The presence and quality of the RNA was checked by running the product on a 1.5% agarose gel and judged by the presence of 18S and 28S ribosomal RNA bands and a lack of RNA degradation products

The concentration and degree of contamination of the RNA was checked by spectrophotometry at wavelengths of 260 nm and 280 nm. The reading at 260 nm allowed calculation of RNA in the sample. An OD of 1 corresponds to ~ 40 µg/ml for single stranded RNA. The ratio of the readings at 260nm and 280 nm ( $OD_{260}: OD_{280}$ ) provides an estimate of the purity of the RNA. Pure preparations of RNA have  $OD_{260}: OD_{280}$  ratio value of 2. In this protocol, lower ratio values were considered as suggestive of significant contamination with protein or phenol.

- The extracted total RNA was stored at -80 °C until used.

**b) First strand cDNA synthesis**

- First strand cDNA was synthesized using a First Strand cDNA Synthesis Kit (MBI Fermentas). The kit relies on a cloned enzyme, Moloney Murine Leukemia Virus (M-MuLV) reverse transcriptase. In brief, the protocol is as follows:

The following reagents were placed in an RNase-free microcentrifuge tube:

- Total RNA 5 $\mu$ g
- Primer: oligo(dT)<sub>18</sub> 0.5 $\mu$ g
- deionized water (nuclease free) to 11 $\mu$ l.

The solution was incubated at 70°C for 5 minutes and chilled on ice. The following reagents were added in the following order:

- 5X reaction buffer (250 mM Tris-HCl, pH 8.3 at 25°C, 250 mM KCl, 20 mM MgCl<sub>2</sub>, 50 mM DTT) 4 $\mu$ l
- 10mM 4 dNTP mix 2 $\mu$ l (1.0mM - final concentration)
- ribonuclease inhibitor 20 units
- deionized water (nuclease free) to 19 $\mu$ l.

The solution was then incubated at 37°C for 5 minutes and 40 units of M-MuLV reverse transcriptase were added. The reaction mixture containing oligo(dT)<sub>18</sub> was then incubated at 37°C for 60 minutes. The reaction was stopped by heating to 70°C for 10 minutes.

**c) PCR amplification of a portion of the chicken guanylate cyclase and rhodopsin cDNAs**

Amplification of a portion of the chicken guanylate cyclase gene spanning the site of the *rd* mutation was performed using a forward primer flanking the deletion site within exon 4 (SPJ 342 -5' - CCTTCCCCCTGCCCTACCAC) and a reverse primer flanking exon 7 (SPJ 343 -5' - TAATGATGCCGATGCCGTAAACGT) with total retinal cDNA as a template. PCR amplification of rhodopsin as a positive control was also performed (forward primer: Rho-1 -5' – CATCATGGGGGTCGCGTTCTCCT and reverse primer: Rho-2 - 5' - CCATGCGGGTCACTTCCTTCTC). The PCR mixtures were as follows: 50 µl reaction volume containing 200 mM Tris-HCl, pH 8.4; 50 mM KCl; 1.5 mM Mg Cl<sub>2</sub>; 1% bovine serum albumin and 0.1 mM each of dATP, dCTP, dGTP and dTTP; 0.5 µM of each primer; and 1 unit of *Taq* DNA polymerase (Invitrogen, Life Technologies). The cycling conditions were: denaturing at 95°C for 3 minutes, followed by 45 cycles of denaturing at 95°C, 30 seconds; annealing at 60°C, 30 seconds; extension at 72°C, 30 seconds and a final cycle of extension at 72°C for 5 minutes.

The PCR products were analyzed by electrophoresis of an aliquot on 1.5% agarose in TAE buffer. For visualization of the bands, ethidium bromide was added in the concentration of 0.5 µg/ml before the gel solidified. PCR products were mixed with loading buffer (0.25% bromophenol blue; 40% (w/v) sucrose in water), in a 1:6 dilution. The gels were run with 1x TAE buffer (40 mM Tris-acetate; 2 mM EDTA, pH 8.0) at 80 V/cm. A commercial DNA size marker (1 kb DNA Ladder BioLabs) was run in adjacent lanes and used to estimate the size of the PCR product.

#### 6.2.2. Mapping of the *rge* region

A group at the Roslin Institute found that microsatellite marker LEI0071 on chromosome 1 was linked to the *rge* phenotype . The LEI0071 region on chicken chromosome 1 is a region with poor comparative synteny to man. The region is equivalent to the following portions of the human genome: 12p13, 7q35, 22p13.31 and 1p13.1. The Roslin group also investigated positional candidate genes: ABCA4, mutated in Stargardt macular dystrophy in humans ; IMPDH1, the gene underlying the RP10 retinal dystrophy in humans; and TIMP3, a gene mutated in humans with Sorsby's Fundus Dystrophy . Their studies excluded those genes . In order to refine the Roslin Institute group mapping, *rge* affected sires were mated to clinically normal carrier hens to produce a population with approximately 50% *rge* and 50% carrier progeny. These were typed using markers that mapped to chicken chromosome 1.

Blood was collected for DNA isolation from the jugular vein using a 1 ml syringe with a 30-gauge needle. Blood was then transferred to EDTA tubes and placed on ice if extraction was to be performed immediately, or stored at -20°C until processed. Frozen blood was thawed on ice and processed in 5 ml aliquots. A typical method for mammalian DNA extraction was used:

- The blood sample was gently mixed with an equal volume of 2x red blood cell lysis solution (0.65 M sucrose; 20 mM Tris-HCl, pH 7.8; 10 mM MgCl<sub>2</sub>; 2% triton X-100 v/v)
- Following incubation on ice for 15 minutes the solution was centrifuged at 2,360 rpm for 12 minutes at 4°C and the supernatant was discarded. If heavy contamination with hemoglobin remained, a further volume of 2x lysis buffer was added and the centrifugation repeated

- The red blood cell nuclei and leukocyte pellet was resuspended in 2 ml of 75 mM NaCl; 24 mM EDTA by pipetting and the suspension transferred to a Phase Lock gel light tube (Brikmann Eppendorf) and 100 µl of 10 mg/ml proteinase K (in 50 mM Tris-HCl, pH 8.5; 5 mM CaCl<sub>2</sub>) added and then sodium lauryl sulfate (SDS) added to a final concentration of 1% w/v and the mixture incubated overnight at 37°C, mixing gently. This results in liberation of DNA and digestion of protein
- A phenol extraction was then performed. 4 ml of phenol was added to the mixture followed by gentle shaking to mix the two phases. The suspension was centrifuged at 3000 rpm for 5 minutes to separate the phenol and aqueous phases
- The aqueous phase was decanted into a fresh Phase Lock gel light tube and an extraction performed as above but using 4 ml of a 50/50 (v/v) phenol chloroform mixture
- The DNA was precipitated by adding 100 µl of 2 M KCl, mixing and then overlaying with 5 ml of 95% ethanol. The two phases were mixed by gently swirling the tube and the precipitated DNA strands removed with a glass pipette, washed in 70% ethanol and after the excess ethanol had dripped off placed in 200 µl of TE (10 mM Tris-HCl, pH 7.8; 1 mM EDTA)
- The DNA was allowed to dissolve by leaving it overnight at 4 °C
- Since the avian blood has nucleated red blood cells, and the extraction protocol was designed for mammalian blood, the resulting concentration

of DNA was typically higher and had to be further diluted. The DNA was further diluted prior to PCR reactions.

The quantity and purity DNA was checked by spectrophotometry at wavelengths of 260 nm and 280 nm. The reading at 260 nm allowed calculation of RNA in the sample. An OD of 1 corresponds to ~ 50 µg/ml for double stranded DNA. The ratio between the readings at 260nm and 280 nm (OD<sub>260</sub>: OD<sub>280</sub>) provides an estimate of the purity of the DNA. Pure preparations of DNA have OD<sub>260</sub>: OD<sub>280</sub> ratio value of 1.8. Lower values were considered as suggestive of significant contamination with protein or phenol.

To identify linked markers to *rge*, selected microsatellite markers from the region of chicken chromosome 1 were screened and the allelic patterns compared between DNA pools from 32 carrier (heterozygous) and 31 affected (homozygous) chicks. Informative microsatellite markers were genotyped on all the progeny; primers were fluorescently-labeled for use on ABI automated sequencers. Linkage analysis was performed using Map Manager 7, which is a program that determines marker order by pairwise comparisons. This portion of the work was performed at Dr. Hans Cheng's laboratory at the USDA's Avian Disease and Oncology Laboratory in East Lansing, MI.

#### 6.2.3. Mapping and sequencing of candidate genes

Positional candidate genes were selected based on the refined mapping of the *rge* locus. The region of the human genome (12 p11-13) that was the equivalent to the refined confidence interval chicken chromosome 1 was scanned for genes involved in retinal function using the Human Genome Browser (<http://genome.ucsc.edu/>). Particular



attention was given to genes expressed in structures of the outer plexiform layer, for example those involved in synaptogenesis, synaptic vesicle formation and synaptic ribbon formation (see Chapter 5). If the chicken homologue of the candidate gene had not been sequenced, then the coding sequence of the gene (for human) was screened against chicken trace sequences and expressed sequence tags (ESTs) (400,000+ and growing) by BLAST, via NCBI website (<http://www.ncbi.nlm.nih.gov/blast/tracemb.shtml/>). If a gene was not represented in the chicken trace sequences or ESTs, primers were designed from well-conserved regions of the gene that were identified by comparing the gene sequence in other species (typically human and mouse). We have found that approximately 50% of primer pairs designed by such a technique yield the correct product.

Primers were designed using the program PrimerQuest (<http://biotools.idtdna.com/primerquest/>), to generate small exonic products (200 to 500 bp) for Radiation Hybrid mapping. PCRs were performed using DNA from homozygous normal and *rge* chicks as template. The conditions for most of the PCR reactions were: denaturing at 95°C for 3 minutes, followed by 35 cycles at denaturing at 95°C, 30 seconds; annealing at 60°C, 30 seconds; and extending at 72°C, 30 seconds with a final extension of 72°C for 5 minutes. To confirm that the selected candidate gene was mapped to the same region of chicken chromosome 1 as the *rge* locus, they were mapped using a chicken radiation hybrid panel. A 6,000 rad chicken radiation hybrid (RH) panel developed by Alain Vignal and co-workers was used (INRA, France; ). The DNA from 90 pools of chicken-hamster hybrid cells were used in PCR reactions using the gene specific primer pairs that had previously been shown to amplify the correct product. The

results from the PCR reactions using the DNA of each hybrid cell were submitted to Alain Vignal and co-workers and a correlation analysis was performed in order to map the chromosomal location of the gene being investigated. In brief, the closer the gene is to the microsatellite marker on a chromosome, the less likely it is that an x-ray induced break will occur between them; as a result, two genes in physical proximity are retained in many of the same hybrids, whereas genes that are not close together usually reside on different chromosome fragments and therefore are usually not present in the same hybrids. The statistical analysis will indicate how often two genes are concordant in radiation hybrid clones provides a measure of distance between the genes . The RH work was performed at Dr. Jerry Dodgson's laboratory, at Michigan State University.

Positional candidate genes that were confirmed as candidates by RH mapping underwent sequencing. Primers were designed to PCR-amplify (as described above) the exonic and exonic/intronic boundaries of the gene. The primers were designed in such a way that the expected sizes of the products were always around 500 to 700 bp.

The products of the PCR reactions were analyzed by electrophoresis on 1.5% agarose gel (as described above).

When the PCR product produced a visible band of the expected size, the DNA fragment band was excised from the agarose gel with a scalpel blade and its DNA content was extracted using a QIAquick Gel Extraction Kit (Qiagen) as follows:

- The gel slice was weighted and placed in a colorless 1.5 ml tube. Three volumes of Buffer QG (solubilization and binding buffer, which contains the chaotropic salt guanidine thiocyanate) were added to one volume of gel

- The tube was then incubated at 50°C for 10 min (or until the gel slice has completely dissolved). The tube was then vortexed every 3 minutes during the incubation
- One gel volume of isopropanol was added to the solution and mixed by vortexing. The solution was then placed in a spin column inside a 2 ml collection tube and centrifuged at 13,000 rpm for 1 min
- The flow-through was discarded and the spin column was placed back in the same collection tube. 0.75 ml of Buffer PE (wash buffer in which the basic component is ethanol) was added to the spin column and centrifuged at 13,000 rpm for 1 minute
- The flow-through was again discarded and the spin column was centrifuged at 13,000 rpm for an additional 1 minute
- The spin-column was placed into a clean 1.5 ml microcentrifuge tube and to elute the bound DNA 30 µl of Buffer EB (10 mM Tris·Cl, pH 8.5) was added to the center of the spin column membrane
- The column was left at room temperature for 1 min, and then centrifuged one more time at 13,000 rpm for 1 minute. The flow-through contained the purified DNA.

The amount of DNA in the purified product was evaluated by comparative analysis on an agarose gel using DNA weight markers of a known loading (DNA Ladder BioLabs). Each gel-purified product (containing a minimum concentration of 20 ng of DNA) was then submitted for sequencing in two tubes, containing 30 pmoles of the forward or reverse primer (two separate reactions) in a total reaction volume of 12 µl.

Sequencing was then performed using an ABI PRISM® 3100 Genetic Analyzer, which is a multi-color fluorescence-based DNA analysis system, at MSU's Genomics Technology Support Facility ([http://genomics.msu.edu/GTSF/DNA\\_Sequencing.html/](http://genomics.msu.edu/GTSF/DNA_Sequencing.html/)).

Sequences were analyzed with BioEdit Sequence Alignment Editor for Windows software (<http://www.mbio.ncsu.edu/BioEdit/bioedit.html>).

## **6.3. Results**

### **6.3.1. Testing the *rge* chicken for the deletion of the guanylate cyclase gene present in the *rd* chicken**

Primers designed to amplify the region corresponding to exons 4 to 7 of the chicken guanylate cyclase resulted in two products (Figure 6.1) that corresponded to the expected sizes (1416 and 1329 bp). The smaller fragment corresponded to a splice variant 87-bp shorter, which is unique to avian species . Amplification of *rge* and carrier retinal cDNA also produced two products of the same size as the normal control.

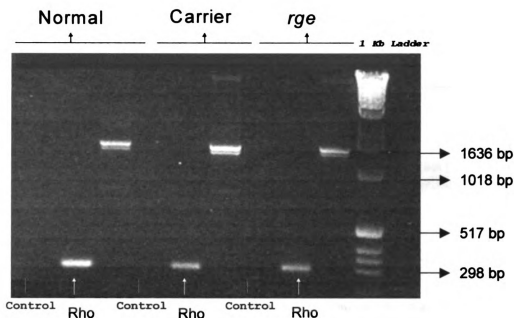


**Figure 6.1** - Result of RT-PCR from retinal tissue from a normal, a carrier and an *rge* bird on 1.5% agarose electrophoresis gel. All samples showed the correct expected fragment (around 1500 bp with a 87bp shorter fragment produced by alternative splicing) indicating the absence of the *rd*-chicken mutation (a deletion on the guanylate cyclase gene). A known rhodopsin product (around 300 bp) served as the positive control for each test. A reaction in which no cDNA template was added served as a negative control. Key = GC = guanylate cyclase.

### 6.3.2. Mapping of the *rge* region

It was confirmed that microsatellite marker LEI0071 on chromosome 1 is linked to the *rge* defect. This linkage to *rge* was confirmed by individual genotyping of all progeny using LEI0071 and MCW0058, another microsatellite that co-segregates with LEI0071 on the East Lansing genetic map (see Figure 6.2). One recombinant was revealed, a single carrier (chick #683C) was homozygous instead of the expected heterozygous genotype for both markers. Assuming complete penetrance of the *rge* trait, this would indicate that LEI0071 and MCW0058 are approximately 2 cM or less from the

*rge* locus. Another microsatellite marker, MCW0318, however, was found to absolutely co-segregate with *rge*, showing no recombination.

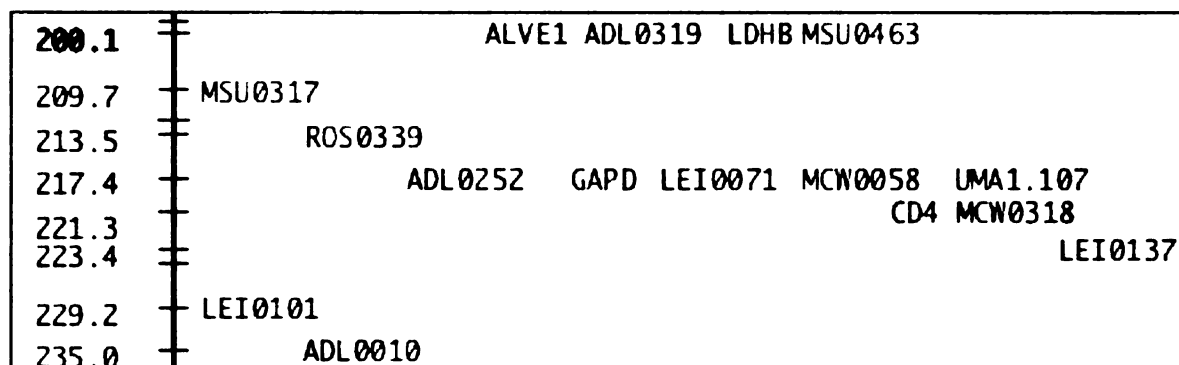


**Figure 6.2** - Genetic map for the *rge* region. East Lansing genetic map with the marker (MCW0318) tightly linked to *rge* (highlighted).

Unlike most regions of the chicken genome, the *rge* region does not show a single conserved synteny to the human genome. However, human 12p11-13, which contains GAPD and CD4 (Figure 6.3), is the region that exhibits the highest amount of conservation for that map region. Therefore, this was the region from which potential candidate genes were selected.

| Locus           | Chicken<br>Position | Human     |             | Mouse    |              |
|-----------------|---------------------|-----------|-------------|----------|--------------|
|                 |                     | Chr.      | Band        | Chr.     | Position     |
| ASCL1           | 160                 | 12        | q22-q23     | 10       |              |
| IGF1            | 172                 | 12        | q22-q23     | 10       | 48.00        |
| TRA1            | 174                 | 12        | q22-q23     | 10       | 49.00        |
| ITPR2           | S                   | 12        | p11         | 6        | S            |
| LDHB            | 204                 | 12        | p12.2-p12.1 | 6        | 62.00        |
| CCND2           | 230                 | 12        | p13         | 6        | 60.00        |
| <b>GAPD/CD4</b> | <b>241</b>          | <b>12</b> | <b>p13</b>  | <b>6</b> | <b>56.00</b> |
| TCRB            | 230                 | 7         | q35         | 6        | 20.50        |
| PPARA           | 240                 | 22        | q13.31      | 15       | 48.80        |
| HSD3B1          | 254                 | 1         | p13.1       | 3        | 49.10        |
| EPHA3           | 274                 | 3         | p11.2       | 16       | S            |

**Figure 6.3** - Interspecies comparative genetic map (chicken, human and mouse) for the *rge* region. Note that the human GAPD gene is located at the chromosome 12p13. This region is analogous to mouse chromosome 6. Key – S = chromosomal location obtained with somatic cell hybrids.

### 6.3.2.i. Selection of candidate genes

#### 6.3.2. i.a. Cyclin-dependent kinase inhibitor (Kip1)

The cyclin-dependent kinase inhibitor p27kip1, or Kip1, maps to human chromosome 12 p13.2. This gene product has an important role in determining cell fate during retinogenesis and more specifically regulates cell cycle withdrawal of late multipotent progenitor cells in the retina . Kip1 was chosen because mutations in other genes involved in retinal cell fate (*NR2E3* and *Nrl*), cause retinal dystrophies. Namely *NR2E3* mutations cause enhanced S-cone syndrome in humans and the *rd7* degeneration in mice. *Nrl* mutations cause a similar phenotype .



#### 6.3.2.i.b. Synaptobrevin (Vamp1)

Vesicle associated membrane protein (Vamp1; also known as synaptobrevin) maps to the human chromosome 12p13.31. Vamp1 is part of the SNARE protein complex . These proteins have critical functions during regulated vesicular release of retinal neurotransmitter. In addition, Vamp1 also plays a critical role during neurite outgrowth and synaptogenesis in the mammalian retina . Since it was possible to observe abnormally shaped photoreceptor pedicles and spherules with abnormally shaped vesicles ultrastructurally, Vamp1 was a natural candidate gene.

#### 6.3.3. Mapping and sequencing of candidate genes

##### 6.3.3.i. Radiation-hybrid (RH) mapping

Kip1 and Vamp1 were mapped using the chicken RH panel. A correlation analysis of the results indicates that Kip1 and Vamp1 are indeed located at chromosome 1. The correlation scores from Vamp1 and the microsatellite marker MCW0318 were higher (closer to 1) than Kip1 (see Figure 6.4).

| <b>Correlations</b> |                |                |                |                |             |                  |                  |
|---------------------|----------------|----------------|----------------|----------------|-------------|------------------|------------------|
| <b>Variable</b>     | <b>LEI0071</b> | <b>MCV0058</b> | <b>MCV0318</b> | <b>LEI0137</b> | <b>KIP1</b> | <b>VAMP 0795</b> | <b>VAMP 8974</b> |
| <b>LEI0071</b>      | 1.0000         | 0.4818         | 0.3187         | 0.3416         | 0.2835      | 0.5897           | 0.5897           |
| <b>MCV0058</b>      | 0.4818         | 1.0000         | 0.4919         | 0.5237         | 0.3067      | 0.7429           | 0.7429           |
| <b>MCV0318</b>      | 0.3187         | 0.4919         | 1.0000         | 0.6928         | 0.3668      | 0.5026           | 0.5828           |
| <b>LEI0137</b>      | 0.3416         | 0.5237         | 0.6928         | 1.0000         | 0.2971      | 0.5514           | 0.6380           |
| <b>KIP1</b>         | 0.2835         | 0.3067         | 0.3668         | 0.2971         | 1.0000      | 0.3380           | 0.4916           |
| <b>VAMP 0795</b>    | 0.5897         | 0.7429         | 0.5026         | 0.5514         | 0.3380      | 1.0000           | 0.8253           |
| <b>VAMP 8974</b>    | 0.5897         | 0.7429         | 0.5828         | 0.6380         | 0.4916      | 0.8253           | 1.0000           |

**Figure 6.4** - RH correlation for several microsatellite markers linked to the *rge* region. Note that Vamp1 markers (VAMP 0795 and VAMP 8974) show higher scores than KIP1.

### **6.3.3.ii. Sequencing of candidate genes**

Since Vamp 1 was the candidate gene showing the best correlation with the microsatellite MCW0318, the gene was sequenced from affected and control DNA using the following sequencing primers:

- VAMP 1. 6 Forward: 5' – TTTGGAATACGTATGCTGGAGAGGCCG,  
Reverse: 5' - AAGCTCTGACAGTTTCTGGTCTCG
- SPJ VAMP 1. 8 Forward: 5' - TTAGCAGTGTGCTAGGGTCTTTCC,  
Reverse: 5' - GGAAGTAGTGTTCCAACGCTACCA
- SPJ VAMP 1. 9 Forward: 5' - TCAGCATCTGCCTTATGTTCCCTC,  
Reverse: 5' - TGGATTCAGGCAAGAAGAGACAGG
- SPJ VAMP 1. 13 Forward: 5' - TGTTACGTTCTCTCTGCCCTTGTG,  
Reverse: 5' - GCCTCTCCAGCATACGTATTCCAA
- SPJ VAMP 1. 14 Forward: 5' - CCGAGGGAGGGACTGGATTATTT,  
Reverse: 5' - AATCTAGCAGGTCTGCTCCCTAGA

No difference was found in the sequence of Vamp1 from the DNA of rge and control chicks. When the first exon of the human Vamp1 gene was screened for chicken trace sequences and ESTs, no match was found. Therefore, primers could not be designed to amplify that region of the chicken Vamp1 gene. However, human exon 1 contains the AT coding nucleotides of the ATG start codon. The chicken sequence obtained for the Vamp1 gene is shown below:

1 GTAGGTGGAA ACAACCCCG **AGGGAGGGAC** TGGATTATT TATTATGTTT (SPJ VAMP 1. 14 FORWARD)  
 51 GCGCTGCATA GGGCGACATA GTGGCGGCT GTTTGGTTCC CTTCCTCCCC  
 101 TTTTGGGGG GGGGGCGGG GCGGGGGCC CGGCCGGCC CCGACCCGCA  
 151 GAATGCCCTGC AGCCGCTCCG GGAGCAGCTA AGGGGGGATT TGGCAGGGG  
 201 GGTGTTGCC CTCCTCTCAC CTTCAGCGCT GGTAGCTCGG GGGGGGCATC  
 251 TGTCTTTGA CAGCTGAGG CGTGATGTTA **CGTTCTCTCT** GCCCTTGTGT (SPJ VAMP 1. 13 FORWARD)  
 301 GTTCCCATAG **GT**TTGAACCA GCTCAGCAGC CTGCTCCTGG GGGCCCGGAA  
 351 GGGGAGCCC CTGCCGGGG CCCCCGGGG CCACCCCCCA ATCTGAGCAG  
 401 TAACCGTCGG CTGCAGCAGA CGCAGGCCCA GGTGGAGGAG GTCAGTAGCT  
 451 GTGCTGCTTC CCTTGGGCTG TATGGGCGCT TGCCTGCTT TGCTGCAGTG  
 501 GTGCTCTTGT TAAGTGATG TTGCTGAAGG GGTGGATGCT TTTGGAATAC (SPJ VAMP 1. 13 REVERSE)  
 551 GTATGCTGGA GAAGCGCTAA TAATCAATGC AAGGACAGTG TCTGATCTGT (SPJ VAMP 1. 6 FORWARD)  
 601 AAACGGGAG GAGCTGAGAT GAAATAGCTT TATATTTAAA AGCAGTGTA  
 651 TTTTGGTTAT GACATCTAGG GAGCAGACCT GCTAGATTCC TTGTACTTCA (SPJ VAMP 1. 14 REVERSE)  
 701 TATGACACGA GTATCATAGA AATAAACCTC TATGGGATCC AGAACTACTC  
 751 TTAATCCCTG CCGGGTGAAC AGTTAGAGTG CGCGTTCAAT GTAAACGTCG  
 801 AACATTACCT GACTTCGCAG AGTGCAAGTA CTCCCTTATG CCTCGCTGGG  
 851 GCAGCAACAC GTAGCTCTAA GTTGTCTTTG CAGTTATCTT CCCTTGAGCA  
 901 TGTGATTGCA GGGGTAGAGG GGGTTGCTCT AATCCTGATG GACTTGGGAA  
 951 CTTTCAAAA CAAGTGAGAG TAGTGTGCTG CAAGTGAGA TTAATTATAC  
 1001 TTGAAAGGAT GCTTTAGCAG **TGTCTAGGG** TCTTTCCCA TTTTCGAGTA (SPJ VAMP 1. 8 FORWARD)  
 1051 GGCAATGACC TGAAAGCTGT TTTTCTTTA CTCTCATCTT TATTCTTGT  
 1101 TTCAGGCTTT TACTTGTAG TAGTATCTTA GCGTTGCTGT GTTACTGCTC  
 1151 TTACTTTCAA CCCTGTGAA CCGCTATGAC TACTGCTACT GTTTTCCTT  
 1201 CTGCAGGTGG TTGATATAAT GCGTGTAAT GTCGACAAGG TACTGGAACG  
 1251 **AGACCAGAAA** CTGTCAGAGC TTGATGACCG GGCAGATGCA CTTCAGGCTG (SPJ VAMP 1. 6 REVERSED)  
 1301 GTGCCTCAGT ATTTGAAAGT AGTGAGCAA AACTCAAAAG GAAGTACTGG  
 1351 TGGAAGAACT GTAAGGTGAG TTTCTTAGTG CCGTGATTTC TTTCAATTAGA  
 1401 AGGGAATTTG ATTAGTTTTC TTCAGGGCTT TCTGAGGATA GTTGGGACAT  
 1451 AATAACTATT ATAACAATTT CAAATGCTTA GGATTATTTC ACTGTGGAAG  
 1501 GTCTTTGAGG CCTCAGCTGT CCTGCCTTCA GCATCTGCCT TATGTTCCCT (SPJ VAMP 1. 9 FORWARD)  
 1551 CATTTGTCATG GAACTGTGA ACTCAGCAGT CTGTTTGTAG TATTACTATC  
 1601 TGACAATCTC TCTTTTGA **TGATGATCAT** GATGGGAGTG ATTTGTGCCA  
 1651 TTGTGGTGGT GGTGATGTGA AGTAAGTACT GAAAAGCCCA GGATTACAGG  
 1701 TGAAGAAGCC GTAACACCAG AGTACTTTAA AACTTTTGCT TTTTGGTTTA  
 1751 TGATCTGGAG GGTCTTGTTC GCATAAGTGG TAACTTCTTT CCTTGGGAAA  
 1801 GGGAGTGGT AGCGTTGGAA CACTAGTTCC AGTTACTGTG GAAATAGTAT (SPJ VAMP 1. 8 REVERSE)  
 1851 GCTTTACAGA GCAAGGAAAG GAAGTGGGG TGGCCATCAA TGTAAGAGTG  
 1901 AGACATTTTA TTACCAGGTC AAATAAACCT GTAAATATGA GGGACAGATA  
 1951 CTTGAAGTG GGTGGGTTTG CAAGCCCTT TCCTGGTGGG GGATTTTGGA  
 2001 GGTCTCTGGG GGACCTTTGA TGTAACCTGC CCTTCTGTTT TTTCTTTT  
 2051 TTCCCTCTTA AGGTATGTCC AGTCTACTTT TTTACTTGAA TGTAGCCCT  
 2101 **AAAGGCTGCA** ACCTGCTGTC CCCTGTACCC TTGCCTGTCT CTTCCTGCCT (SPJ VAMP 1. 9 REVERSE)  
 2151 **GAATCCACCC** ACATGAGTAC TGCCAAAAA A

**Figure 6.5** - Chicken Vamp1 sequence derived from chicken trace sequences. Underlined = exon 2 to 5. The AT of the start codon is on exon 1. The end of the start codon is marked ( ). The stop codon is highlighted in bold. The primers used are shaded in gray.

## 6.4. Discussion

We were able to demonstrate that the mutation present in the *rge* chicken is not the same present in the *rd* chicken.

The early research efforts to identify potential candidate genes through comparative mapping were slightly confounded by the fact that the initial *rge* confidence interval did not show a single conserved synteny to the human genome.

The more refined mapping of the *rge* defect on chromosome 1 indicated that human chromosome region 12 p11-13 is the most likely region to contain the human homolog of the *rge* gene. Among the investigated genes in the study, Vamp1 had the best correlation to the microsatellite marker that absolutely co-segregated with the *rge* locus (MCW0318). However, sequence analysis revealed no differences in the coding regions and splice sites of the gene in *rge* birds compared to controls. Sequence differences in the first exon, which contains 2 of the start codon nucleotides, however, could not be analyzed because no matching chicken sequences were found for that exon. A possible future plan for the completion of the analysis of the Vamp1 sequence would be using the 5' Rapid Amplification of cDNA Ends (5' RACE) technique to obtain the 5' end of the chicken Vamp1 cDNA for sequencing. Nevertheless, immunohistochemically stained retinal sections using an anti-Vamp1 antibody revealed no differences in labeling patterns between control and *rge* birds (Chapter 5). Therefore, it seems unlikely that this gene contains the *rge*-causing mutation.

Most autosomal recessive inherited retinal diseases are reportedly due to nonsense mutations. These often result from the introduction of a premature stop codon. It is much

less likely that recessive diseases are caused by misense mutations that cause a change in protein sequence and thus protein function or localization. Therefore we anticipate finding the causative mutation in the coding region or exon/intron splice sites. This would be expected to show a lack of expression in immunohistochemistry studies.

Alternatively, it is conceivable that the causal mutation lies outside the coding region or the splice site of the gene involved (e.g., in a promoter or regulatory region) or in a gene that has not previously been identified and fails to support the comparative map (e.g., translocation). Micro-rearrangements will hopefully become apparent when the Chicken Genome Project is concluded.

## CHAPTER 7

### CONCLUSIONS & FUTURE STUDIES

The results of this work show that the *rge* chick has an unusual form of retinal dystrophy with electroretinographic and morphological changes quite unlike the previously described retinal dystrophies in any species.

The electroretinographic changes observed in *rge* birds progressively deteriorated with age and were characterized initially by a reduction in photoreceptor sensitivity, marked decrease in oscillatory potentials, an increase in b-wave amplitudes (supernormal b-waves) and delayed implicit times of a- and b-waves (Chapter 3). The results obtained with the intravitreal injection of APB, PDA, barium and ornithine (Chapter 4) also suggest an abnormal transmission from the photoreceptors to the second order neurons in the *rge* retinas. Application of drugs that block the generation of the b-wave in normal birds has little effect on the ERG in the *rge* chick. This suggests that normal transmission to the inner retina of *rge* birds does not occur. Furthermore the processes that occur in the normal retina do not generate the b-wave in *rge* birds. The only two agents used that caused a change in the *rge* ERG were barium and ornithine. The supernormal component of the *rge* ERG was blocked by ornithine, a known pharmacological RPE blocker that might also affect photoreceptors. The amplitude of the supernormal b-waves was even further elevated after intravitreal injections of barium chloride, a known potassium channel blocker of Müller cells. The specific cellular origin of the supernormal b-wave, however, remains uncertain. RPE and photoreceptors, and less likely Müller cells, still remain as candidates. Future ERG studies with additional drugs are planned to further

dissect the components of the *rge* ERG, such as the use of sodium iodate to destroy the RPE cells and cobalt, which may act directly on the photoreceptors. Intraretinal ERG recording might also be used to identify which retinal layer is responsible for the abnormal components of the *rge* ERG. However it is also conceivable that identification of the underlying gene defect may be required to fully explain the ERG abnormalities.

The apparent absence of inner retinal components of the ERG in the *rge* bird is in keeping with ultrastructural studies showing abnormalities in the synapses between the photoreceptors and second order retinal neurons. This abnormal signaling of photoreceptors to inner retinal cells and the resultant loss of visual acuity may be functionally equivalent to form-deprivation, and thereby, as in this environmentally induced ametropia, result in excessive ocular growth. It is likely that functional coupling of photoreceptor responses to the growth-regulating mechanisms of the inner retina are disrupted in *rge* birds. The fact that the marked morphological globe changes that develop in the *rge* chick occur after electrophysiological and ultrastructural evidence of retinal abnormality supports the supposition that they are most likely secondary to retinal dysfunction. However, in turn they are likely to account for some of the retinal changes in the later stages of the disease. These morphological changes are similar to those that develop in constant light exposure chicks (e.g. increased corneal thickness, low IOP, hyperopia, radial globe enlargement and linear fundus lesions). There is evidence to show that melatonin plays a role in these changes in the constant light exposure chick and might, therefore also play a role in the *rge* chick. To address this possibility, a future collaborative effort with Drs. Howard Howland and Tong Li from Cornell University, to measure retinal levels of melatonin in *rge* chicks, is planned.



The recent mapping of the *rge* locus to chicken chromosome 1 and our refined mapping results suggest a number of candidate genes to investigate as candidates for the genetic basis of the *rge* defect (Chapter 6). *Vamp1*, among the investigated genes in the study, had the best correlation to the microsatellite marker with which *rge* cosegregated completely. However, sequence analysis revealed no differences in the *rge* birds compared to controls.

The most pressing future work will be to try to identify the causal gene mutation for the *rge* defect. Further candidate genes are discussed below:

Calcium channel L-type alpha 1 subunit maps to human chromosome 12p13.33. This gene was chosen as a positional candidate for the *rge* defect because calcium ( $\text{Ca}^{2+}$ ) L-type channels are closely associated with synaptic ribbons of photoreceptor pedicles and spherules.  $\text{Ca}^{2+}$  influx through voltage-gated channels stimulates a variety of neural activities, including process outgrowth, neurotransmission, and synaptic plasticity. In general, L-type channels control  $\text{Ca}^{2+}$  influx into the soma and dendrites of the cells of the nervous system, whereas other  $\text{Ca}^{2+}$  channel types control presynaptic activities. Neurons that make ribbon synapses, however, are among a select group of nerve cells whose presynaptic  $\text{Ca}^{2+}$ -dependent secretion is linked to L-type channels.

GABA(A) receptor-associated protein like 1 maps to human chromosome 12p13.2. This gene was also chosen as a positional candidate for the *rge* defect because of the remarkable increase in globe size observed in the *rge* chicks (Chapter 2). It is known that GABA(A), GABA(A<sub>0r</sub>), and GABA(B) receptors modulate eye growth and refractive development. Additionally, GABA(A) receptors occur in both OPL and IPL and distinct types of amacrine cell somata. GABA(A<sub>0r</sub>) receptors also

localize to both plexiform layers and to the processes of bipolar cells. Due to the involvement in the control of eye globe size and for the localization of GABA receptors in the retina, a gene related to the GABA receptor family is a potential candidate for the *rge* defect.

The gene responsible for dynamin-1 like protein, isoforms 1 to 3, maps to human chromosome 12p11.21. This gene is another positional candidate for the *rge* defect because several lines of evidence indicate that dynamin 1, a very similar gene, is required to separate synaptic vesicles attached to the photoreceptor presynaptic membrane during endocytosis .

The above candidate genes should first be RH mapped in order to confirm them as good positional candidate genes for the *rge* defect prior to sequencing them.

The upcoming release of the complete chicken genome sequence will serve as an invaluable resource to enhance our ability to select and screen other positional candidate genes for potential causative mutations. The complete genome sequence may also provide additional markers to fill marker gaps.

An avian model of retinal dystrophy such as the *rge* demonstrates some advantages over other animal models such as those in mice and dogs. Mice are popular for the study of different types of inherited retinal disease, with both spontaneously occurring models and engineered ones. Mice have some advantages as a research model over others species; they reproduce quickly and are relatively inexpensive to maintain and have a highly investigated genome. Disadvantages are that mice have a rod-dominated retina and small sized eyes.

A breeding colony of chickens also is relatively inexpensive to establish and maintain. Genetic abnormalities progress rapidly compared to those in other models such as dogs, since adult chickens are sexually mature in 4-5 months.

Normal retinal function in humans relies heavily on cone function. The cone-rich human macula is the most important area in the human retina, with the highest acuity for color and daylight vision. Since chickens have a cone-dominated retina, models of retinal dystrophy in this species are valuable research model for cone development and function in human vision. Birds, similarly to humans and unlike mice and dogs, are diurnal species. Human and chick eyes grow significantly over their lives and have optics of good quality. These are the main reasons that the chicken eye has become a widely used model for refraction studies. Additionally, human and chicken eyes are closer in size than human and mice eyes. This feature of the avian eye permits surgical manipulations (such as delivery of intravitreal drugs and/or gene therapy vectors) using techniques comparable to those used in humans. Whereas in the mouse the small size of the eye and certain anatomical features such as the large lens and small vitreal cavity size mean that it is not a good model for procedures that are ultimately aimed for use in humans.

In conclusion, the *rge* chick is not only a unique model of retinal dystrophy, understanding of which may improve our knowledge of retinal function and also of the generation of the ERG, but it is also valuable for ametropy studies and is the only spontaneous model of the complications of globe enlargement such as the formation of lacquer crack lesions.

## BIBLIOGRAPHY

- Adler, R., C. Curcio, et al. (1999). "Cell death in age-related macular degeneration." Mol Vis **5**: 31.
- Aguirre, G., J. Alligood, et al. (1982). "Pathogenesis of progressive rod-cone degeneration in miniature poodles." Invest Ophthalmol Vis Sci **23**(5): 610-30.
- Akhmedov, N. B., N. I. Piriev, et al. (2000). "A deletion in a photoreceptor-specific nuclear receptor mRNA causes retinal degeneration in the rd7 mouse." Proc Natl Acad Sci U S A **97**(10): 5551-6.
- Allikmets, R., N. F. Shroyer, et al. (1997). "Mutation of the Stargardt disease gene (ABCR) in age-related macular degeneration." Science **277**(5333): 1805-7.
- Araki, M., Y. Fukada, et al. (1990). "Localization of iodopsin in the chick retina during in vivo and in vitro cone differentiation." Invest Ophthalmol Vis Sci **31**(8): 1466-73.
- Arshavsky, V. Y., T. D. Lamb, et al. (2002). "G proteins and phototransduction." Annu Rev Physiol **64**: 153-87.
- Arushanian, E. B. and K. B. Ovanesov (1999). "Melatonin lowers the threshold of light sensitivity of the human retina." Eksp Klin Farmakol **62**(2): 58-60.
- Autzen, T. and L. Bjornstrom (1989). "Central corneal thickness in full-term newborns." Acta Ophthalmol (Copenh) **67**(6): 719-20.
- Baich, A. and K. Ratzlaff (1980). "Ornithine aminotransferase in chick embryo tissues." Invest Ophthalmol Vis Sci **19**(4): 411-4.
- Ballesta, J., G. Terenghi, et al. (1984). "Putative dopamine-containing cells in the retina of seven species demonstrated by tyrosine hydroxylase immunocytochemistry." Neuroscience **12**(4): 1147-56.
- Barishak, Y. R. (2001). Embryology of the eye and its adnexa. Basel, NY, Karger.
- Barlow, H. B. and T. J. Ostwald (1972). "Pecten of the pigeon's eye as an inter-ocular eye shade." Nat New Biol **236**(64): 88-90.

- Bauerfeind, R., T. Galli, et al. (1996). "Molecular mechanisms in synaptic vesicle recycling." J Neurocytol **25**(12): 701-15.
- Beebe, D. C. and J. M. Coats (2000). "The lens organizes the anterior segment: specification of neural crest cell differentiation in the avian eye." Dev Biol **220**(2): 424-31.
- Beresford, J. A., S. G. Crewther, et al. (2001). "Comparison of refractive state and circumferential morphology of retina, choroid, and sclera in chick models of experimentally induced ametropia." Optom Vis Sci **78**(1): 40-9.
- Bergmann, M., D. Grabs, et al. (1999). "Developmental expression of dynamin in the chick retinotectal system." J Histochem Cytochem **47**(10): 1297-306.
- Berson, E. L. (1993). "Retinitis pigmentosa. The Friedenwald Lecture." Invest Ophthalmol Vis Sci **34**(5): 1659-76.
- Bessant, D. A., G. E. Holder, et al. (2003). "Phenotype of retinitis pigmentosa associated with the Ser50Thr mutation in the *NRL* gene." Arch Ophthalmol **121**(6): 793-802.
- Birch, D. G. and J. L. Anderson (1992). "Standardized full-field electroretinography. Normal values and their variation with age." Arch Ophthalmol **110**(11): 1571-6.
- Bok, D. and R. W. Young (1979). Phagocytic Properties of the Retinal Pigment Epithelium. The Retinal Pigment Epithelium. K. M. Zinn and M. F. Marmor. Cambridge, MA, Harvard University Press: 148-174.
- Bowmaker, J. K. and A. Knowles (1977). "The visual pigments and oil droplets of the chicken retina." Vision Res **17**(7): 755-64.
- Bownds, D., J. Dawes, et al. (1972). "Phosphorylation of frog photoreceptor membranes induced by light." Nat New Biol **237**(73): 125-7.
- Bowne, S. J., L. S. Sullivan, et al. (2002). "Mutations in the inosine monophosphate dehydrogenase 1 gene (*IMPDH1*) cause the RP10 form of autosomal dominant retinitis pigmentosa." Hum Mol Genet **11**(5): 559-68.

- Brach**, V. (1975). "The effect of intraocular ablation of the pecten oculi of the chicken." Invest Ophthalmol **14**(2): 166-8.
- Bringmann**, A. and A. Reichenbach (2001). "Role of Muller cells in retinal degenerations." Front Biosci **6**: E72-92.
- Brown**, K. T. (1968). "The electroretinogram: its components and their origins." Vision Res **8**(6): 633-77.
- Bruesch**, S. and L. Arey (1942). "The number of myelinated and unmyelinated fibers in the optic nerve of vertebrates." Journal of Comparative Neurology **77**: 631-665.
- Bruhn**, S. L. and C. L. Cepko (1996). "Development of the pattern of photoreceptors in the chick retina." J Neurosci **16**(4): 1430-9.
- Burt**, D. W., D. R. Morrice, et al. (2003). "Analysis of the rdd locus in chicken: a model for human retinitis pigmentosa." Mol Vis **9**: 164-70.
- Bush**, R. A. and P. A. Sieving (1994). "A proximal retinal component in the primate photopic ERG a-wave." Invest Ophthalmol Vis Sci **35**(2): 635-45.
- Butler**, A. B. and W. Hodos (1996). Comparative Vertebrate Neuroanatomy: Evolution and Adaptation. New York, NY, Wiley-Liss.
- Carroll**, J., C. J. Murphy, et al. (2001). "Photopigment basis for dichromatic color vision in the horse." J Vis **1**(2): 80-7.
- Chen**, Y., M. Hu, et al. (2003). "Changes in somal growth and dendritic patterns of the retinal ganglion cells in the chicks and chick embryos." J Vet Med Sci **65**(10): 1135-7.
- Cherqui**, S., C. Sevin, et al. (2002). "Intralysosomal cystine accumulation in mice lacking cystinosin, the protein defective in cystinosis." Mol Cell Biol **22**(21): 7622-32.
- Coleman**, P. A., P. L. Carras, et al. (1987). "Barium reverses the transretinal potassium gradient of the amphibian retina." Neurosci Lett **80**(1): 61-5.

- Cook, C. S. (1995). "Embryogenesis of congenital eye malformations." Veterinary & Comparative Ophthalmology 5: 109-23.
- Cook, C. S. (1999). Ocular embryology and congenital malformations. Veterinary Ophthalmology. K. N. Gelatt. Philadelphia, PA, Lippincott Williams & Wilkins: 3-17.
- Coulombre, A. J. (1955). "Correlations of structural and biochemical changes in the developing retina of the chick." Am J Anat 96(1): 153-89.
- Cremona, O. and P. De Camilli (1997). "Synaptic vesicle endocytosis." Curr Opin Neurobiol 7(3): 323-30.
- Crewther, D. P., S. G. Crewther, et al. (1996). "Changes in eye growth produced by drugs which affect retinal ON or OFF responses to light." J Ocul Pharmacol Ther 12(2): 193-208.
- Crozier, W. J. and E. Wolf (1944). "Flicker response contours for the sparrow and the theory of the avian pecten." Journal of General Physiology 27: 315-24.
- Curtin, B. J. (1985). Ocular findings and complications. The Myopias: Basic Science and Clinical Management. B. J. Curtin. Philadelphia, PA, Harper and Row: 277-347.
- Curtis, P. E., J. R. Baker, et al. (1987). "Impaired vision in chickens associated with retinal defects." Vet Rec 120(5): 113-4.
- Curtis, R., J. R. Baker, et al. (1988). "An inherited retinopathy in commercial breeding chickens." Avian Pathology 17: 87-99.
- Czepita, D. (2002). "Myopia - epidemiology, pathogenesis, present and coming possibilities of treatment." Clinical Practice Review 3: 294-300.
- De Camilli, P. (1995). "Neurotransmission. Keeping synapses up to speed." Nature 375(6531): 450-1.
- Dowling, J. E. (1960). "Chemistry of visual adaptation in the rat." Nature 188: 114-8.
- Duke-Elder, S. (1958). System of Ophthalmology. London, Henry Kimpton.

- Dyer, M. A. and C. L. Cepko (2000). "Control of Muller glial cell proliferation and activation following retinal injury." Nat Neurosci **3**(9): 873-80.
- Emeis, D., H. Kuhn, et al. (1982). "Complex formation between metarhodopsin II and GTP-binding protein in bovine photoreceptor membranes leads to a shift of the photoproduct equilibrium." FEBS Lett **143**(1): 29-34.
- Emmerton, J. and J. D. Delius (1980). "Wavelength discrimination in the 'visible' and ultraviolet spectrum in pigeons." Journal of Comparative Physiology **141**: 47-52.
- Evans, L. S., N. S. Peachey, et al. (1993). "Comparison of three methods of estimating the parameters of the Naka-Rushton equation." Doc Ophthalmol **84**(1): 19-30.
- Farahbakhsh, Z. T., K. Hideg, et al. (1993). "Photoactivated conformational changes in rhodopsin: a time-resolved spin label study." Science **262**(5138): 1416-9.
- Ferrari, P. A. and W. E. Koch (1984). "Development of the iris in the chicken embryo. I. A study of growth and histodifferentiation utilizing immunocytochemistry for muscle differentiation." J Embryol Exp Morphol **81**: 153-67.
- Ferrari, P. A. and W. E. Koch (1984). "Development of the iris in the chicken embryo. II. Differentiation of the irideal muscles in vitro." J Embryol Exp Morphol **81**: 169-83.
- Fischer, A. J., J. J. McGuire, et al. (1999). "Light- and focus-dependent expression of the transcription factor ZENK in the chick retina." Nat Neurosci **2**(8): 706-12.
- Fischer, A. J., R. L. Seltner, et al. (1998). "Immunocytochemical characterization of quisqualic acid- and N-methyl-D-aspartate-induced excitotoxicity in the retina of chicks." J Comp Neurol **393**(1): 1-15.
- Fischer, A. J., R. L. Seltner, et al. (1997). "N-methyl-D-aspartate-induced excitotoxicity causes myopia in hatched chicks." Can J Ophthalmol **32**(6): 373-7.
- Fulton, A. B., K. V. Fite, et al. (1982). "Retinal degeneration in the delayed amelanotic (DAM) chicken: an electroretinographic study." Curr Eye Res **2**(11): 757-63.



- Gabella, G. and E. Clarke (1983). "Embryonic development of the smooth and striated musculatures of the chicken iris." Cell Tissue Res **229**(1): 37-59.
- Gallemore, R. P. and R. H. Steinberg (1991). "Cobalt increases photoreceptor-dependent responses of the chick retinal pigment epithelium." Invest Ophthalmol Vis Sci **32**(12): 3041-52.
- Garamszegi, L. Z., A. P. Moller, et al. (2002). "Coevolving avian eye size and brain size in relation to prey capture and nocturnality." Proc R Soc Lond B Biol Sci **269**(1494): 961-7.
- Gilger, B. C., R. D. Whitley, et al. (1991). "Canine corneal thickness measured by ultrasonic pachymetry." Am J Vet Res **52**(10): 1570-2.
- Goebel, H. H., A. Kohlschutter, et al. (1978). "Ultrastructural observations on the retina in type II glycogenosis (Pompe's disease)." Ophthalmologica **176**(2): 61-8.
- Goldsmith, T. H. (1980). "Hummingbirds see near ultraviolet light." Science **207**(4432): 786-8.
- Goldsmith, T. H., J. S. Collins, et al. (1984). "The cone oil droplets of avian retinas." Vision Res **24**(11): 1661-71.
- Gomez, A., J. Cedano, et al. (2001). "The gene causing the Best's macular dystrophy (BMD) encodes a putative ion exchanger." DNA Seq **12**(5-6): 431-5.
- Gouras, P., H. M. Eggers, et al. (1983). "Cone dystrophy, nyctalopia, and supernormal rod responses. A new retinal degeneration." Arch Ophthalmol **101**(5): 718-24.
- Gouras, P. and C. J. MacKay (1992). "Supernormal cone electroretinograms in central retinal vein occlusion." Invest Ophthalmol Vis Sci **33**(3): 508-15.
- Granit, R. (1933). "The components of the retinal action potential in mammals and their relation to the discharge in the optic nerve." Journal of Physiology **77**: 207-39.
- Greenlee, M. H., C. B. Roosevelt, et al. (2001). "Differential localization of SNARE complex proteins SNAP-25, syntaxin, and VAMP during development of the mammalian retina." J Comp Neurol **430**(3): 306-20.

- Griff, E. R., Y. Shirao, et al. (1985). "Ba<sup>2+</sup> unmasks K<sup>+</sup> modulation of the Na<sup>+</sup>-K<sup>+</sup> pump in the frog retinal pigment epithelium." J Gen Physiol **86**(6): 853-76.
- Grossniklaus, H. E. and W. R. Green (1992). "Pathologic findings in pathologic myopia." Retina **12**(2): 127-33.
- Hacker, G. (2000). "The morphology of apoptosis." Cell Tissue Res **301**(1): 5-17.
- Hagerman, G. S. and L. V. Johnson (1991). The photoreceptor-retinal pigmented epithelium interface. Principles and Practice of Clinical Electrophysiology of Vision. J. R. Heckenlively and G. B. Arden. St. Louis, Mosby Year Book: 53-68.
- Haider, N. B., S. G. Jacobson, et al. (2000). "Mutation of a nuclear receptor gene, *NR2E3*, causes enhanced S cone syndrome, a disorder of retinal cell fate." Nat Genet **24**(2): 127-31.
- Haider, N. B., J. K. Naggert, et al. (2001). "Excess cone cell proliferation due to lack of a functional *NR2E3* causes retinal dysplasia and degeneration in rd7/rd7 mice." Hum Mol Genet **10**(16): 1619-26.
- Hamm, H. E. and M. Menaker (1980). "Retinal rhythms in chicks: circadian variation in melatonin and serotonin N-acetyltransferase activity." Proc Natl Acad Sci U S A **77**(8): 4998-5002.
- Hayasaka, S., T. Shiono, et al. (1980). "Ornithine ketoacid aminotransferase in the bovine eye." Invest Ophthalmol Vis Sci **19**(12): 1457-60.
- Heidelberger, R. and G. Matthews (1992). "Calcium influx and calcium current in single synaptic terminals of goldfish retinal bipolar neurons." J Physiol **447**: 235-56.
- Hirata, A. and A. Negi (1998). "Lacquer crack lesions in experimental chick myopia." Graefes Arch Clin Exp Ophthalmol **236**(2): 138-45.
- Hiroi, K., F. Yamamoto, et al. (1995). "Effects of ornithine on the electroretinogram in cat retina." Invest Ophthalmol Vis Sci **36**(8): 1732-7.
- Hong, F. T. (1995). "Magnetic field effects on biomolecules, cells, and living organisms." Biosystems **36**(3): 187-229.

- Hood, D. C. (1990). The ERG and sites and mechanisms of retinal disease, adaptation and development. Advances in Photoreception: Proceedings of a Symposium on Frontiers of Visual Science. Washington, DC, The National Academies Press: 41-58.
- Hood, D. C. and D. G. Birch (1996). "Assessing abnormal rod photoreceptor activity with the a-wave of the electroretinogram: applications and methods." Doc Ophthalmol **92**(4): 253-67.
- Howland, H. C. and F. Schaeffel (1989). Development of accommodation and refractive state in the eyes of humans and chickens. Development of the Vertebrate Retina. B. L. Finlay and D. R. Sengelaub. New York, Plenum: 267-282.
- Humayun, M. S., M. Prince, et al. (1999). "Morphometric analysis of the extramacular retina from postmortem eyes with retinitis pigmentosa." Invest Ophthalmol Vis Sci **40**(1): 143-8.
- Inglehearn, C. F., D. R. Morrice, et al. (2003). "Genetic, ophthalmic, morphometric and histopathological analysis of the Retinopathy Globe Enlarged (rge) chicken." Mol Vis **9**: 295-300.
- Inoue, Y., Y. Sugihara, et al. (1980). "Atypical neural sheaths formed by Muller cells in chicken retina." Okajimas Folia Anat Jpn **57**(2-3): 79-88.
- Kandel, E. R., J. H. Schwartz, et al. (1991). Principles of Neural Science. Norwalk, Connecticut, Appleton & Lange.
- Karten, H. J. and W. J. H. Nauta (1968). "Organization of retinothalamic projections in the pigeon and owl." Anatomical Record **160**: 373.
- Karten, H. J. and A. M. Revzin (1966). "The afferent connections of the nucleus rotundus in the pigeon." Brain Res **2**(4): 368-77.
- Kasahara, M., T. Matsuzawa, et al. (1986). "Immunohistochemical localization of ornithine aminotransferase in normal rat tissues by Fab'-horseradish peroxidase conjugates." J Histochem Cytochem **34**(11): 1385-8.
- Keep, J. M. (1972). "Clinical aspects of progressive retinal atrophy in the Cardigan Welsh Corgi." Aust Vet J **48**(4): 197-9.

- Kefalov, V., Y. Fu, et al. (2003). "Role of visual pigment properties in rod and cone phototransduction." Nature **425**(6957): 526-31.
- Kirschfeld, K. (1982). "Carotenoid pigments: their possible role in protecting against photooxidation in eyes and photoreceptor cells." Proc R Soc Lond B Biol Sci **216**(1202): 71-85.
- Klein, R. M. and B. J. Curtin (1975). "Lacquer crack lesions in pathologic myopia." Am J Ophthalmol **79**(3): 386-92.
- Klein, R. M. and S. Green (1988). "The development of lacquer cracks in pathologic myopia." Am J Ophthalmol **106**(3): 282-5.
- Kolb, H. (1991). The neural organization of the human retina. Principles and Practices of Clinical Electrophysiology of Vision. J. R. Heckenlively and G. B. Arden. St. Louis, Mosby Year Book Inc. **6**: 25-52.
- Kolb, H. and L. E. Lipetz (1991). The anatomical basis for colour vision in the vertebrate retina. Vision and Visual Dysfunction, The Perception of Colour. London, UK, Macmillan Press Ltd. **6**: 128-45.
- Komenda, J. K. and K. V. Fite (1983). "Optokinetic nystagmus in progressive retinal degeneration." Behav Neurosci **97**(6): 928-36.
- Koutalos, Y. and T. G. Ebrey (1986). "Recent progress in vertebrate photoreception." Photochem Photobiol **44**(6): 809-17.
- Krill, A. E. and G. B. Lee (1963). "The electroretinogram in albinos and carriers of the ocular albino trait." Arch Ophthalmol **69**: 32-8.
- Kuwabara, T. (1979). Photic and photo-thermal effects on the retinal pigment epithelium. The Retinal Pigment Epithelium. K. M. Zinn and M. F. Marmor. Cambridge, MA, Harvard University Press: 293-313.
- Lahiri, D. and C. F. Bailey (1993). "A comparison of phagocytosis by the retinal pigment epithelium in normal and delayed amelanotic chickens." Exp Eye Res **56**(6): 625-34.

- Lam, K. W., J. Zwaan, et al. (1993). "Detection of ascorbic acid in the eye of the early chicken embryo by silver staining." Exp Eye Res **56**(5): 601-4.
- LaVail, M. M. (1976). "Rod outer segment disk shedding in rat retina: relationship to cyclic lighting." Science **194**(4269): 1071-4.
- Lei, B. and I. Perlman (1999). "The contributions of voltage- and time-dependent potassium conductances to the electroretinogram in rabbits." Vis Neurosci **16**(4): 743-54.
- Levine, E. M., J. Close, et al. (2000). "p27(Kip1) regulates cell cycle withdrawal of late multipotent progenitor cells in the mammalian retina." Dev Biol **219**(2): 299-314.
- Li, T. and H. C. Howland (1999). "The effect of melatonin on eye growth in chicks raised under constant light." Investigative Ophthalmology and Visual Science [ARVO Abstract] **40**: S847.
- Li, T., H. C. Howland, et al. (2000). "Diurnal illumination patterns affect the development of the chick eye." Vision Res **40**(18): 2387-93.
- Li, T., D. Troilo, et al. (1995). "Constant light produces severe corneal flattening and hyperopia in chickens." Vision Res **35**(9): 1203-9.
- Li, Z. Y., I. J. Kljavin, et al. (1995). "Rod photoreceptor neurite sprouting in retinitis pigmentosa." J Neurosci **15**(8): 5429-38.
- Liebner, S., H. Gerhardt, et al. (1997). "Maturation of the blood-retina barrier in the developing pecten oculi of the chicken." Brain Res Dev Brain Res **100**(2): 205-19.
- Lythgoe, J. N. (1979). The ecology of vision. Oxford, U.K., Clarendon Press.
- Manly, K. F. and J. M. Olson (1999). "Overview of QTL mapping software and introduction to map manager QT." Mamm Genome **10**(4): 327-34.
- Massey, S. C., D. A. Redburn, et al. (1983). "The effects of 2-amino-4-phosphonobutyric acid (APB) on the ERG and ganglion cell discharge of rabbit retina." Vision Res **23**(12): 1607-13.

- McCall, M. A., R. G. Gregg, et al. (1996). "Morphological and physiological consequences of the selective elimination of rod photoreceptors in transgenic mice." Exp Eye Res **63**(1): 35-50.
- Mears, A. J., M. Kondo, et al. (2001). "*Nrl* is required for rod photoreceptor development." Nat Genet **29**(4): 447-52.
- Meyer, D. B. (1977). The avian eye. Handbook of Sensory Physiology. The Visual System in Vertebrates. F. Crescitelli. Berlin, Springer: 549-612.
- Milam, A. H., L. Rose, et al. (2002). "The nuclear receptor *NR2E3* plays a role in human retinal photoreceptor differentiation and degeneration." Proc Natl Acad Sci U S A **99**(1): 473-8.
- Mito, T., T. Shiono, et al. (1989). "Immunocytochemical localization of ornithine aminotransferase in human ocular tissues." Arch Ophthalmol **107**(9): 1372-4.
- Mizota, A., E. Sato, et al. (2001). "Facilitatory and neurotoxic effects of intravitreal ornithine on the electroretinographic responses of albino rats." Ophthalmic Res **33**(2): 91-7.
- Molday, R. S. (1998). "Photoreceptor membrane proteins, phototransduction, and retinal degenerative diseases. The Friedenwald Lecture." Invest Ophthalmol Vis Sci **39**(13): 2491-513.
- Montiani-Ferreira, F., S. Petersen-Jones, et al. (2003). "Early postnatal development of central corneal thickness in dogs." Vet Ophthalmol **6**(1): 19-22.
- Morgan, I. G. (1983). "The organization of amacrine cell types which use different transmitters in chicken retina." Prog Brain Res **58**: 191-9.
- Morisson, M., A. Lemiere, et al. (2002). "ChickRH6: a chicken whole-genome radiation hybrid panel." Genet Sel Evol **34**(4): 521-33.
- Morris, V. B. (1970). "Symmetry in a receptor mosaic demonstrated in the chick from the frequencies, spacing and arrangement of the types of retinal receptor." J Comp Neurol **140**(3): 359-98.

- Morris, V. B. (1982). "An afoveate area centralis in the chick retina." J Comp Neurol **210**(2): 198-203.
- Morris, V. B. and C. D. Shorey (1967). "An electron microscope study of types of receptor in the chick retina." J Comp Neurol **129**(4): 313-40.
- Murphy, C. J. (1993). Raptor ophthalmology. Zoo and Wildlife Medicine. M. E. Fowler. Philadelphia, PA, W.B. Saunders: 211-21.
- Nachman-Clewner, M., R. St Jules, et al. (1999). "L-type calcium channels in the photoreceptor ribbon synapse: localization and role in plasticity." J Comp Neurol **415**(1): 1-16.
- Narfstrom, K., A. Wrigstad, et al. (1989). "The Briard dog: a new animal model of congenital stationary night blindness." Br J Ophthalmol **73**(9): 750-6.
- Nussbaum, R. L., R. E. McInnes, et al. (2001). Thompson & Thompson Genetics in Medicine. Philadelphia, PA, W B Saunders.
- Oakley, B., 2nd and D. G. Green (1976). "Correlation of light-induced changes in retinal extracellular potassium concentration with c-wave of the electroretinogram." J Neurophysiol **39**(5): 1117-33.
- Ohno-Matsui, K., M. Ito, et al. (1996). "Subretinal bleeding without choroidal neovascularization in pathologic myopia. A sign of new lacquer crack formation." Retina **16**(3): 196-202.
- Ohno-Matsui, K., T. Yoshida, et al. (2003). "Patchy atrophy and lacquer cracks predispose to the development of choroidal neovascularisation in pathological myopia." Br J Ophthalmol **87**(5): 570-3.
- Ookawa, T. (1971). "Further studies on the ontogenetic development of the chick electroretinogram." Poult Sci **50**(4): 1185-90.
- Ookawa, T. (1971). "On the ontogenetic study of the chick ERG." Nippon Seirigaku Zasshi **33**(5): 317-8.

- Ookawa, T. (1971). "The onset and development of the chick electroretinogram: the A- and B-waves." Poult Sci **50**(2): 601-8.
- Ookawa, T. and K. Takahashi (1971). "The ontogenetic development of the c-wave in the chick ERG." Experientia **27**(4): 407-9.
- Osorio, D., M. Vorobyev, et al. (1999). "Colour vision of domestic chicks." J.Exp.Biol. **202** ( Pt 21): 2951-9.
- Pacione, L. R., M. J. Szego, et al. (2003). "Progress toward understanding the genetic and biochemical mechanisms of inherited photoreceptor degenerations." Annu Rev Neurosci **26**: 657-700.
- Pardue, M. T., M. A. McCall, et al. (1998). "A naturally occurring mouse model of X-linked congenital stationary night blindness." Invest Ophthalmol Vis Sci **39**(12): 2443-9.
- Paton, I. R., J. Smith, et al. (2003). "Mapping the ABCA4, IMPDH2 and TIMP3 genes in chicken." Anim Genet **34**(5): 395-6.
- Pearlman, J. T. and H. M. Burian (1964). "Electroretinographic findings in thyroid dysfunction." American Journal of Ophthalmology **58**: 216-25.
- Pepperberg, D. R., P. K. Brown, et al. (1978). "Visual pigment and photoreceptor sensitivity in the isolated skate retina." J Gen Physiol **71**(4): 369-96.
- Petters, R. M., C. A. Alexander, et al. (1997). "Genetically engineered large animal model for studying cone photoreceptor survival and degeneration in retinitis pigmentosa." Nat Biotechnol **15**(10): 965-70.
- Pittack, C., G. B. Grunwald, et al. (1997). "Fibroblast growth factors are necessary for neural retina but not pigmented epithelium differentiation in chick embryos." Development **124**(4): 805-16.
- Pleyer, U. (2001). "Gene therapy in hereditary retinal degeneration and the tower of Babel." Br J Ophthalmol **85**(3): 255.



- Pollock, B. J., M. A. Wilson, et al. (1982). Preliminary observations of a new blind chick mutant (beg). Problems of normal and genetically abnormal retinas. R. M. Clayton, H. W. Reading, J. Haywood and A. Wright. London, UK, Academic Press: 241-7.
- Prada, C., J. Puga, et al. (1991). "Spatial and Temporal Patterns of Neurogenesis in the Chick Retina." Eur J Neurosci 3(6): 559-69.
- Pugh, E. N. J. and T. D. Lamb (2000). Phototransduction in Vertebrate Rods and Cones: Molecular Mechanisms of Amplification, Recovery and Light Adaptation. Handbook of Biological Physics. D. G. Stavenga, W. J. DeGrip and E. N. J. Pugh. Amsterdam, Elsevier. 3: 183-254.
- Qiu, H., E. Fujiwara, et al. (2002). "Evidence that a-wave latency of the electroretinogram is determined solely by photoreceptors." Jpn J Ophthalmol 46(4): 426-32.
- Rager, G. (1979). "The cellular origin of the b-wave in the electroretinogram -- a developmental approach." J Comp Neurol 188(2): 225-44.
- Randall, C. J., M. A. Wilson, et al. (1983). "Partial retinal dysplasia and subsequent degeneration in a mutant strain of domestic fowl (rdd)." Exp Eye Res 37(4): 337-47.
- Rando, R. R. (1990). "The Chemistry of Vitamin A and Vision." Angewandte Chemie International Edition 29: 461-80.
- Rao-Mirotznik, R., A. B. Harkins, et al. (1995). "Mammalian rod terminal: architecture of a binary synapse." Neuron 14(3): 561-9.
- Rodieck, R. W. p. S. F., CA: Freeman. (1973). The vertebrate retina: Principles of structure and function. San Francisco, CA, Freeman.
- Romanoff, A. L. (1960). The Avian Embryo: Structural and Functional Development. New York, NY, The Macmillan Company.
- Rothman, J. E. (1994). "Mechanisms of intracellular protein transport." Nature 372(6501): 55-63.

- Schaeffel, F. and H. C. Howland (1987). "Corneal accommodation in chick and pigeon." J.Comp Physiol [A] **160**(3): 375-384.
- Schaeffel, F., D. Troilo, et al. (1990). "Developing eyes that lack accommodation grow to compensate for imposed defocus." Vis Neurosci **4**(2): 177-83.
- Scher, J., E. Wankiewicz, et al. (2002). "MT(1) melatonin receptor in the human retina: expression and localization." Invest Ophthalmol Vis Sci **43**(3): 889-97.
- Schmid, K. L. and C. F. Wildsoet (1996). "Effects on the compensatory responses to positive and negative lenses of intermittent lens wear and ciliary nerve section in chicks." Vision Res **36**(7): 1023-36.
- Semple-Rowland, S. L. and K. M. Cheng (1999). "rd and rc chickens carry the same GC1 null allele (GUCY1\*)." Exp Eye Res **69**(5): 579-81.
- Semple-Rowland, S. L. and N. R. Lee (2000). "Avian models of inherited retinal disease." Methods Enzymol **316**: 526-36.
- Semple-Rowland, S. L., N. R. Lee, et al. (1998). "A null mutation in the photoreceptor guanylate cyclase gene causes the retinal degeneration chicken phenotype." Proc Natl Acad Sci U S A **95**(3): 1271-6.
- Sherry, D. M., M. M. Wang, et al. (2003). "Differential distribution of vesicle associated membrane protein isoforms in the mouse retina." Molecular Vision **9**: 673-688.
- Sherry, D. M., M. M. Wang, et al. (2003). "Differential distribution of vesicle associated membrane protein isoforms in the mouse retina." Mol Vis **9**: 673-88.
- Sherry, D. M., H. Yang, et al. (2001). "Vesicle-associated membrane protein isoforms in the tiger salamander retina." J Comp Neurol **431**(4): 424-36.
- Shibuya, K., H. Yamazaki, et al. (2002). "Hereditary visual impairment in a new mutant strain of chicken, GSN/1." Acta Neuropathol (Berl) **103**(2): 137-44.
- Sillman, A. J. (1973). Avian vision. Avian Biology. D. S. Farner and J. R. King. New York, NY, Academic Press. **3**: 349-83.

- Slaughter, M. M. and R. F. Miller (1981). "2-amino-4-phosphonobutyric acid: a new pharmacological tool for retina research." Science **211**(4478): 182-5.
- Slaughter, M. M. and R. F. Miller (1983). "An excitatory amino acid antagonist blocks cone input to sign-conserving second-order retinal neurons." Science **219**(4589): 1230-2.
- Slaughter, M. M. and R. F. Miller (1983). "The role of excitatory amino acid transmitters in the mudpuppy retina: an analysis with kainic acid and N-methyl aspartate." J Neurosci **3**(8): 1701-11.
- Smyth, J. R., Jr., R. E. Boissy, et al. (1981). "The DAM chicken: a model for spontaneous postnatal cutaneous and ocular amelanosis." J Hered **72**(3): 150-6.
- Smyth, J. R., Jr., R. E. Boissy, et al. (1981). "Retinal dystrophy associated with a postnatal amelanosis in the chicken." Invest Ophthalmol Vis Sci **20**(6): 799-803.
- Spence, S. G. and J. A. Robson (1989). "An autoradiographic analysis of neurogenesis in the chick retina in vitro and in vivo." Neuroscience **32**(3): 801-12.
- Spiwoks-Becker, I., L. Vollrath, et al. (2001). "Synaptic vesicle alterations in rod photoreceptors of synaptophysin-deficient mice." Neuroscience **107**(1): 127-42.
- Sprague, J. B. and W. B. Wilson (1981). "Electrophysiologic findings in bilateral optic nerve hypoplasia." Arch Ophthalmol **99**(6): 1028-9.
- Steinberg, R. H., R. Schmidt, et al. (1970). "Intracellular responses to light from cat pigment epithelium: origin of the electroretinogram c-wave." Nature **227**(259): 728-30.
- Stevenson, G. W., M. Kiupel, et al. (1999). "Ultrastructure of porcine circovirus in persistently infected PK-15 cells." Vet Pathol **36**(5): 368-78.
- Stone, R. A., T. Lin, et al. (1989). "Retinal dopamine and form-deprivation myopia." Proc Natl Acad Sci U S A **86**(2): 704-6.

- Stone, S. and P. Witkovsky (1984). "The actions of gamma-aminobutyric acid, glycine and their antagonists upon horizontal cells of the *Xenopus* retina." J Physiol **353**: 249-64.
- Swain, P. K., D. Hicks, et al. (2001). "Multiple phosphorylated isoforms of *NRL* are expressed in rod photoreceptors." J Biol Chem **276**(39): 36824-30.
- Teakle, E. M., C. F. Wildsoet, et al. (1993). "The spatial organization of tyrosine hydroxylase-immunoreactive amacrine cells in the chicken retina and the consequences of myopia." Vision Res **33**(17): 2383-96.
- Thanos, S. and F. Bonhoeffer (1983). "Investigations on the development and topographic order of retinotectal axons: anterograde and retrograde staining of axons and perikarya with rhodamine in vivo." J Comp Neurol **219**(4): 420-30.
- Thompson, I. (1991). Considering the evolution of the vertebrate neural retina. Vision and Visual Dysfunction. J. R. Cronly-Dillon and R. L. Gregory. Boca Raton, FL, CRC Press. **2**: 136-51.
- Troilo, D., M. D. Gottlieb, et al. (1987). "Visual deprivation causes myopia in chicks with optic nerve section." Curr Eye Res **6**(8): 993-9.
- Ulshafer, R. J., C. Allen, et al. (1984). "Hereditary retinal degeneration in the Rhode Island Red chicken. I. Histology and ERG." Exp Eye Res **39**(2): 125-35.
- Ulshafer, R. J. and C. B. Allen (1985). "Hereditary retinal degeneration in the Rhode Island Red chicken: ultrastructural analysis." Exp Eye Res **40**(6): 865-77.
- Vigh, J., T. Banvolgyi, et al. (2000). "Amacrine cells of the anuran retina: morphology, chemical neuroanatomy, and physiology." Microsc Res Tech **50**(5): 373-83.
- Vorobyev, M. (2003). "Coloured oil droplets enhance colour discrimination." Proc R Soc Lond B Biol Sci **270**(1521): 1255-61.
- Wack, M. A., N. S. Peachey, et al. (1989). "Electroretinographic findings in human oculocutaneous albinism." Ophthalmology **96**(12): 1778-85.

- Wallman, J. (1993). "Retinal control of eye growth and refraction." Progress in Retinal Eye Research **12**: 133-53.
- Wang, H. and X. Yang (1996). "Cobalt ions enhance light responsiveness of carp cone horizontal cells in low calcium." Sci China C Life Sci **39**(3): 258-66.
- Weber, B. H., G. Vogt, et al. (1994). "Mutations in the tissue inhibitor of metalloproteinases-3 (TIMP3) in patients with Sorsby's fundus dystrophy." Nat Genet **8**(4): 352-6.
- Weber, B. H., G. Vogt, et al. (1994). "Sorsby's fundus dystrophy is genetically linked to chromosome 22q13-qter." Nat Genet **7**(2): 158-61.
- Wen, R. and B. Oakley, 2nd (1990). "K(+)-evoked Muller cell depolarization generates b-wave of electroretinogram in toad retina." Proc Natl Acad Sci U S A **87**(6): 2117-21.
- Wildsoet, C. and J. Wallman (1995). "Choroidal and scleral mechanisms of compensation for spectacle lenses in chicks." Vision Res **35**(9): 1175-94.
- Williams, C. V. and S. C. McLoon (1991). "Elimination of the transient ipsilateral retinotectal projection is not solely achieved by cell death in the developing chick." J Neurosci **11**(2): 445-53.
- Witzel, D. A. and C. W. Smith (1976). Electroretinography. Applied electronics for Veterinary Medicine and Animal Physiology. W. R. Klemm. Springfield, Charles C. Thomas Publisher: 365-93.
- Won, M. H., T. C. Kang, et al. (2000). "Glial cells in the bird retina: immunochemical detection." Microsc Res Tech **50**(2): 151-60.
- Wurziger, K., T. Lichtenberger, et al. (2001). "On-bipolar cells and depolarising third-order neurons as the origin of the ERG-b-wave in the RCS rat." Vision Res **41**(8): 1091-101.
- Yang, H., K. M. Standifer, et al. (2002). "Synaptic protein expression by regenerating adult photoreceptors." J Comp Neurol **443**(3): 275-88.

Yazulla, S. (1986). "GABAergic mechanisms in the retina." Progress in Retinal Research 5: 1-52.

Yinon, U. and K. C. Koslowe (1986). "Hypermetropia in dark reared chicks and the effect of lid suture." Vision Res 26(6): 999-1005.

Young, R. W. and D. Bok (1969). "Participation of the retinal pigment epithelium in the rod outer segment renewal process." J Cell Biol 42(2): 392-403.

Zars, T. and D. R. Hyde (1996). "*rdgE*: a novel retinal degeneration mutation in *Drosophila melanogaster*." Genetics 144(1): 127-38.

Zimmerman, T. J., W. W. Dawson, et al. (1973). "I. Electroretinographic changes in normal eyes during administration of prednisone." Ann Ophthalmol 5(7): 757-65.

MICHIGAN STATE UNIVERSITY LIBRARIES



3 1293 02504 4425